Novel Roles for CHD7 and SOX11 in CHARGE Syndrome Pathogenesis and the Developing Ear

by

Ethan Douglas Sperry

A dissertation submitted in partial fulfillment
of the requirements for the degree of
Doctor of Philosophy
(Human Genetics)
in the University of Michigan
2017

Doctoral Committee:

Professor Donna M. Martin, Chair
Associate Professor Anthony Antonellis
Associate Professor Scott Barolo
Professor John V. Moran
Professor Yehoash Raphael

“The songs are in your eyes /
I see them when you smile /
I’ve had enough, I’m not giving up /
On a miracle drug /
Of science and the human heart /
There is no limit /
There is no failure here sweetheart /
Just when you quit”

- “Miracle Drug” by U2

“Follow the energy and you will understand the science.”

- Thomas E. Wilson, M.D., Ph.D.

Ethan D. Sperry

esperry@umich.edu

ORCID ID: 0000-0003-1233-4502

© Ethan D. Sperry 2017

Dedication

For my parents and sister;
this was only possible because of you.

Acknowledgments

No monumental task, such as a doctoral dissertation, is completed without an impressive supporting cast. First and foremost, what follows has only been possible because of the dedicated, persistent, generous, and intelligent mentorship by Dr. Donna Martin. Through all of the many disruptive medical issues I have faced during the past five years, you have stood by me and remained firm in your belief in my abilities and potential. I have learned so much from you about developmental genetics, inner ear biology, medical genetics, and maintaining a career as a physician-scientist. As a compassionate physician, discerning scientist, supportive mentor, and good friend, you represent the best of your profession. Indeed, you are the quintessential physician-scientist to whom I aspire.

Words are not enough to convey my appreciation to members of the Martin Laboratory. Jennifer, you are the foundation of Donna's laboratory. I have learned so many technical skills under your tutelage; however, and perhaps most importantly, you have provided me with invaluable knowledge about how to run a lab efficiently and effectively. I will certainly apply these skills and knowledge during my career. Ronus, I have been very lucky to have the privilege to mentor you during your tenure in the laboratory. Your enthusiasm for science has kept me motivated to learn, teach, and experiment over these past few years. I look forward to seeing you become a

compassionate and capable physician. Hui, Sophie, and Gilson; thank you all for your support and friendship. I must also thank Joe and Liz; you both provided me with the early intellectual foundation and support I needed to excel during my time in the lab. Finally, I thank Mark for our many intellectual discussions about genetics in addition to his friendship and support.

I sincerely appreciate the support of my doctoral dissertation committee: Drs. Tony Antonellis, Scott Barolo, John Moran, and Yehoash Raphael. I will carry forward the lessons learned from each of you about how to be an ever-curious, rigorous, and discerning scientist. Your support of my doctoral research, even during the difficult times, has been exceptional and I thank each of you for your efforts to help me become a better scientist.

The Department of Human Genetics has been a wonderful academic home for me during my doctoral training. In particular, I thank Drs. Thomas Gelehrter, Julie Douglas, Didi Robins, and JoAnn Sekiguchi for the many thoughtful discussions and support of my genetics education during these past five years. I also thank the entire administrative staff for the Department; your work "behind-the-scenes" has made my training a smooth process.

I am sincerely and eternally grateful to the entire University of Michigan Medical Scientist Training Program; I will never forget the moment I opened my admission letter back in February 2010. It means so much to me that I have been afforded the opportunity to become a physician-scientist. Dr. Ron Koenig, you have been a phenomenal program director, mentor, and friend over these past seven years. I am indebted to your support of, and belief in, me throughout my training here at UM. I have learned so much from you about what it means to be a physician-scientist. I also thank Drs. Katy Keegan and Juanita

Merchant for your support of the MSTP and my training. To Ellen Elkin, Hilkka Ketola, Laurie Koivupalo, and Justine Hein, I thank each of you for helping me navigate the administrative aspects of medical and doctoral training here at the University. Ellen and Hilkka, I am especially grateful for our many morale-boosting talks and for assisting me with all of the administrative and financial details surrounding my open heart surgery in early 2017.

Many close friends have helped keep me motivated during my medical and doctoral training. First, I wish to acknowledge the support of the MSTP class of 2010: Arthur Brannon III, Anup Das, Xixi Du, Andrew Freddo, Laurie Griffin, Zach Harvanek, Mangala Iyengar, Beth Pedersen-Schuler, Dave Rogawski, and Natasha Weiser. It has been so much fun spending time and learning from each of you over these past several years. I also greatly appreciate the friendship and support of Jon and Mia Bell, Erin Chapman, Amanda Harvanek (and Bennett and Emilia!), Ania Owczarczyk, Stacey Vosters, Nathan Wells, and Matt Windisch (and Callen!).

I realized my love for biology years ago in 7th grade science class at Honey Creek Middle School. I credit the enthusiasm of my science teacher Mrs. Carol Tolin for introducing me to fundamental experimental biology. You let me stay during lunch hour each day to dissect spare frogs, use the microscopes, and answer my many questions. Thank you, Mrs. Tolin; you are the teacher that "changed my life." Additionally, I thank Drs. Rusty Gonser and Elaina Tuttle for their mentorship of my high school science fair projects. I learned so much from both of you about how to perform experimental science. Your unparalleled mentorship and unwavering support of my science education has provided me with many of the tools I use to this day.

Finally, none of this would have been possible without the unwavering love and support from my family: Drs. Douglas and Linda Sperry and my sister Emma. Dad and Mom, you remain my greatest sources of inspiration. Through twenty-eight years, thirty-eight major surgeries, hundreds of medical appointments, and dozens of life-threatening medical events, you have been there for me. You have both remained steadfast in your belief that despite all of my medical issues, I can realize my dream of helping people burdened by, and of understanding the biology underlying, genetic disorders. Because of you, I will achieve my greatest goal: becoming a physician-scientist. Each day I strive to follow in your footsteps as I chart my own path in medicine, in academia, and in life. Emma, you are the best little sister I could have asked for twenty-two years ago. You have opened my eyes to the many injustices and humanitarian needs around the world and I will be sure to use this knowledge as I practice medicine. I am so proud of you and I cannot wait to watch you change the world.

Table of Contents

Dedication ..... **ii**

Acknowledgments ..... **iii**

List of Tables ..... **ix**

List of Figures ..... **x**

Abstract ..... **xii**

Chapter I: Introduction **1**

Clinical presentation of CHARGE syndrome 1

Phenotypic spectrum and mimics of CHARGE syndrome 4

Genotypic spectrum of CHARGE syndrome 5

Mouse models of Chd7 haploinsufficiency 6

The CHD family of ATP-dependent chromatin remodelers 9

Current understanding of functional roles for CHD7 in metazoans 11

CHD7 and SoxC transcription factors 13

Inner ear development 14

Summary 18

References 23

Chapter II: The chromatin remodeling protein CHD7, mutated in CHARGE syndrome, is necessary for proper craniofacial and tracheal development **32**

Introduction 33

Results 34

Discussion 41

Experimental Procedures 47

Acknowledgements 50

References 58

Chapter III: Duplication 2p25 in a Child with Clinical Features of CHARGE Syndrome **62**

Introduction 63

Materials and Methods 64
Results 65
Discussion 68
Acknowledgments 71
References 80
Chapter IV: SOX11 and CHD7 Act in a Common Gene Regulatory Network to Promote Inner Ear Development 83
Abstract 83
Introduction 84
Methods 87
Results 91
Discussion 99
Acknowledgments 104
References 116
Chapter V: Discussion and Future Directions 121
Summary of dissertation 121
CHD7 in craniofacial and tracheal development 121
Duplication 2p25 in a child with clinical features of CHARGE syndrome 124
SOX11 and CHD7 act in a common gene regulatory network to promote inner ear development 125
Conclusion 129
References 130

List of Tables

Table 1.1. Gene families and associated genes implicated in Coffin-Siris syndrome..... 21

Table 2.1. Foxg1-Cre or Wnt1-Cre conditional loss of Chd7 in mice results in multiple skeletal abnormalities..... 52

Table 3.1: Clinical features of pure trisomy 2p patients..... 73

Table 3.2: Probes utilized in FISH experiments..... 76

Table 3.3: Primers utilized in experiments..... 77

Table 3.4: Summary of relevant 2p duplication cases from ClinGen Database..... 78

Table 3.5: Summary of relevant 2p duplication cases from DECIPHER Database..... 79

Table 4.1. TaqMan probes used in this study..... 105

List of Figures

Figure 1.1: CHD7 is an ATP-dependent chromatin remodeler 22

Figure 2.1. Conditional deletion of Chd7 results in ocular hypoplasia and cranial bone dysplasia..... 53

Figure 2.2. Chd7 conditional mutants have shortened intraocular and intersquamosal distances, hypoplasia of the maxillary shelves, and dysplasia of nasal conchae. 54

Figure 2.3. Conditional Chd7 deletion results in palatal and nasal epithelial dysplasia.. 55

Figure 2.4. Neural crest-derived cardiac structures develop normally in Wnt1-CHet and Wnt1-CKO mice. 56

Figure 2.5. Foxg1-CKO mice have reduced numbers of cartilaginous tracheal rings..... 57

Figure 3.1: Clinical features of the proband. 74

Figure 3.2: Chromosomal microarray analysis revealed a gain of genomic material on chromosome 2p25.3-p25.2, confirmed by FISH, and shared with three other cases. 75

Figure 4.1. Sox11 mutant mice exhibit lateral and posterior semicircular canal dysplasia. 106

Figure 4.2. Posterior canal projections fail to form in Sox11-null mice despite normal EMT gene expression along the fusion plate. 107

Figure 4.3. Sox11-null mouse ears demonstrate impaired cellular proliferation..... 108

Figure 4.4. Germline absence of Sox11 results in misexpression of several genes critical for vestibular development. 109

Figure 4.5. Loss of Sox11 results in expansion of Bmp4, but not Otx1/2, expression at E10.5. 110

Figure 4.6. Bmp4 expression is expanded across the presumptive lateral and anterior cristae of E11.5 $Sox11^{-/-}$ mice. 111

Figure 4.7. CHD7 positively regulates Sox11 expression in the developing inner ear. 112

Figure 4.8. SOX11 protein levels are reduced in Chd7 mutant inner ears but CHD7 protein levels are preserved in Sox11-null ears. 113

Figure 4.9. Mice doubly heterozygous for Chd7 and Sox11 exhibited lateral and posterior semicircular canal dysplasia. 114

Figure 4.10. Model of CHD7 and SOX11 function in the lateral crista ampullaris and adjacent canal genesis zone. 115

Abstract

Tight regulation of gene expression is dependent on interactions of transcription factors and chromatin architecture. Haploinsufficiency of *CHD7*, which encodes a chromatin remodeling protein, is seen in individuals with CHARGE syndrome, a multiple anomaly disorder that presents with ocular colobomata, heart defects, choanal atresia, growth retardation, genital anomalies, and ear malformations. Mouse models of *Chd7* deficiency have provided extensive insight into the role of this ATP-dependent chromatin remodeler in development of the central nervous system, inner ear, and olfactory system. Nevertheless, many questions remain as to the role of CHD7 in mammalian embryogenesis. In this dissertation, I address the mechanistic relationships between CHD7 and the transcription factor SOX11 in development of embryologic structures affected in CHARGE syndrome. First, I present results of a careful examination of murine craniofacial and cardiorespiratory structures in two conditional *Chd7*-null mouse models. Further, I show that proper expression of *Chd7* is necessary for development of nasal, oropharyngeal, and tracheal structures through its function in migrating neural crest cells and developing bone. I then report on an individual with clinical features of CHARGE syndrome but no pathogenic variants within the *CHD7* locus, and show that partial duplication of chromosome 2p is associated with a CHARGE-like phenotype. This study highlights the importance of clinical phenotyping and the inherent similarities between

CHARGE and other syndromes. Finally, I examine the transcription factor SOX11 during vestibular morphogenesis. Using *Sox11*$^{+/+}$ and *Sox11*$^{-/-}$ mice, I conclude that SOX11 impacts development of the lateral and posterior semicircular canals through disruption of fusion plate formation and periotic mesenchymal cell proliferation. Further, I show that *Sox11* modulates *Bmp4* signaling in the crista ampullaris of developing semicircular canals and may be a putative downstream effector of CHD7 in the inner ear. Together, these studies advance our understanding of CHD7 and SOX11 function during craniofacial and inner ear morphogenesis and provide new insights into genetic mechanisms in CHARGE syndrome.

Chapter I: Introduction

CHARGE syndrome is a multiple anomaly disorder that presents with ocular colobomata, heart defects, choanal atresia, growth retardation, genital anomalies, and ear malformations[1-3]. First described in 1979 as an association of phenotypes exhibiting an autosomal dominant inheritance pattern, CHARGE is now understood to be a Mendelian disorder, caused by heterozygous pathogenic variants in the ATP-dependent chromatin remodeler CHD7[4,5]. CHARGE syndrome presents with a characteristic phenotype impacting the structure and function of the craniofacial, cardiorespiratory, neurosensory, endocrine, and urogenital systems[6,7]. Individuals with CHARGE experience a lifetime of medical, surgical, and psychosocial therapy and a diagnosis of CHARGE represents a life-altering event for affected families[8-10]. Continued scientific research into CHARGE and CHD7 will positively affect clinical outcomes for affected individuals and their families as well as further collective understanding of epigenetic and transcriptional regulation during mammalian development.

Clinical presentation of CHARGE syndrome

CHARGE syndrome represents one of the more common "rare" genetic disorders, with an incidence of 1 in 10,000 individuals[5,6]. Individuals with CHARGE present with classic craniofacial features, including square-shaped facies, facial asymmetry, external ear

anomalies, cleft lip and/or palate, cranial nerve palsies, and torticollis[11,12]. As all human neonates are obligate nasal breathers, many infants with CHARGE experience respiratory distress secondary to physical occlusion of the nasopharyngeal airway, often a direct consequence of choanal atresia[12]. Additionally, 75-95% of individuals diagnosed with CHARGE exhibit complex cardiac malformations resulting from abnormal development and septation of the conotruncus and the great vessels[5,12,13]. These life-threatening cardiorespiratory findings in newborns with CHARGE often result in extensive medical and surgical intervention from birth.

In addition to the classic craniofacial and cardiac features seen in CHARGE, patients also exhibit several brain, endocrine, and urogenital phenotypes[12,14-17]. Some individuals with CHARGE exhibit anatomic abnormalities of the developing cerebrum (specifically the ventricular system and corpus callosum) and cerebellum[18,19]. Additionally, many individuals with CHARGE experience developmental and neurobehavioral phenotypes, including autism spectrum disorder, likely related to microscopic changes in neural patterning and function in these structures[8-10]. Cranial nerve involvement is highly prevalent in individuals with CHARGE syndrome[20]. Specifically, disruptions to cranial nerves V, VII, IX, and X most commonly manifest as motor and sensory deficits affecting facial expression, sucking, mastication, and swallowing. Further, endocrine and urogenital dysfunction, including growth hormone deficiency and hypogonadotropic hypogonadism, are prevalent in individuals with CHARGE[16,17,21,22].

Ocular and otic abnormalities represent the most penetrant of the phenotypes in the CHARGE spectrum[5,12]. Indeed, CHARGE is the most common monogenic cause of hereditary deaf-blindness[23]. Individuals with CHARGE experience lifelong issues with

visual acuity, hearing, and balance. Vision loss in CHARGE is the result of ocular coloboma which is defined as a failed approximation of the iris and, in some cases, the retina during optic cup formation[24]. At their most limited, ocular colobomata impact the ability of the affected eye to adapt to changes in ambient light intensity[25]. Individuals with retinal colobomata experience visual field loss corresponding to the region of retina which has not properly fused.

Development of the ear is disrupted in nearly all individuals diagnosed with CHARGE syndrome[5,12]. For these patients, it is most common to uncover outer, middle, and inner ear abnormalities which ultimately affect hearing and balance sensation[26-28]. Individuals with CHARGE present with external ear malformations including low-set, posteriorly-rotated auricles with over-folded helices[29]. Within the middle ear, tympanic membrane prolapses, dysplastic ossicles, and small middle ear cavities are highly prevalent[26,27,30]. Furthermore, the course of the chorda tympani, a branch of CN-VII (facial), is often aberrant in these individuals[28]. Inner ear abnormalities are commonly reported in CHARGE syndrome, with significant disruptions to both the cochlear and vestibular components[12,23,31,32]. Anatomically, Mondini malformation and cochlear atresia are very common along with narrowing, truncation, or absence of one or more semicircular canals[23,33]. Innervation of the inner ear is also perturbed in most individuals with CHARGE, as evidenced by altered course or ablation of portions or all of the vestibulocochlear nerve (CN-VIII)[34].

Phenotypic spectrum and mimics of CHARGE syndrome

The phenotypic spectrum of CHARGE is broad and an area of intense study by several laboratories around the world. Most current clinical paradigms indicate a positive diagnosis of CHARGE in patients who present with various core combinations of the classic clinical features and genetic findings. Specifically, a clinical diagnosis of CHARGE is made when an affected individual presents with two or more of the following "major" criteria: coloboma, choanal atresia or cleft palate, abnormal external, middle, or inner ears, or a pathogenic *CHD7* variant[6]. In addition, most individuals with CHARGE exhibit other hallmarks of the disorder, including cranial nerve dysfunction, structural brain anomalies, developmental delay, intellectual disability, autism spectrum disorder, hypothalamo-hypophyseal dysfunction, cardiac malformations, tracheoesophageal fistula, renal anomalies, and axial skeletal anomalies.

Between unrelated individuals, the clinical presentation of CHARGE can vary dramatically. While the core "major" features are nearly universally observed in any individual diagnosed with CHARGE, the severity of presentation is frequently highly variable[5-7]. For example, dysplasia of the lateral semicircular canal (a major criterion) is commonly observed in CHARGE; however, one child may present with hypoplasia while another may have no recognizable canal[28]. Interestingly, this phenotypic variability is preserved in families with multiple affected individuals and even in mouse models of *Chd7* haploinsufficiency (to be discussed later)[35,36].

CHARGE syndrome is one of several phenotypically and developmentally similar disorders, all of which are considered within the differential diagnosis of an individual presenting with the appropriate symptom cluster. Specifically, the differential diagnosis for CHARGE typically includes 22q11.2 Deletion, Kallmann, Kabuki, Renal-Coloboma,

Joubert, and Branchio-Oto-Renal syndromes in addition to VACTERL association (comprised of vertebral defects, anal atresia, cardiac defects, trachea-esophageal fistula, renal anomalies, and limb abnormalities). Of these disorders, only Kallmann and Kabuki syndromes present with a high degree of similarity to CHARGE, particularly with regard to the major diagnostic criteria[37-42].

Genotypic spectrum of CHARGE syndrome

Up to 95% of individuals with a clinical diagnosis of CHARGE syndrome are believed to harbor *de novo* heterozygous deleterious mutations in *CHD7*[5]. Specifically, the majority (75%) of pathogenic *CHD7* mutations are nonsense (40%) or frameshift (35%)[23,43]. The remaining 25% of CHARGE-relevant *CHD7* mutations include missense (8%) and splice site (12%) mutations, along with complex chromosomal microdeletions, microduplications, and rearrangements (5%)[4,44,45]. While mutations in critical CHD7 protein domains, including the two N-terminal chromodomains and the paired helicase domains, are abundant within the population of individuals with CHARGE, pathogenic mutations exist along the entire length of the protein coding sequence.

There is often poor correlation between specific *CHD7* mutations and clinical presentation; indeed, a few anecdotal reports have described parent-child transmission of a given mutation with highly variable phenotypic presentations[35,46]. In these reports, the parent is most commonly mildly affected in the setting of a severely affected child, suggesting potential roles for parental somatic mosaicism (affecting the germline) or genetic anticipation[35,46]. To date, one confirmed case of paternal somatic mosaicism has been reported[46]. Finally, given the putative role of CHD7 as a regulator of chromatin

accessibility, it is feasible that individual variability in this accessibility could differentiate phenotypes across generations.

Of the 10-30% of individuals diagnosed with CHARGE but without detectable mutations in *CHD7*, it is possible that regulatory mutations affecting *CHD7* expression levels are responsible. One isolated case of CHARGE has been described in which the patient had a predicted pathogenic variant in the semaphorin gene *SEMA3E*[47]. Additionally, because of the phenotypic heterogeneity in CHARGE and its similarity with other disorders as described earlier, some individuals with other genetic variants more commonly associated with different disorders may meet the clinical criteria for CHARGE[38,48]. One such example is presented in Chapter III in this dissertation: in this case, a patient who met criteria for CHARGE syndrome presented with a genetic diagnosis of partial trisomy 2p but no mutations or other genetic changes in and around the *CHD7* locus.

Mouse models of Chd7 haploinsufficiency

Following the discovery of *CHD7* mutations as causative for the majority of people diagnosed with CHARGE syndrome, significant efforts were undertaken to develop a tractable mouse model for further study of CHD7[4]. Inroads towards understanding the function of *CHD7* began when Bosman and colleagues identified a *Chd7* haploinsufficient mouse model in a large-scale ENU mutagenesis system[49]. Specifically, they observed head-bobbing and circling behavior consistent with a vestibular defect. They identified *Chd7* expression in the semicircular canal pouches, developing cochlea, and in the vestibulocochlear ganglion (CN-VIII). Additionally, loss of *Chd7* generated sporadic

craniofacial defects including choanal atresia and cleft palate. Septal heart defects, predominantly ventricular septal defects, were also observed. Keratoconjunctivitis sicca was observed in *Chd7* mutant mice as were genital abnormalities involving the vulva and clitoris. Subsequently, Hurd and colleagues developed a gene-trapped mouse model of *Chd7* haploinsufficiency (*Chd7*$^{Gt/+}$) whereby truncation of the lateral and posterior semicircular canals was confirmed as well as reduced vestibular sensory epithelial innervation, providing a mechanism for the behavioral phenotype of head-bobbing and circling[15]. As *Chd7*-null mice do not survive past embryonic day 10.5 (E10.5), a *Foxg1-Cre* recombinase was employed to generate mice with conditional deletion of *Chd7* activity in neural tissues, including neural crest-derived structures[50]. Mice with *Foxg1-Cre* conditional *Chd7* deletion demonstrate severe hypoplasia of both semicircular canals and cochlea corresponding to observed reduction in inner ear neuroblasts. Follow-up studies in *Chd7*$^{Gt/+}$ mice have expanded on these findings to confirm physiologic hearing deficits as well as protection against further noise-induced hearing loss, perhaps secondary to stapedial fusion, hinting at a role for *Chd7* in bone formation and maintenance[51].

This same gene-trapped mouse model (*Chd7*$^{Gt/+}$) also exhibits olfactory bulb neurogenesis deficiency secondary to a neural stem cell proliferation defect[17]. The role of CHD7 in neural stem cell proliferation was more recently extended to include development of the subventricular zone (SVZ), where it was found to be required for proliferation, differentiation, and self-renewal of the SVZ neural stem cell niche[52]. Endocrine dysfunction in *Chd7*$^{Gt/+}$ mice has also been reported with specific defects in gonadotropin releasing hormone-producing neurons, having downstream effects on reproductive development and function[16]. A second mouse model of CHARGE syndrome (*whirligig*)

has been used to demonstrate neurogenesis defects along the hypothalamic-pituitary axis affecting the olfactory and genitourinary systems, which correlates well with the clinical findings of hypo/anosmia and hypogonadotropic hypogonadism in adolescent individuals with CHARGE syndrome[53]. These findings confirm a role for *CHD7* in neurogenesis within the olfactory and endocrine systems.

More recently, a *Chd7*-null zebrafish model was generated, showing disruption of multiple neurologic and musculoskeletal aspects of the developing embryo and confirming that CHD7 has a similar role across the vertebrate sub-phylum[54,55]. These studies in mice and zebrafish point towards neural crest migration as a common mechanism of developmental dysfunction secondary to loss of CHD7. Indeed, direct evidence for CHD7 participating in the formation of multipotent, migratory neural crest cells was provided by Bajpai and colleagues in *Xenopus*[56]. Cells populating the cranial neural crest are responsible for diverse structures, throughout the head, neck, and thorax of developing vertebrates, principally the branchial arches. More recently, the *whirligig* mouse model was used to demonstrate that loss of *Chd7* impairs neural crest cell guidance into the pharyngeal arches[57]. Many of the structural deformities in individuals with CHARGE, including those involving the outer (structural malformation of the auricle) and middle (stapedial fusion, cranial nerve VII dysfunction) ear, eyes (coloboma), nose (choanal atresia, hyposmia), and heart (septal defects) in individuals with CHARGE can be explained by inappropriate migration and failed regulation of neural crest cells at those sites[56,58]. Embryologic patterning is heavily influenced by interactions between migrating neural crest and the overlying ectoderm and underlying endoderm, making possible the broad array of phenotypic disruptions seen in CHARGE syndrome[59]. Thus, mutations in

CHD7 could be indirectly influencing neural patterning throughout the developing embryo via tissue- and temporally-selective access to genes involved in neural crest development, migration, and differentiation.

As previously mentioned, craniofacial abnormalities are among the more recognizable features seen in individuals with CHARGE syndrome. Proper craniofacial development depends on adequate neural crest cell formation and migration and disruption of CHD7 impairs neural crest cell development[56,57,59]. Thus, one important question is how CHD7 functions during morphogenesis of mammalian facial structures. While the human craniofacial phenotype has been extensively studied, until recently it was unknown whether mouse models for CHARGE syndrome reproducibly exhibited similar defects. Chapter II of this dissertation highlights research into the craniofacial and cardiorespiratory phenotypes present in mice with germline, gene-trapped, and conditional *Chd7* deletion.

The CHD family of ATP-dependent chromatin remodelers

The identification of *CHD7* as the causative gene for human CHARGE syndrome has served as the foundation for a large body of research into the role of chromatin remodelers in mammalian development[4]. The process of chromatin remodeling is critical for regulation of chromatin openness to binding by transcription factors and other regulatory factors necessary for gene expression[60-62]. Regulation of chromatin organization is maintained by three separate biologic processes. First, the association of nucleosomes to DNA can be affected by the DNA sequence itself; indeed, many high- and low-affinity binding sequences have been identified[63]. These high-affinity sites are known as "nucleosome positioning sequences" and typically include AA and TT dinucleotides

spaced at regular intervals across a stretch of DNA[64]. Second, nucleosomes can be recruited and ejected from certain regions via changes in the chemical structures of the constituent histones[61]. Enzymes involved in this process include the histone de/acetylases and de/methylases, kinases and phosphorylases, and de/ubiquitinases. Third, nucleosome positioning along DNA can be actively changed by ATP-dependent chromatin remodeling complexes[61]. These complexes translocate nucleosomes, allowing specific regions of DNA to become accessible, or inaccessible, to transcriptional regulatory factors and machinery[65].

CHD7 is one of nine members of the chromodomain helicase DNA-binding family of enzymes which belong to the SNF2 superfamily of ATP-dependent chromatin remodelers[66,67]. Together with SWI-like proteins, SNF remodelers work in large complexes to translocate nucleosomes along DNA. To accomplish their part in this task, CHD proteins variably contain several domains critical for their function and specificity. In particular, CHD7 has two N-terminal chromodomains, two helicase domains, a Swi3/Ada2/N-Cor/TFIIIB (SANT) domain, and two Brahma/Kismet (BRK) domains[68,69]. Each chromodomain is thought to help CHD7 associate with specific regions of chromatin while the paired helicase domains serve to slide nucleosomes in an ATP-dependent fashion (Figure 1.1). The SANT domain may help CHD7 utilize specific histone marks to guide its nucleosome sliding functionality while the role of the twin BRK domains remains under investigation[68,70].

Current understanding of functional roles for CHD7 in metazoans

CHD7 is a member of a family of nine proteins encoding ATP-dependent chromatin remodelers, whose nucleosome sliding function has been recently confirmed for CHD6, CHD7, and CHD8[71,72]. Efforts have been made to better understand the role of CHD7 in gene expression in a diverse range of cell types and organisms. The *CHD7* orthologue *kismet* in *Drosophila* has a role in elongation of mRNA transcripts by RNA polymerase II, specifically by recruiting trithorax group histone methyltransferases to promote methylation of H3K27 sites which, in turn, results in transcriptional activation by inhibiting the transcription-repressive function of nearby Polycomb group proteins[73]. These findings have been demonstrated to affect axonal development in *Drosophila* leading to defects in neuronal function, specifically memory formation, motor function, and retinal development[74,75].

Studies in mouse embryonic stem cells (ESCs) have demonstrated localization of CHD7 at H3K4-methylated sites along potential enhancer regions in a cell type-specific fashion[76]. Specifically, CHD7 appears to be critical for fine-tuning expression of ESC gene expression, both via co-activation and co-repression with other proteins associated with enhancers including P300 and the ESC master regulators OCT4, SOX2, and NANOG[77]. CHD7 is also a known regulator of ribosomal RNA biogenesis[78]. Specifically, ChIP experiments have demonstrated that CHD7 is physically associated with hypomethylated, active ribosomal DNA (rDNA). Upon siRNA-mediated depletion of *Chd7*, rDNA promoters become hypermethylated and 45S rRNA levels are reduced. Together, these studies suggest that CHD7 has wide-ranging effects on genomic and ribosomal DNA expression in early-formed cells in development.

CHD7 functions in nucleosome remodeling complexes alongside several other proteins at regulatory elements across the genome. CHD7 binds SOX2, a SRY-related HMG box-containing transcription factor, at specific binding sites along the human genome in neural stem cells, resulting in target gene-specific regulation[79]. CHD7-SOX2 interactions have provided a possible mechanism for clinical similarities seen between CHARGE syndrome and SOX2 anophthalmia syndrome. In mouse embryonic stem cells, CHD7 also co-immunoprecipitates with P300, a histone acetyltransferase and marker of functional enhancer elements[77]. As a transcriptional co-activator, P300 often associates with CREB-binding protein at DNaseI hypersensitive sites[80]. P300 is then able to acetylate histone residues H3K27 and H3K18, which, in turn, allows recruitment of the transcription complex including RNA polymerase II[80]. Mutations in P300 and CREB-binding protein are associated with Rubinstein-Taybi syndrome[81]. In mouse embryonic stem cells, CHD7 represses target gene expression through enhancer occupancy[77].

Other CHD family members also participate in large protein complexes, presumably allowing them to effectively modulate chromatin structure. CHD8, another ATP-dependent chromatin remodeling enzyme functioning at histone sites throughout the genome, associates with CHD7 *in vitro*[82]. CHD8 is important in regulating the expression of homeobox transcription factors and genes involved in cell cycle control[83,84]. There is immense complexity of chromatin remodeling enzyme function in metazoans and interplay between CHDs could indicate roles in super-structural chromatin complexes which allow for selective access to genes designated for transcription.

CHD7 and SoxC transcription factors

In mouse central nervous system neural stem cells CHD7 regulates transcription of *Sox4* and *Sox11*, which encode SRY-related HMG box-containing transcription factors (Feng 2013). In humans, heterozygous mutations in *SOX11* cause a phenotypically mild, rare variant of Coffin-Siris syndrome[85]. Individuals with Coffin-Siris syndrome generally exhibit craniofacial dysmorphisms, microcephaly, posteriorly rotated ears, intellectual disability, endocrine deficiencies, congenital heart defects, and hypo/aplasia of the fifth finger/toenails[86-91]. Developmental delay is common in Coffin-Siris and some children exhibit autism spectrum disorder and sensorineural hearing loss[87,89,92]. Most cases of Coffin-Siris syndrome have been attributed to mutations in one of the five subunits found in the human SWI/SNF (BAF) complex (*ARID1A/B* and *SMARCA4/B1/E1*), placing this condition within the rapidly expanding group of neurodevelopmental disorders caused by defects in chromatin remodeling with significant ramifications for embryologic development (Table 1.1)[89-91,93,94].

SOX11 primarily acts as a transcriptional activator, modulating transcription via three protein domains. Common to all SOX transcription factors, SOX11 contains a core High Mobility Group (HMG) DNA binding domain which binds the minor groove of DNA at a 5'-(A/T)(A/T)CAA(A/T)G-3' sequence[95]. Further, like many Sox proteins, SOX11 also contains a carboxy-terminal transcription activation domain (TAD) which allows SOX11 to bind protein complexes destined to activate downstream transcription[96]. Additionally, SOX11 has a central acid-rich domain which demonstrates auto-inhibitory function *in vivo*, suggesting that SOX11 auto-regulates its own transcription[97]. Further, SOX11 displays a high degree of homology with the pro-apoptotic poly-glycine domain of SOX4[98]. Finally, the POU family of transcription factors work in synergy to promote

SOX11 function in early neural progenitors[99]. Through these various mechanisms, SOX11 exhibits an important role in regulating cell number, particularly in neuronal tissues, during embryogenesis and adulthood; findings which are consistent with the reported proliferative role of SOX4 and SOX11 in embryonic and adult brain development[100].

There are significant phenotypic similarities between Coffin-Siris and CHARGE syndromes, including involvement of craniofacial structures, brain, endocrine system, heart, and the ear. Studies in the developing mouse highlight the importance of SOX11 for proper embryogenesis. *Sox11* germline mutant mice exhibit abnormalities in craniofacial, axial skeletal, cardiopulmonary, and neurologic structures[101]. SOX11 was recently studied in the developing murine utricle and found to be important for cell proliferation in the utricular macula[102]. *Sox11* deficiency also led to reduced proliferation of otic sensory progenitor cells and impaired differentiation of otic progenitors into hair cells versus supporting cells. Given that 1) *Sox11* is widely expressed in the developing chicken ear, 2) SOX11 is critical for utricular neurogenesis in the developing mouse ear, and 3) CHD7 associates at the promoter of *Sox11* in mouse neural stem cells, SOX11 has emerged as a potential factor downstream of CHD7 during inner ear development[102-104].

Inner ear development

Proper structure-function morphogenesis in the mammalian inner ear requires rapid and accurate cellular proliferation and differentiation. Functionally, the inner ear serves as the starting point for the detection and processing of pressure waves (sound) and of three-dimensional motion. External auditory and vestibular signals are received by the inner ear and transmitted to the brain via the eighth cranial nerve to generate the sensations of

hearing and balance. Inner ear morphogenesis begins with the formation of the otic placode from the pre-placodal region of the developing rhombencephalon[105,106]. Subsequently, the otic placode elongates along the ectodermal ridge and invaginates to form the otic cup and later the otic vesicle, located between the ectodermal layer and the lateral wall of the neural tube[106]. Over the next several days of development (E9.5-E15.5 in the mouse), the otic vesicle grows and segregates into the various epithelial compartments (e.g. semicircular canals, cochlea) and sensory structures (sensory cristae, maculae, and the organ of Corti) of the inner ear. Coordination of this complex developmental process depends on accurate spatiotemporal control of gene expression via transcriptional networks in the cell nucleus[106-108].

As mentioned previously, *CHD7* haploinsufficiency affects development of the outer, middle, and inner ear, resulting in difficulties with sound capture, transduction, and signal processing. Individuals with CHARGE exhibit highly penetrant lateral and posterior semicircular canal abnormalities manifesting in balance disturbances[109]. Studies in *Chd7* haploinsufficient mice largely replicate the inner ear findings reported in humans, including hearing loss, lateral and posterior semicircular canal malformations, and vestibular innervation defects[50,110-112]. The effects of *Chd7* haploinsufficiency on mouse inner ear development are complex, profound, and likely result from early stage (E8.5-E9.5) disruption to the genetic integrity of the developing ear.

Loss of *Chd7* also results in major disruptions to the transcriptome in several CHARGE-relevant cell types and tissues. Microarray analysis and RNA-sequencing of *Chd7* mutant mouse embryonic stem, neural stem, and cerebellar granule precursor cells have uncovered abnormalities in expression of hundreds of genes involved in several

developmental signaling pathways[79,103,113,114]. Germline loss of a single copy of *Chd7* in the developing mouse inner ear also results in broad disruptions to the transcriptome. In the E10.5 *Chd7* heterozygous ear, several transcription factors, signaling molecules, and structural proteins exhibit significantly altered expression, illuminating the genetic basis for the broad phenotypic impact of this chromatin remodeler on ear development[50,112]. However, studies of the *Chd7* mutant ear have thus far relied on analysis of individual genes using *in situ* hybridization or immunohistochemistry.

Changes in the distribution, or complete absence, of several genes critical for specification of the E10.5-E11.5 ear have been extensively reported in *Chd7* deficient mice. Loss of *Chd7* results in reduced expression of the critical otic placode inducers BMP2, BMP4, and FGF10[115-117]. Semicircular canal development is impaired in *Chd7* mutant mice, along with disrupted expression of several genes important for canal morphogenesis, including *Bmp2*, *Bmp4*, *Fgf10*, *Msx1*, *Otx1*, *Otx2*, and *Ntn1*[112]. Finally, neurogenesis in the inner ear, as partially marked by FGF10, OTX2, and NGN1 is also disrupted in *Chd7* mutant mice[50]. Unsurprisingly, vestibulocochlear ganglion size is subsequently reduced in *Chd7* mutant mice when compared with wild type mice, concomitant with expansion of *Tbx1*, a suppressor of neurogenesis.

Studies of SOX11 in the developing inner ear have been primarily limited to the utricle, one of two sensory structures responsible for detecting linear acceleration[102]. Expression data indicate that *Sox11* is highly expressed throughout the ventral, medial, and lateral quadrants of the developing chicken otocyst[104]. Work performed more recently suggests that SOX11 promotes cell proliferation in sensory organ development, and leads

to reduced proliferation of otic sensory progenitor cells and impaired differentiation of otic progenitors into hair cells versus supporting cells[102].

In the developing ear, CHD7 and SOX11 act within a complex three-dimensional space marked by dynamic cellular differentiation and morphogenetic events. The E10.5 otocyst comprises a sphere whose domains of gene expression lead to the compartment-boundary model originally proposed by Fekete (1996) as octants containing cells that behave similarly and express related genes[106]. The domains of gene expression in the developing ear are thought to behave in a similar fashion to other segmented anatomic structures, including the *Drosophila* wing and vertebrate brain, where cells occupy specific compartments that act synergistically or antagonistically to establish borders and specific identities. For example, antagonism between members of the SHH and WNT signaling pathways help specify the dorsal and ventral halves of the otocyst, while the neurosensory patches require localized TGFB and Notch signaling[106,118]. Moreover, individual structures in the ear (e.g. endolymphatic duct, semicircular canals, cochlea) reproducibly derive from specific regions of the vertebrate otocyst, suggesting links between gene expression boundaries and structural differentiation. For example, anatomically, the ear can be divided into the dorsal and ventral compartments which give rise to the vestibular and auditory systems, respectively. Other structures in the developing ear, including the lateral semicircular canal, are generally understood to arise from lateral compartments, while neuroblasts that migrate from the otocyst to the vestibulocochlear (VIII) ganglion arise from the ventrolateral compartment and migrate medially before delamination[119].

Fekete and others have hypothesized that master genetic regulators likely direct this highly organized and complex developmental process. Given the broad impact of CHD7

loss on the mammalian ear, CHD7 may also play important roles in early otic patterning. While the specific molecular genetic mechanisms by which CHD7 impacts inner ear development are incompletely understood, the emergence of SoxC transcription factors as critical for ear development provide an intriguing avenue for further exploration of this chromatin remodeler. Chapter IV of this dissertation explores the hypothesis that SOX11 functions as a downstream effector of CHD7 during semicircular canal morphogenesis.

Summary

The scope of this dissertation is broad. In Chapter II, I discuss my research into the role of CHD7 during mouse craniofacial and oropharyngeal development. Specifically, I found that CHD7 is required for mouse head and neck morphogenesis including disruptions to ocular formation and nasal architecture. Further, the affected structures in *Chd7*-deficient mice are identical to those affected in humans with CHARGE syndrome. My work found that loss of *Chd7* in mice recapitulates some of the phenotypic variability seen in humans, specifically the variability in incidence of cleft palate. Further, I demonstrated a direct effect of CHD7 on tracheal formation, with *Chd7* mutant embryos exhibiting a reduction in tracheal cartilage morphogenesis. This was the first non-human evidence for *Chd7* deletion causing tracheomalacia, a serious condition experienced by many individuals with CHARGE. Results from this study 1) highlight the role of *Chd7* in craniofacial and respiratory development, including development of cartilage and bone, 2) demonstrate that *Chd7* is required for proper generation of the surface ectoderm, endoderm, and migrating neural crest cells, and 3) confirm the utility of available *Chd7* mutant mouse models in studying these phenotypes.

In Chapter III, I report on an individual diagnosed with clinical features of CHARGE syndrome who did not exhibit any genetic aberrations in or around the *CHD7* locus. This study was inspired by continuing efforts in the field to better understand the genetic causes of CHARGE as well as the high degree of clinical overlap between CHARGE and phenotypically similar syndromes. I confirmed that this patient exhibited a complicated duplication of chromosome 2, including increased dosage of *SOX11*. In this chapter, I discuss the importance of clinical phenotyping and the inherent similarities between CHARGE and other syndromes.

In Chapter IV, I present results of my analysis of the role of SOX11 in the developing mouse ear. Extensive phenotypic similarity between *Chd7* and *Sox11* mutant mice led me to hypothesize that SOX11 may have a complementary role during inner ear development. Consistent with this, CHD7 had been shown by others to act as an upstream regulator of *Sox11* expression in neural stem cells[103]. While loss of *Chd7* has been reported by others to impact gene expression and morphologic development of the mouse inner ear, the precise genetic mechanism underlying CHD7's role in inner ear development is unknown. I hypothesized that, similar to its role in neural stem cell development, CHD7 may directly regulate *Sox11* during ear development. I focused my studies on the most highly penetrant inner ear phenotype observed in *Chd7* mutant mice, that of lateral and posterior semicircular canal dysplasia. Consistent with this, I showed that loss of *Sox11* impacted development of these semicircular canals. Next, I determined that SOX11 positively regulates cell proliferation around the lateral and posterior canal anlagen and is required for canal fusion plate formation. Further, I found *Sox11* is important for restricting expression of *Bmp4*, a gene critical for specifying the semicircular canal crista ampullaris

and adjacent canal genesis zones. Finally, I determined that loss of *Chd7* disrupts *Sox11* expression in the developing ear and may indicate that *Sox11* resides downstream of *Chd7* in semicircular canal morphogenesis.

Together, the data presented in my dissertation expand our understanding of roles for CHD7 in craniofacial and inner ear development. Importantly, my studies highlight the necessity for CHD7 in craniofacial and respiratory development and expand on the role of this chromatin remodeler in neural crest cell-dependent developmental processes. Further, I described a chromosome 2 duplication in an individual with clinical features of CHARGE syndrome. This work broadens our understanding of the genetic etiologies underlying human CHARGE phenotypes. Finally, I have demonstrated that SOX11 is required for lateral and posterior semicircular canal development in the mouse and may serve as a putative effector of CHD7 function in the developing ear, complementary to its published role in the central nervous system[103].

Gene Family	Genes Implicated in Coffin-Siris Syndrome
AT-rich interacting domain (ARID)-containing factor	*ARID1A, ARID1B*
Switching defective/sucrose non-fermenting related, matrix associated, actin dependent regulators of chromatin (SMARC)	*SMARCA4, SMARCB1, SMARCE1*
SRY-related high mobility group box-containing (SOX) transcription factor	*SOX11*

Table 1.1. Gene families and associated genes implicated in Coffin-Siris syndrome.

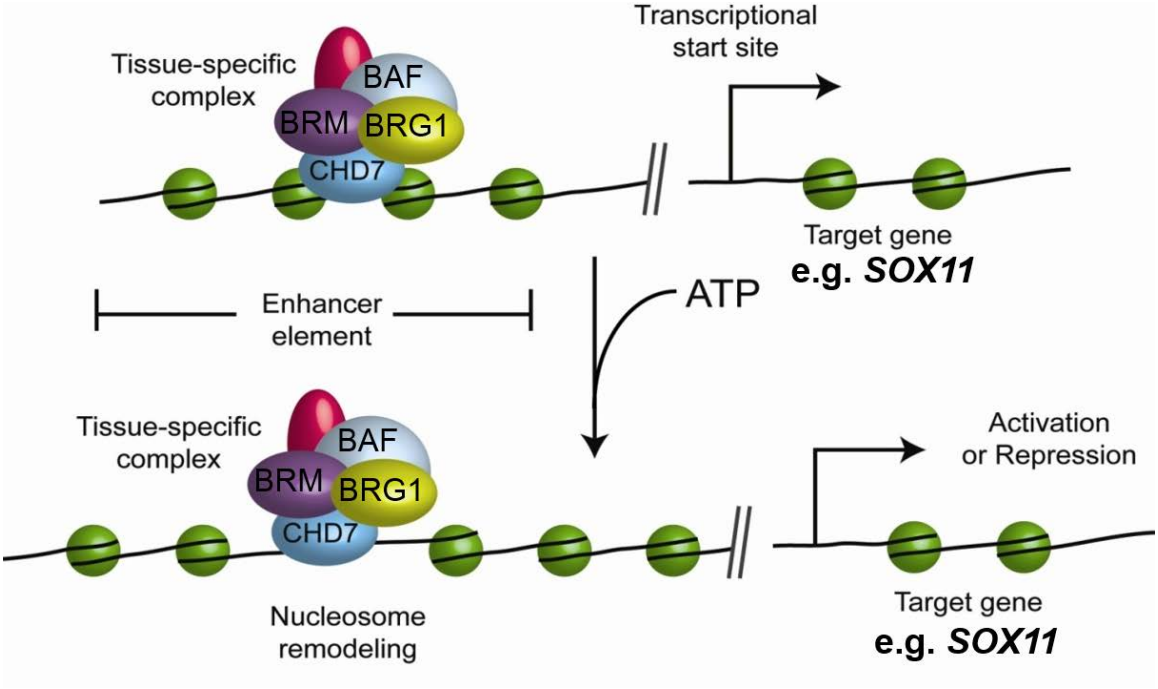


Figure 1.1: CHD7 is an ATP-dependent chromatin remodeler.
Upon hydrolysis of ATP, CHD7 functions in complex with other SWI/SNF proteins to slide nucleosomes along DNA, regulating DNA accessibility and access by transcription factor complexes to nearby genes.

References

1. Hall, B. D. Choanal atresia and associated multiple anomalies. *J Pediatr* **95**, 395-398 (1979).

2. Hittner, H. M., Hirsch, N. J., Kreh, G. M. & Rudolph, A. J. Colobomatous microphthalmia, heart disease, hearing loss, and mental retardation--a syndrome. *Journal of Pediatric Ophthalmology & Strabismus* **16**, 122-128 (1979).

3. Pagon, R. A., Graham, J. M., Jr., Zonana, J. & Yong, S. L. Coloboma, congenital heart disease, and choanal atresia with multiple anomalies: CHARGE association. *J Pediatr-Us* **99**, 223-227 (1981).

4. Vissers, L. E. *et al.* Mutations in a new member of the chromodomain gene family cause CHARGE syndrome. *Nat Genet* **36**, 955-957 (2004).

5. Janssen, N. *et al.* Mutation update on the CHD7 gene involved in CHARGE syndrome. *Hum Mutat* **33**, 1149-1160 (2012).

6. Hale, C. L., Niederriter, A. N., Green, G. E. & Martin, D. M. Atypical phenotypes associated with pathogenic CHD7 variants and a proposal for broadening CHARGE syndrome clinical diagnostic criteria. *Am J Med Genet A* **170A**, 344-354 (2016).

7. Verloes, A. Updated diagnostic criteria for CHARGE syndrome: a proposal. *Am J Med Genet A* **133**, 306-308 (2005).

8. Hartshorne, T. S., Grialou, T. L. & Parker, K. R. Autistic-like behavior in CHARGE syndrome. *Am J Med Genet A* **133**, 257-261 (2005).

9. Hartshorne, T. S., Hefner, M. A. & Davenport, S. L. Behavior in CHARGE syndrome: introduction to the special topic. *Am J Med Genet A* **133A**, 228-231 (2005).

10. Hartshorne, T. S., Nicholas, J., Grialou, T. L. & Russ, J. M. Executive function in CHARGE syndrome. *Child Neuropsychol* **13**, 333-344 (2007).

11. Hughes, S. S., Welsh, H. I., Safina, N. P., Bejaoui, K. & Ardinger, H. H. Family history and clefting as major criteria for CHARGE syndrome. *Am J Med Genet A* **164A**, 48-53 (2014).

12. Zentner, G. E., Layman, W. S., Martin, D. M. & Scacheri, P. C. Molecular and phenotypic aspects of CHD7 mutation in CHARGE syndrome. *Am J Med Genet A* **152A**, 674-686 (2010).

13. Bergman, J. E. H. *et al.* CHD7 mutations and CHARGE syndrome: the clinical implications of an expanding phenotype. *Journal of Medical Genetics* **48**, 334-342 (2011).

14. Bergman, J. E. H., Bocca, G., Hoefsloot, L. H., Meiners, L. C. & van Ravenswaaij-Arts, C. M. A. Anosmia Predicts Hypogonadotropic Hypogonadism in CHARGE Syndrome. *J Pediatr-Us* **158**, 474-479 (2011).

15. Hurd, E. A. *et al.* Loss of Chd7 function in gene-trapped reporter mice is embryonic lethal and associated with severe defects in multiple developing tissues. *Mamm Genome* **18**, 94-104 (2007).

16. Layman, W. S., Hurd, E. A. & Martin, D. M. Reproductive dysfunction and decreased GnRH neurogenesis in a mouse model of CHARGE syndrome. *Hum Mol Genet* **20**, 3138-3150 (2011).

17. Layman, W. S. *et al.* Defects in neural stem cell proliferation and olfaction in Chd7 deficient mice indicate a mechanism for hyposmia in human CHARGE syndrome. *Hum Mol Genet* **18**, 1909-1923 (2009).

18. Becker, R., Stiemer, B., Neumann, L. & Entezami, M. Mild ventriculomegaly, mild cerebellar hypoplasia and dysplastic choroid plexus as early prenatal signs of CHARGE association. *Fetal Diagn Ther* **16**, 280-283 (2001).

19. Sohn, Y. B. *et al.* Cerebellar vermis hypoplasia in CHARGE syndrome: clinical and molecular characterization of 18 unrelated Korean patients. *J Hum Genet* **61**, 235-239 (2016).

20. Blake, K. D., Hartshorne, T. S., Lawand, C., Dailor, A. N. & Thelin, J. W. Cranial nerve manifestations in CHARGE syndrome. *Am J Med Genet A* **146A**, 585-592 (2008).

21. Asakura, Y. *et al.* Endocrine and radiological studies in patients with molecularly confirmed CHARGE syndrome. *J Clin Endocrinol Metab* **93**, 920-924 (2008).

22. Khadilkar, V. V., Cameron, F. J. & Stanhope, R. Growth failure and pituitary function in CHARGE and VATER associations. *Arch Dis Child* **80**, 167-170 (1999).

23. Lalani, S. R. *et al.* Spectrum of CHD7 Mutations in 110 Individuals with CHARGE Syndrome and Genotype-Phenotype Correlation. *Am J Hum Genet* **78**, 303-314 (2006).

24. Nishina, S. *et al.* Ophthalmic features of CHARGE syndrome with CHD7 mutations. *Am J Med Genet A* **158A**, 514-518 (2012).

25. Onwochei, B. C., Simon, J. W., Bateman, J. B., Couture, K. C. & Mir, E. Ocular colobomata. *Surv Ophthalmol* **45**, 175-194 (2000).

26. Edwards, B. M., Kileny, P. R. & Van Riper, L. A. CHARGE syndrome: a window of opportunity for audiologic intervention. *Pediatrics* **110**, 119-126 (2002).

27. Shah, U. K. *et al.* Otologic management in children with the CHARGE association. *Int J Pediatr Otorhinolaryngol* **44**, 139-147 (1998).

28. Vesseur, A. C. *et al.* CT findings of the temporal bone in CHARGE syndrome: aspects of importance in cochlear implant surgery. *Eur Arch Otorhinolaryngol* **273**, 4225-4240 (2016).

29. Legendre, M. *et al.* Antenatal spectrum of CHARGE syndrome in 40 fetuses with CHD7 mutations. *J Med Genet* (2012).

30. Derbent, M. *et al.* Middle and inner ear anomalies in a patient with CHARGE association. *Genet Couns* **14**, 367-368 (2003).

31. Green, G. E., Huq, F. S., Emery, S. B., Mukherji, S. K. & Martin, D. M. CHD7 mutations and CHARGE syndrome in semicircular canal dysplasia. *Otol Neurotol* **35**, 1466-1470 (2014).

32. Wineland, A. *et al.* Prevalence of Semicircular Canal Hypoplasia in Patients With CHARGE Syndrome: 3C Syndrome. *JAMA Otolaryngol Head Neck Surg* **143**, 168-177 (2017).

33. Wright, C. G., Brown, O. E., Meyerhoff, W. L. & Rutledge, J. C. Auditory and temporal bone abnormalities in CHARGE association. *Annals of Otology, Rhinology & Laryngology* **95**, 480-486 (1986).

34. Holcomb, M. A., Rumboldt, Z. & White, D. R. Cochlear nerve deficiency in children with CHARGE syndrome. *Laryngoscope* **123**, 793-796 (2013).

35. Delahaye, A. *et al.* Familial CHARGE syndrome because of CHD7 mutation: clinical intra- and interfamilial variability. *Clin Genet* **72**, 112-121 (2007).

36. Jongmans, M. C. J. *et al.* Familial CHARGE syndrome and the CHD7 gene: A recurrent missense mutation, intrafamilial recurrence and variability. *American Journal of Medical Genetics Part A* **146A**, 43-50 (2008).

37. Badalato, L. *et al.* KMT2D p.Gln3575His segregating in a family with autosomal dominant choanal atresia strengthens the Kabuki/CHARGE connection. *Am J Med Genet A* **173**, 183-189 (2017).

38. Jongmans, M. C. *et al.* CHD7 mutations in patients initially diagnosed with Kallmann syndrome--the clinical overlap with CHARGE syndrome. *Clin Genet* **75**, 65-71 (2009).

39. Kim, H. G. *et al.* Mutations in CHD7, encoding a chromatin-remodeling protein, cause idiopathic hypogonadotropic hypogonadism and Kallmann syndrome. *Am J Hum Genet* **83**, 511-519 (2008).

40. Ming, J. E., Russell, K. L., Bason, L., McDonald-McGinn, D. M. & Zackai, E. H. Coloboma and other ophthalmologic anomalies in Kabuki syndrome: distinction from charge association. *Am J Med Genet A* **123A**, 249-252 (2003).

41. Patel, N. & Alkuraya, F. S. Overlap between CHARGE and Kabuki syndromes: more than an interesting clinical observation? *Am J Med Genet A* **167A**, 259-260 (2015).

42. Schulz, Y. *et al.* CHARGE and Kabuki syndromes: a phenotypic and molecular link. *Hum Mol Genet* **23**, 4396-4405 (2014).

43. Jongmans, M. C. J. *et al.* CHARGE syndrome: the phenotypic spectrum of mutations in the CHD7 gene. *Journal of Medical Genetics* **43**, 306-314 (2006).

44. Kaliakatsos, M. *et al.* Combined microdeletions and CHD7 mutation causing severe CHARGE/DiGeorge syndrome: clinical presentation and molecular investigation by array-CGH. *J Hum Genet* **55**, 761-763 (2010).

45. Lehman, A. M. *et al.* A characteristic syndrome associated with microduplication of 8q12, inclusive of CHD7. *Eur J Med Genet* **52**, 436-439 (2009).

46. Jongmans, M. C. *et al.* Familial CHARGE syndrome and the CHD7 gene: a recurrent missense mutation, intrafamilial recurrence and variability. *Am J Med Genet A* **146**, 43-50 (2008).

47. Lalani, S. R. *et al.* SEMA3E mutation in a patient with CHARGE syndrome. *J Med Genet* **41**, E94 (2004).

48. Bergman, J. E. H. *et al.* A novel classification system to predict the pathogenic effects of CHD7 missense variants in CHARGE syndrome. *Hum Mutat* **33**, 1251-1260 (2012).

49. Bosman, E. A. *et al.* Multiple mutations in mouse Chd7 provide models for CHARGE syndrome. *Hum Mol Genet* **14**, 3463-3476 (2005).

50. Hurd, E. A., Poucher, H. K., Cheng, K., Raphael, Y. & Martin, D. M. The ATP-dependent chromatin remodeling enzyme CHD7 regulates pro-neural gene expression and neurogenesis in the inner ear. *Development* **137**, 3139-3150 (2010).

51. Hurd, E. A. *et al.* Mature middle and inner ears express Chd7 and exhibit distinctive pathologies in a mouse model of CHARGE syndrome. *Hear Res* (2011).

52. Micucci, J. A. *et al.* CHD7 and retinoic acid signaling cooperate to regulate neural stem cell and inner ear development in mouse models of CHARGE syndrome. *Hum Mol Genet* **23**, 434-448 (2014).

53. Bergman, J. E., Bosman, E. A., van Ravenswaaij-Arts, C. M. & Steel, K. P. Study of smell and reproductive organs in a mouse model for CHARGE syndrome. *Eur J Hum Genet* **18**, 171-177 (2010).

54. Asad, Z. *et al.* Rescue of neural crest-derived phenotypes in a zebrafish CHARGE model by Sox10 downregulation. *Hum Mol Genet* **25**, 3539-3554 (2016).

55. Patten, S. A. *et al.* Role of Chd7 in zebrafish: a model for CHARGE syndrome. *PLoS One* **7**, e31650 (2012).

56. Bajpai, R. *et al.* CHD7 cooperates with PBAF to control multipotent neural crest formation. *Nature* **463**, 958-962 (2010).

57. Schulz, Y. *et al.* CHD7, the gene mutated in CHARGE syndrome, regulates genes involved in neural crest cell guidance. *Hum Genet* **133**, 997-1009 (2014).

58. Gong, S. G. Cranial neural crest: migratory cell behavior and regulatory networks. *Exp Cell Res* **325**, 90-95 (2014).

59. Walker, M. B. & Trainor, P. A. Craniofacial malformations: intrinsic vs extrinsic neural crest cell defects in Treacher Collins and 22q11 deletion syndromes. *Clin Genet* **69**, 471-479 (2006).

60. Ho, L. & Crabtree, G. R. Chromatin remodelling during development. *Nature* **463**, 474-484 (2010).

61. Hota, S. K. & Bruneau, B. G. ATP-dependent chromatin remodeling during mammalian development. *Development* **143**, 2882-2897 (2016).

62. Zhou, V. W., Goren, A. & Bernstein, B. E. Charting histone modifications and the functional organization of mammalian genomes. *Nat Rev Genet* **12**, 7-18 (2011).

63. Eslami-Mossallam, B., Schiessel, H. & van Noort, J. Nucleosome dynamics: Sequence matters. *Adv Colloid Interface Sci* **232**, 101-113 (2016).

64. Radman-Livaja, M. & Rando, O. J. Nucleosome positioning: how is it established, and why does it matter? *Dev Biol* **339**, 258-266 (2010).

65. Bowman, G. D. Mechanisms of ATP-dependent nucleosome sliding. *Curr Opin Struct Biol* **20**, 73-81 (2010).

66. Hall, J. A. & Georgel, P. T. CHD proteins: a diverse family with strong ties. *Biochem Cell Biol* **85**, 463-476 (2007).

67. Marfella, C. G. & Imbalzano, A. N. The Chd family of chromatin remodelers. *Mutat Res* **618**, 30-40 (2007).

68. Boyer, L. A., Latek, R. R. & Peterson, C. L. The SANT domain: a unique histone-tail-binding module? *Nat Rev Mol Cell Biol* **5**, 158-163 (2004).

69. Layman, W. S., Hurd, E. A. & Martin, D. M. Chromodomain proteins in development: lessons from CHARGE syndrome. *Clinical genetics* **78**, 11-20 (2010).

70. Allen, M. D., Religa, T. L., Freund, S. M. & Bycroft, M. Solution structure of the BRK domains from CHD7. *J Mol Biol* **371**, 1135-1140 (2007).

71. Bouazoune, K. & Kingston, R. E. Chromatin remodeling by the CHD7 protein is impaired by mutations that cause human developmental disorders. *Proceedings of the National Academy of Sciences of the United States of America* **109**, 19238-19243 (2012).

72. Manning, B. J. & Yusufzai, T. The ATP-dependent chromatin remodeling enzymes CHD6, CHD7, and CHD8 exhibit distinct nucleosome binding and remodeling activities. *J Biol Chem* **292**, 11927-11936 (2017).

73. Srinivasan, S., Dorighi, K. M. & Tamkun, J. W. Drosophila Kismet regulates histone H3 lysine 27 methylation and early elongation by RNA polymerase II. *PLoS genetics* **4**, e1000217 (2008).

74. Melicharek, D. J., Ramirez, L. C., Singh, S., Thompson, R. & Marenda, D. R. Kismet/CHD7 regulates axon morphology, memory and locomotion in a Drosophila model of CHARGE syndrome. *Hum Mol Genet* **19**, 4253-4264 (2010).

75. Ghosh, R. *et al.* Kismet positively regulates glutamate receptor localization and synaptic transmission at the Drosophila neuromuscular junction. *PLoS One* **9**, e113494 (2014).

76. Schnetz, M. P. *et al.* Genomic distribution of CHD7 on chromatin tracks H3K4 methylation patterns. *Genome Res* **19**, 590-601 (2009).

77. Schnetz, M. P. *et al.* CHD7 targets active gene enhancer elements to modulate ES cell-specific gene expression. *PLoS Genet* **6**, e1001023 (2010).

78. Zentner, G. E. *et al.* CHD7 functions in the nucleolus as a positive regulator of ribosomal RNA biogenesis. *Hum Mol Genet* **19**, 3491-3501 (2010).

79. Engelen, E. *et al.* Sox2 cooperates with Chd7 to regulate genes that are mutated in human syndromes. *Nat Genet* **43**, 607-611 (2011).

80. Holmqvist, P. H. & Mannervik, M. Genomic occupancy of the transcriptional co-activators p300 and CBP. *Transcription* **4**, 18-23 (2013).

81. Milani, D. *et al.* Rubinstein-Taybi syndrome: clinical features, genetic basis, diagnosis, and management. *Ital J Pediatr* **41**, 4 (2015).

82. Batsukh, T. *et al.* CHD8 interacts with CHD7, a protein which is mutated in CHARGE syndrome. *Hum Mol Genet* **19**, 2858-2866 (2010).

83. Durak, O. *et al.* Chd8 mediates cortical neurogenesis via transcriptional regulation of cell cycle and Wnt signaling. *Nat Neurosci* **19**, 1477-1488 (2016).

84. Wang, P. *et al.* CRISPR/Cas9-mediated heterozygous knockout of the autism gene CHD8 and characterization of its transcriptional networks in cerebral organoids derived from iPS cells. *Mol Autism* **8**, 11 (2017).

85. Tsurusaki, Y. *et al.* De novo SOX11 mutations cause Coffin-Siris syndrome. *Nature communications* **5**, 4011 (2014).

86. Coffin, G. S. & Siris, E. Mental retardation with absent fifth fingernail and terminal phalanx. *Am J Dis Child* **119**, 433-439 (1970).

87. Fleck, B. J., Pandya, A., Vanner, L., Kerkering, K. & Bodurtha, J. Coffin-Siris syndrome: review and presentation of new cases from a questionnaire study. *Am J Med Genet* **99**, 1-7 (2001).

88. Haspeslagh, M., Fryns, J. P. & van den Berghe, H. The Coffin-Siris syndrome: report of a family and further delineation. *Clin Genet* **26**, 374-378 (1984).

89. Hoyer, J. *et al.* Haploinsufficiency of ARID1B, a member of the SWI/SNF-a chromatin-remodeling complex, is a frequent cause of intellectual disability. *Am J Hum Genet* **90**, 565-572 (2012).

90. Santen, G. W. *et al.* Mutations in SWI/SNF chromatin remodeling complex gene ARID1B cause Coffin-Siris syndrome. *Nat Genet* **44**, 379-380 (2012).

91. Tsurusaki, Y. *et al.* Mutations affecting components of the SWI/SNF complex cause Coffin-Siris syndrome. *Nat Genet* **44**, 376-378 (2012).

92. Kellermayer, R. *et al.* Upper gastrointestinal malformations in Coffin-Siris syndrome. *Am J Med Genet A* **143A**, 1519-1521 (2007).

93. Kleefstra, T. *et al.* Disruption of an EHMT1-associated chromatin-modification module causes intellectual disability. *Am J Hum Genet* **91**, 73-82 (2012).

94. Wieczorek, D. *et al.* A comprehensive molecular study on Coffin-Siris and Nicolaides-Baraitser syndromes identifies a broad molecular and clinical spectrum converging on altered chromatin remodeling. *Hum Mol Genet* **22**, 5121-5135 (2013).

95. Prior, H. M. & Walter, M. A. SOX genes: architects of development. *Mol Med* **2**, 405-412 (1996).

96. Dy, P. *et al.* The three SoxC proteins--Sox4, Sox11 and Sox12--exhibit overlapping expression patterns and molecular properties. *Nucleic Acids Res* **36**, 3101-3117 (2008).

97. Wiebe, M. S., Nowling, T. K. & Rizzino, A. Identification of novel domains within Sox-2 and Sox-11 involved in autoinhibition of DNA binding and partnership specificity. *J Biol Chem* **278**, 17901-17911 (2003).

98. Hur, E. H. *et al.* Functional identification of the pro-apoptotic effector domain in human Sox4. *Biochem Biophys Res Commun* **325**, 59-67 (2004).

99. Tanaka, S. *et al.* Interplay of SOX and POU factors in regulation of the Nestin gene in neural primordial cells. *Mol Cell Biol* **24**, 8834-8846 (2004).

100. Wang, Y., Lin, L., Lai, H., Parada, L. F. & Lei, L. Transcription factor Sox11 is essential for both embryonic and adult neurogenesis. *Dev Dyn* **242**, 638-653 (2013).

101. Sock, E. *et al.* Gene targeting reveals a widespread role for the high-mobility-group transcription factor Sox11 in tissue remodeling. *Mol Cell Biol* **24**, 6635-6644 (2004).

102. Gnedeva, K. & Hudspeth, A. J. SoxC transcription factors are essential for the development of the inner ear. *Proc Natl Acad Sci U S A* **112**, 14066-14071 (2015).

103. Feng, W. *et al.* The chromatin remodeler CHD7 regulates adult neurogenesis via activation of SoxC transcription factors. *Cell Stem Cell* **13**, 62-72 (2013).

104. Sinkkonen, S. T. *et al.* Serial analysis of gene expression in the chicken otocyst. *J Assoc Res Otolaryngol* **12**, 697-710 (2011).

105. Alsina, B. & Whitfield, T. T. Sculpting the labyrinth: Morphogenesis of the developing inner ear. *Semin Cell Dev Biol* **65**, 47-59 (2017).

106. Fekete, D. M. Cell fate specification in the inner ear. *Curr Opin Neurobiol* **6**, 533-541 (1996).

107. Fekete, D. M., Homburger, S. A., Waring, M. T., Riedl, A. E. & Garcia, L. F. Involvement of programmed cell death in morphogenesis of the vertebrate inner ear. *Development* **124**, 2451-2461 (1997).

108. Fekete, D. M. & Wu, D. K. Revisiting cell fate specification in the inner ear. *Curr Opin Neurobiol* **12**, 35-42 (2002).

109. Sanlaville, D. *et al.* Phenotypic spectrum of CHARGE syndrome in fetuses with CHD7 truncating mutations correlates with expression during human development. *J Med Genet* **43**, 211-217 (2006).

110. Adams, M. E. *et al.* Defects in vestibular sensory epithelia and innervation in mice with loss of Chd7 function: implications for human CHARGE syndrome. *J Comp Neurol* **504**, 519-532 (2007).

111. Hurd, E. A. *et al.* Mature middle and inner ears express Chd7 and exhibit distinctive pathologies in a mouse model of CHARGE syndrome. *Hear Res* **282**, 184-195 (2011).

112. Hurd, E. A., Micucci, J. A., Reamer, E. N. & Martin, D. M. Delayed fusion and altered gene expression contribute to semicircular canal defects in Chd7 deficient mice. *Mech Dev* **129**, 308-323 (2012).

113. Feng, W. *et al.* Chd7 is indispensable for mammalian brain development through activation of a neuronal differentiation programme. *Nat Commun* **8**, 14758 (2017).

114. Whittaker, D. E. *et al.* The chromatin remodeling factor CHD7 controls cerebellar development by regulating reelin expression. *J Clin Invest* **127**, 874-887 (2017).

115. Chang, W., Brigande, J. V., Fekete, D. M. & Wu, D. K. The development of semicircular canals in the inner ear: role of FGFs in sensory cristae. *Development* **131**, 4201-4211 (2004).

116. Chang, W., ten Dijke, P. & Wu, D. K. BMP pathways are involved in otic capsule formation and epithelial-mesenchymal signaling in the developing chicken inner ear. *Dev Biol* **251**, 380-394 (2002).

117. Omata, Y. *et al.* Role of Bone morphogenetic protein 4 in zebrafish semicircular canal development. *Dev Growth Differ* **49**, 711-719 (2007).

118. Groves, A. K. & Fekete, D. M. Shaping sound in space: the regulation of inner ear patterning. *Development* **139**, 245-257 (2012).

119. Kantarci, H., Gerberding, A. & Riley, B. B. Spemann organizer gene Goosecoid promotes delamination of neuroblasts from the otic vesicle. *Proc Natl Acad Sci U S A* **113**, E6840-E6848 (2016).

Chapter II: The chromatin remodeling protein CHD7, mutated in CHARGE syndrome, is necessary for proper craniofacial and tracheal development[1]

Abstract

Heterozygous mutations in the chromatin remodeling gene *CHD7* cause CHARGE syndrome, a developmental disorder with variable craniofacial dysmorphisms and respiratory difficulties. The molecular etiologies of these malformations are not well understood. Homozygous *Chd7* null mice die by E11, whereas $Chd7^{Gt/+}$ heterozygous null mice are a viable and excellent model of CHARGE. We explored skeletal phenotypes in $Chd7^{Gt/+}$ and *Chd7* conditional knockout mice, using *Foxg1-Cre* to delete *Chd7* (*Foxg1*-CKO) in the developing eye, ear, nose, pharyngeal pouch, forebrain, and gut and *Wnt1-Cre* (*Wnt1*-CKO) to delete *Chd7* in migrating neural crest cells. *Foxg1*-CKO mice exhibited postnatal respiratory distress and death, dysplasia of the eye, concha, and frontal bone, hypoplastic maxillary shelves and nasal epithelia, and reduced tracheal rings. *Wnt1*-CKO mice exhibited frontal and occipital bone dysplasia, hypoplasia of the maxillary shelves and mandible, and cleft palate. In contrast, heterozygous $Chd7^{Gt/+}$ mice had apparently normal skeletal development. Conditional deletion of *Chd7* in ectodermal and endodermal derivatives (*Foxg1-Cre*) or migrating neural crest cells (*Wnt1-Cre*) results in varied and more severe craniofacial defects than in $Chd7^{Gt/+}$ mice. These studies indicate that CHD7 has an important, dosage-dependent role in development of several different craniofacial tissues.

Introduction

Heterozygous mutations in the gene encoding CHD7, a chromatin remodeling protein, are found in the majority of individuals diagnosed with CHARGE syndrome, a multiple anomaly disorder defined by ocular coloboma, heart defects, atresia of the choanae, retarded growth and development, genital and/or urinary abnormalities, and ear abnormalities[1,2]. Craniofacial dysmorphisms are common in CHARGE syndrome, and include square-shaped facies, facial asymmetry, external ear anomalies, cleft lip and/or palate, cranial nerve palsies, and torticollis[3,4]. In addition, less penetrant phenotypes are associated with CHARGE and include vertebral and limb anomalies, renal anomalies, and tracheal hypoplasia or tracheo-esophageal fistula[2,4,5].

Understanding the role of CHD7 during organogenesis is critical for the development of effective therapies. We have generated mouse models of CHARGE syndrome to examine molecular mechanisms of *Chd7* deficiency, including *Chd7* loss of function ($Chd7^{Gt}$) and *Chd7* conditional deletion ($Chd7^{flox}$) alleles[6,7]. Previous studies indicate that heterozygous *Chd7* mutant mice exhibit many phenotypes similar to human CHARGE, including vestibular disorders, deafness, reduced growth, pubertal delay, olfactory dysfunction, and brain abnormalities[6-14]. Despite the myriad of skeletal abnormalities reported in humans with CHARGE[15,16], there is no information about skeletal features of *Chd7* mutant mice. Because homozygous $Chd7^{Gt/Gt}$ mice do not survive beyond E11[6,13], we chose to focus on $Chd7^{Gt/+}$ and *Chd7* conditional knockout mice using *Foxg1-Cre* [17] and *Wnt1-Cre*[18] mice. The complementary expression profiles of these two different mouse lines in neural crest (*Wnt1-Cre*) and various ectodermal/endodermal derivatives (*Foxg1-Cre*) provided an opportunity to delineate the effects of loss of *Chd7* in development of various craniofacial structures.

Results

Chd7 deficient mice have craniofacial defects

The developmental origins of CHARGE-related birth defects are not fully understood. Neural crest-derived tissues are commonly affected by CHD7 deficiency[19], yet ectodermal structures including the brain are also affected[5,14]. In order to explore the relative contributions of CHD7 in these tissue derivatives to organ development, we generated mice with loss of *Chd7* using *Foxg1-Cre*, which is expressed by E7.5 in the pharyngeal arches, facial and head ectoderm, otic, optic, nasal and oral epithelium, pharyngeal arches, forebrain, and foregut[17]. We also generated mice with *Chd7* deletion using *Wnt1-Cre*, which is expressed by E8.5 in developing pharyngeal arches, head mesenchyme, inner ear, neural crest, midbrain, spinal cord and nasal neural crest and mesenchyme [18]. Mice with deletion of both *Chd7* alleles by *Foxg1-Cre* or *Wnt1-Cre* are hereafter referred to as *Foxg1*-CKO or *Wnt1*-CKO, respectively.

While $Chd7^{Gt/+}$ mice survive to adulthood[6,13], both *Foxg1*-CKO and *Wnt1*-CKO mice die shortly after birth, likely from respiratory failure (neither *Foxg1*-CKO nor *Wnt1*-CKO pups had milk in their stomachs). We therefore focused our phenotypic analysis of craniofacial and other tissues on postnatal day 1 pups. *Chd7* wild type, $Chd7^{flox/+}$, and $Chd7^{Gt/+}$ mice had no apparent abnormalities of the skull or craniofacial regions (Figure 2.1A-B). In contrast, *Foxg1*-CKO mice had severely hypoplastic eyes (*N*=7/7 mice) and shortened faces (Figure 2.1C) and *Wnt1*-CKO mice had shortened snouts (Figure 2.1D). We performed comprehensive measurements of craniofacial distances on skeletal preparations of postnatal day 1 mice (Figures 2.1E-H, Figure 2.2 and Table 2.1). We observed no differences in the degree of ossification in the skulls or in craniofacial measurements (occipital bone, intersquamosal, interocular, mandible, or rostral-caudal

lengths) between *Chd7*$^{Gt/+}$ mice and wild type or *Chd7*$^{flox/+}$ littermate controls (Table 2.1), suggesting that loss of one *Chd7* allele does not cause major or highly penetrant skeletal defects in mice. We did note mild hypoplasia of the ethmoid bone of *Chd7*$^{Gt/+}$ mice relative to controls (Figure 2.1F).

In contrast, we observed significant frontal bone dysplasia (either reduced ossification or hypoplasia) in both *Foxg1*-CKO (N=7, p<0.05) and *Wnt1*-CKO (N=7, p<0.05) mice compared with littermate controls (Figure 2.1 E-H and Figure 2.2 A-D). Interestingly, there was no dysplasia of the atlas (C1), axis (C2) or parietal/interparietal bones, or change in rostral-caudal lengths of *Chd7*$^{Gt/+}$, *Foxg1*-CKO or *Wnt1*-CKO mice compared to controls. Some mice had dysplastic ribs, but this was infrequent, also occurred in controls, and did not correlate with changes in rib number or vary significantly across genotypes. Clavicles were also normal in mice of all genotypes. Notably, the ethmoid bones were hypoplastic in both *Foxg1*-CKO and *Wnt1*-CKO mice, and the occipital region appeared dysplastic in *Wnt1*-CKO mice (Figure 2.1 G, H). *Foxg1*-CKO mice exhibited significantly shortened interocular distances (mean= 3.72 vs. 4.66 mm, N=7, p<0.05) and intersquamosal distances (mean= 5.90 vs. 6.58 mm, N=7, p<0.05) compared to controls (Figure 2.2C vs. A and Table 2.1), whereas *Wnt1*-CKO mice exhibited normal interocular or intersquamosal distances, occipital bone dysplasia and reduced mandibular length (mean=4.95 vs. 5.55 mm, N=7, p<0.05) (Figure 2.2D vs. A and Table 2.1). Intersquamosal and interocular distances were similar in *Chd7*$^{Gt/+}$ mice (Figure 2.2B) and controls (Figure 2.2A). Thus, whereas *Chd7*$^{Gt/+}$ mice appear normal, both *Foxg1*-CKO and *Wnt1*-CKO mice displayed severe but distinct craniofacial anomalies, suggesting that proper *Chd7*

expression within the facial ectoderm (*Foxg1*) and neural crest (*Wnt1*) is required to ensure normal craniofacial development.

Cre transgene and Chd7 expression in developing retina correlate with ocular defects

Chd7 is expressed in mouse embryonic stem cells[20] and broadly in early (E7.5-E8.5) developing mouse embryos[21], then by mid-gestation (E12.5) becomes restricted to specific organs and tissues such as the brain, pituitary, ear, heart, and craniofacial structures[6]. To characterize *Chd7* expression relative to *Foxg1-Cre* and *Wnt1-Cre* transgene expression, we performed immunofluorescence for CHD7 on E11.5 transgenic embryos that also contained *ZsGreen* reporter[22] alleles (Figure 2.1 I-L). CHD7 was present in the retinae of both *Foxg1-Cre;ZsGreen+* and *Wnt1-Cre;ZsGreen+* E11.5 embryos. Consistent with published results, *Foxg1-Cre*, but not *Wnt1-Cre* expression was observed in the E11.5 mouse retina (Figure 2.1 J vs L)[17,18]. Thus, deletion of *Chd7* in *Foxg1*-CKO retina (with resultant hypoplastic eyes) and preservation of *Chd7* (with normal eyes) in *Wnt1*-CKO mice is expected given these expression patterns.

Foxg1-CKO mice have upper and lower airway abnormalities including conchae dysplasia and hypoplastic nasal epithelia.

Individuals with CHARGE syndrome have highly penetrant respiratory and olfactory deficits, including choanal atresia, tracheoesophageal fistula, and hyposmia or anosmia[4,11,23]. *Chd7* mutant mice are known to have severely reduced olfactory abilities and olfactory bulb hypoplasia, as well as choanal defects[12,13,24], but to date there is no detailed information about upper and lower airway structures. We asked whether *Chd7*

heterozygous and conditional mutant mice also exhibit airway dysplasia by analyzing the structure of the oral/nasal cavity in skeletal preparations of postnatal day 1 pups. The majority of *Chd7*$^{Gt/+}$ mice (*N*=4/6) and all *Foxg1*-CKO (*N*=7/7) and *Wnt1*-CKO (*N*=7/7) mice displayed ventral conchae dysplasia (Figure 2.2 and Table 2.1). Similarly, the majority of *Chd7*$^{Gt/+}$ mice (*N*=5/6) and all *Foxg1*-CKO (*N*=7/7) and *Wnt1*-CKO (*N*=7/7) pups displayed dorsal conchae dysplasia (Figure 2.2 and Table 2.1). Analysis of histologically stained sections revealed normal nasal epithelial tissues in *Chd7*$^{Gt/+}$ and *Wnt1*-CKO mice, despite hypoplasia of the dorsal and ventral conchae in the latter (Figure 2.3B and 2.3C). In contrast, the nasal epithelium in *Foxg1*-CKO mice was severely disorganized and hypoplastic (Figure 2.3D). Comparison of X-gal staining in *Chd7*$^{Gt/+}$ and *Foxg1*-CKO mice (both of which contain the *Chd7*^{Gt} allele that expresses β-galactosidase under the control of the *Chd7* promoter[6]) showed that *Chd7* promoter activity is preserved in the nasal epithelium of both mutants, and that unlike *Chd7*$^{Gt/+}$ mice which exhibit normal nasal epithelia, the *Foxg1*-CKO nasal epithelium is severely disrupted (Figure 2.3E vs. 2.3F). Together, these data suggest that dysplasia of the nasal epithelium in mice with reduced *Chd7* may result primarily from disruption of normal *Chd7* expression in the ectoderm rather than a secondary defect in neural crest cell migration.

Foxg1-CKO and Wnt1-CKO mice have palatal defects

Clefting of the lip and/or palate is reported in 33-48% of individuals with CHARGE syndrome[4,23]. In addition, approximately one-third of *Chd7*$^{whi/+}$ heterozygous mutant mice have cleft palates[13]. By gross morphological analysis, we found no hard or soft palatal defects in postnatal day 1 *Chd7*$^{Gt/+}$pups (Figure 2.2F and 2.3B). *Foxg1*-CKO mice exhibit

mild palatal shelf hypoplasia (*N*=7/7); however, do not exhibit cleft palates (*N*=0/7; Table 2.1, Figure 2.2G and 2.3D). By contrast, all *Wnt1*-CKO mice (*N*=7) exhibited severe palatal shelf hypoplasia and some (*N*=3/7) *Wnt1*-CKO mice displayed complete clefting of the palate resulting in an open oral/nasal pharynx (Figure 2.2D, 2.3C and Table 2.1). X-gal stained sections from *Chd7*$^{Gt/+}$ and *Foxg1*-CKO mice, showed β-galactosidase activity (*Chd7* promoter activity) in epithelial cells lining the palatal shelves (Figure 2.3E, F). Together, these data provide evidence that *Chd7* is highly expressed in the nasal/oral epithelium and may contribute to disrupted palatal formation.

Absence of long bone, vertebral, clavicular, and pelvic defects in Chd7 mutant mice

It has been proposed that CHARGE may be considered a skeletal dysplasia, with clinical reports of limb anomalies[15,25], vertebral defects, and basiooccipital abnormalities[26]. We identified no visible skeletal defects in postnatal day 1 control, *Foxg1-Cre* conditional heterozygous (*Foxg1-Cre;Chd7*$^{+/flox}$), or *Wnt1-Cre* conditional heterozygous (*Wnt1-Cre;Chd7*$^{+/flox}$) mice. Likewise, lengths of bones in the upper extremity (humerus, ulna, or radius), pelvis (intercrest, interspinous, or crest-symphysis) and lower extremity (femur, tibia, or fibula) were similar in control, *Chd7* heterozygous null (*Chd7*$^{Gt/flox}$), *Foxg1*-CKO and *Wnt1*-CKO mice (data not shown). Bones from the right and left sides of the body of all mice were also similar across all genotypes, suggesting that loss of *Chd7* does not affect axial symmetry. We observed no vertebral anomalies suggestive of spinal curvature (data not shown). Analysis of the cervical spine, thoracic spine (rib count or dysplasia) and clavicle revealed no apparent differences between *Chd7*$^{Gt/+}$, *Foxg1*-CKO, *Wnt1*-CKO, and littermate control mice (Table 2.1). Thus, at the level of resolution possible by analysis of

skeletal postnatal day 1 preparations, we found no defects in the long bones, vertebrae, clavicles, or pelvis of *Chd7* mutant mice.

Normal development of neural crest derived cardiac structures in Wnt1-Cre conditional mutant mice

Cardiac defects including abnormal development and septation of the conotruncus and the development of the great vessels, are present in 75-77% of individuals with CHARGE syndrome[2,4,23]. In mice, some *Chd7*$^{Whi/+}$ embryos (heterozygous for a *Chd7* null allele) have been reported to have interventricular septal defects, body edema and cardiac insufficiency[13]. In *Wnt1-Cre* mice, *Cre*-positive neural crest cells (NCCs) migrate to the conotruncus or early cardiac outflow tract, where they participate in septation of this tract into the pulmonary and aortic outflow tracts[27]. Additionally, NCCs migrate from the posterior hindbrain into the third, fourth and sixth pharyngeal arches where they participate in the asymmetric remodeling of the pharyngeal arch arteries (PAA) into the great vessels[28]. We therefore asked whether *Wnt1*-CKO mutant mice also exhibit heart defects similar to or more severe than those previously reported. In order to demonstrate whether NCC-mediated conotruncal development is impacted by *Chd7* deletion, we assessed cardiac outflow tract development in *Wnt1*-CKO embryos. At E16.5, a time point at which cardiac outflow tract septation is complete, we observed grossly normal aortic and pulmonary septation as well as normal formation of the major branches off the aorta (*N*=4 Conditional Heterozygous (CHet) (Figure 2.4A), *N*=5 *Wnt1*-CKO (Figure 2.4B)). Histologic analysis with H&E staining of E16.5 *Wnt1*-CHet (*N*=7; Figure 2.4C) and *Wnt1*-CKO (*N*=6; Figure 2.4D) hearts confirmed normal aorto-pulmonary and right-left outflow

tract septation. To determine whether neural crest-mediated PAA formation was impacted by *Chd7* deletion, we assessed PAA formation at E10.5 by India ink injection in *Wnt1*-Conditional heterozygous (Figure 2.4E) and *Wnt1*-CKO (Figure 2.4F) mice. Third, fourth, and sixth PAA formation in *Wnt1-Cre* expressing neural crest cells was unaffected by *Chd7* deletion (*N*=5 CHet, *N*=6 *Wnt1*-CKO). Thus, we found no evidence for cardiac abnormalities in mice with *Wnt1-Cre* mediated conditional deletion of one or both copies of CHD7.

Foxg1-Cre Chd7 conditional mutants have fewer tracheal rings

Other mediastinal abnormalities, including tracheoesophageal fistula and tracheal agenesis have also been reported at relatively high penetrance (19-29%) in CHARGE syndrome[4,23]. Tracheal cartilage was readily visible in the skeletal preparations of postnatal day 1 pups, allowing us to characterize the mice for tracheal abnormalities. Interestingly, there were, on average, 17-18 tracheal rings in control mice (*N*=16), 19 in $Chd7^{Gt/+}$ mice (*N*=6), and 19 in *Wnt1*-CKO mice (*N*=7) (Figure 2.5 and Table 2.1). In contrast, *Foxg1*-CKO mice had, on average, only 11 tracheal rings ($p<0.001$, *N*=7) (Figure 2.5 and Table 2.1). The severe reduction in tracheal rings may represent a developmental delay or arrest of tracheal development, and could contribute to their early postnatal respiratory distress and death.

We then asked whether *Chd7* and *Wnt1-Cre*/*Foxg1-Cre* transgenes are expressed in the embryonic trachea proper or in surrounding mesenchymal tissues[29]. As in Figures 2.1 and 2.3, we stained cross-sections through E11.5 *Foxg1-Cre;ZsGreen+* and *Wnt1-Cre;ZsGreen+* embryos at the level of the mediastinum for immunofluorescence with anti-

CHD7 antibody (Figure 2.5E-H). We observed abundant CHD7 staining in the presumptive esophagus and trachea, with less bright label in the surrounding mesenchyme of *Foxg1-Cre;ZsGreen+* embryos. Interestingly, *Foxg1-Cre* transgene activity was widespread in both the tracheal epithelium and surrounding mesenchymal tissues (Figure 2.5E, F) whereas *Wnt1-Cre* transgene activity was restricted to the peri-tracheal mesenchyme (Figure 2.5G, H). These data suggest that CHD7 is concentrated in the tracheal primordium, and is also expressed in adjacent mesenchyme, and that loss of CHD7 in the tracheal primordium leads to severely disrupted tracheal development.

Discussion

In this study, we present data showing that *Chd7* is required for certain aspects of murine craniofacial and mediastinal development; specifically, loss of *Chd7* disrupts formation of the orbit and multiple regions of the respiratory tract. By using mice expressing *Cre* recombinase in ectoderm- and endoderm-derived cells of the developing telencephalon and pharyngeal arches (*Foxg1-Cre*) and in migratory neural crest cells (*Wnt1-Cre*), we identified components of the upper and lower respiratory tracts that likely contribute to acute respiratory failure and perinatal death of *Chd7*-conditional mutant mice. Interestingly, *Chd7* is required for proper development of multiple components along the upper and lower respiratory tracts, including the nose, hard palate, and trachea. Complex malformations of each of these organs have been noted in humans with CHARGE syndrome, and postnatal respiratory distress is a common cause for early morbidity and mortality.

Upper and lower airway malformations with Chd7 deficiency

Nasal conchae, or turbinates, are critical for air filtration and proper formation and maintenance of the olfactory epithelium. Specifically, the conchae provide increased nasal epithelial surface area while humidifying the air, which may help protect olfactory nerve axons traveling through the cribriform plate to synapse in the olfactory bulb[30,31]. These structures develop, in part, from the ethmoid bone, a complex structure which forms the caudal nasal cavity[32]. We found that *Chd7*$^{Gt/+}$ mice exhibit mild hypoplasia of the dorsal and ventral conchae as well as the ethmoid bone, whereas conditional deletion of *Chd7* in *Foxg1-Cre*-expressing mice resulted in complete loss of the nasal choanae and ethmoid bone. Interestingly, *Wnt1*-CKO mice also exhibited nasal conchae and ethmoid dysplasia, with little disruption to the nasal passageways. Given the importance of the conchae in olfactory development, their disruption could worsen olfactory neuron dysfunction in *Chd7* mutant mice and contribute to previously reported hyposmia/anosmia phenotypes[12]. In addition to disruption of the nasal conchae, we observed marked disruption of the nasal passageways in *Foxg1*-CKO mice, reminiscent of the posterior nasal aperture blockage or choanal atresia reported in some *Chd7*$^{Whi/+}$ mice[13]. The nose, like most other craniofacial structures, is composed of facial ectoderm and migrating cranial neural crest cells, and *Chd7* may be necessary for proper integration of these cell types. Interestingly, external naris occlusion impairs nasal turbinate development in the mouse[33], evidence that development of the conchae is dependent on proper airflow. We postulate that some of the nasal abnormalities observed in *Chd7* mutant mice reflect underlying contributions of *Chd7* to development of cells derived from neural crest, ectoderm, and underlying mesenchyme.

In addition to choanal atresia, other airway abnormalities such as sinus blockage, cleft palate, and laryngomalacia, are common in CHARGE syndrome[2-4]. We observed thickening and vaulting of the palatal shelves in *Foxg1*-CKO mice and complete cleft of the palate in *Wnt1*-CKO mice. In humans, highly-arched palates indicate disruptions in maxillary shelf development, are often reported following cleft palate repair, and are commonly associated with dental crowding and speech difficulties[34-36]. The occurrence of highly-arched palates has been documented in individuals with CHARGE who have intact palates or following surgical repair of a cleft palate[37]. Both *Foxg1-Cre* and *Wnt1-Cre* are expressed in cells critical for maxillary development; indeed, deletions of other genes including *β-catenin* and *Bmpr1a* using these *Cre* recombinases results in mild and more severe maxillary malformations including complete aplasia[38,39]. Interestingly, we did not observe palatal vaulting or clefting in our $Chd7^{Gt/+}$ mice. This could be a result of low sample size or effects of genetic background. Cleft palate occurs in 25% of $Chd7^{Whi/+}$ mice[13] and 33-48% of humans with CHARGE syndrome[2,4]. Together, these results suggest that *Chd7* plays critical roles in *Wnt1-Cre* derived cranial neural crest cells that contribute to osteogenesis and to the overlying *Foxg1-Cre* derived oral epithelium, both of which are critical for proper maxillary development[40].

In addition to malformations of the upper airway, we observed hypoplasia of tracheal cartilaginous rings in *Foxg1*-CKO mice. This is consistent with high levels of *Cre* expression in the tracheal primordium of *Foxg1-Cre* mice. Tracheal cartilage is critical for maintaining patency of the trachea upon expiration[41]. Thus *Chd7* may play an intrinsic role in tracheal development, consistent with the tracheal abnormalities (malacia, dysgenesis, and agenesis) observed in individuals with CHARGE. The proximity of

foregut derivatives to the trachea and the high incidence of tracheoesophageal fistula in CHARGE suggest that CHD7 may be important for gut development[42]. Further, we observed significant, colocalized *Chd7* and *Foxg1-Cre* activity in the presumptive esophagus suggesting that development of the laryngotracheal groove is critically dependent on proper expression of *Chd7*. More detailed analysis mice will be necessary to determine the extent to which *Chd7* contributes to foregut development.

Potential dual roles for Chd7 in the eye

Development of the eye involves a dual process whereby neuroectoderm forms a proto-retinal outpouching from the rostral telencephalon[43]. Upon contact with growing retinal tissue, the overlying surface ectoderm induces optic cup formation. The lens is the principal structure derived from the overlying surface ectoderm. Recent reports suggest that spatiotemporal localization of lens and retinal tissue is driven by neural crest cells, which themselves differentiate into the sclera separating the developing lens from the retina[44]. These neural crest cells help direct the generation of the optic cup, which involves a complex folding process resulting in formation of the choroid fissure. In the mature eye, the choroidal fissure is almost completely closed, providing continuity to the inferior iris and retina. Defects in choroidal fissure closure present as colobomata.

Ocular colobomata of the retina and/or iris, are sometimes associated with microphthalmia, occur in 75-81% of individuals with CHARGE syndrome[4,23]. Previous studies of *Chd7*$^{Whi/+}$ mice showed keratoconjunctivitis sicca (dry eye)[13], but there are no reports in *Chd7* mutant mice of ocular coloboma or other major eye defects commonly seen in CHARGE syndrome. One of our most striking findings was severe hypoplasia of

the eye in *Foxg1*-CKO mice. Our immunofluorescence results from E11.5 mice also demonstrate high levels of both *Foxg1-Cre* and CHD7 in retinal tissue. Notably, in addition to the high CHD7 in retina, we detected abundant CHD7 in the developing lens. We observe no obvious defects in eye development in *Wnt1*-CKO mice, suggesting that *Chd7* may have subtle or no significant functions in neural crest cells that contribute to ocular development. Recent data from zebrafish (*D. rerio*) have implicated *chd7* in the regulation of retinal cell specification[45]; our data provide the first evidence that loss of *Chd7* within the retina contributes to ocular malformations in mammals. Future studies of *Chd7* function in the developing eye should help determine the mechanistic relationship between ocular hypoplasia and colobomata.

Lack of evidence for Chd7 function in cardiac neural crest cells

Fourth pharyngeal arch artery (PAA) hypoplasia and malformations of the transverse aorta and right subclavian artery (fourth PAA derivatives) have been reported in $Chd7^{Whi/+}$ mice[21]. Importantly, attempted rescue of these malformations using *Wnt1-Cre*, expressed in neural crest cells, and a conditional *Chd7* wild-type allele was unsuccessful, suggesting minimal contributions of *Chd7* in *Wnt1-Cre* lineages to heart formation[21]. Given these observations, we further explored the role of cardiac neural crest by examining conditional deletion of *Chd7* using *Wnt1-Cre*. Neither *Wnt1*-conditional heterozygous nor *Wnt1*-CKO mice exhibited any deformity in PAA development at E10.5 or in arterial branching at E16.5, consistent with minimal or no *Chd7* function in cardiac neural crest cells. Alternatively, *Wnt1-Cre* activity may be mosaic or inefficient in the

cardiac neural crest. Additional studies are necessary to distinguish among these possibilities.

Development of craniofacial structures requires correct spatiotemporal Chd7 expression

Our results demonstrate that proper expression of *Chd7* is necessary for development of the craniofacial structures contributing to the upper respiratory tract and the cartilaginous rings of the trachea. Two complementary themes emerge from our data: (1) *Chd7* expression is required in the surface ectoderm, endoderm, and migrating neural crest cells which all contribute to the development of facial structures and the eye and (2) *Chd7* likely has a significant role in the development of cartilage and bone. *Foxg1-Cre* is highly expressed by E7.5 in surface ectoderm and endoderm which populate the pharyngeal arch and pouch derivatives, respectively[17]. Components of the first pharyngeal arch contribute to many of the facial bones affected in *Chd7* deficient mice and humans, including the ethmoid, maxilla, and mandible[46]. Migrating neural crest cell populations expressing *Wnt1-Cre* invade pharyngeal arch structures and are critical for their proper specification. Loss of *Chd7* in the embryonic frog (*X. laevis*) has been reported to result in failed neural crest cell migration from the dorsal neural tube[19]. We found that disruptions to *Chd7* in *Wnt1-Cre* expressing neural crest cells results in developmental abnormalities in the nose and palate, but not the heart. Interestingly, we observed phenotypic differences in the nose and palate between *Foxg1-CKO* and *Wnt1-CKO* mice that may reflect differences in sites or timing of *Cre* activity. In *Foxg1-Cre* mice, *Cre* is induced around E7.5, which may affect certain populations of pre-migratory neural crest cells[47], whereas *Wnt1-Cre* is activated slightly later, at E8.5, in migratory neural crest[18]. Much remains to

be clarified regarding how CHD7 regulates proper gene expression in both the facial ectoderm and neural crest cells that contribute to craniofacial development.

Our results highlight the potential role that CHD7 has in regulating development of bone. Interestingly, a previous report suggests that CHD7 is required for inducing *Wnt5a*-dependent osteoblastogenesis in mesenchymal stem cells[48]. Indeed, these authors determined that reduction in *Chd7* mRNA levels by RNAi caused a cell fate switch leading to the accumulation of adipocytes. While this research was performed using mesoderm-derived cell populations, CHD7 may function similarly in craniofacial osteoblasts derived from cranial neural crest cells[49]. Further investigation is necessary to determine the specific function(s) of CHD7 in development of craniofacial and tracheal structures affected in CHARGE syndrome.

Experimental Procedures

Mice

Foxg1-Cre;Chd7$^{Gt/+}$ mice and *Chd7*$^{flox/flox}$ mice were generated and genotyped as previously described[6,7]. Specifically, these mice were maintained on a mixed C57BL/6;129S1/SvImJ background and inbred to N=6-8. Mice of the following genotypes were analyzed: control (*Chd7*$^{+/flox}$), *Chd7* heterozygous mutant (*Chd7*$^{Gt/flox}$ or *Chd7*$^{Gt/+}$), *Foxg1* conditional heterozygous mutant (*Foxg1-Cre;Chd7*$^{+/flox}$) and *Foxg1*conditional knockout mutant (*Foxg1-Cre;Chd7*$^{Gt/flox}$ or *Foxg1*-CKO). *Wnt1-Cre;Chd7*$^{+/flox}$ mice were crossed with *Chd7*$^{flox/flox}$ mice, and the following genotypes were analyzed: control (*Chd7*$^{+/flox}$ or *Chd7*$^{flox/flox}$), *Wnt1-Cre* conditional heterozygous mutant (*Wnt1-Cre;Chd7*$^{+/flox}$) and *Wnt1*conditional knockout mutant (*Wnt1-Cre;Chd7*$^{flox/flox}$ or *Wnt1-*

CKO). *ZsGreen Cre* reporter mice[22] (JAX#007906) were crossed with *Foxg1-Cre* or *Wnt1-Cre* mice to identify sites of *Cre* positive cells. The University of Michigan University Committee on the Use and Care of Animals (UCUCA) approved all procedures.

Skeletal Preparations

Postnatal day 1 mice were terminally anaesthetized, eviscerated, and fixed in 95% ethanol overnight and incubated in acetone for three days. Preparations were placed in dye solution (0.06 mg/ml Alizarin Red (Sigma, St. Louis, MO) and 0.18 mg/mL Alcian Blue (Sigma) in 42 mL of 72% ethanol and 3 mL of glacial acetic acid) and agitated gently on a rotary shaker for four days. Skeletons were washed in ddH_2O for two hours to rinse excess dye then placed in 1% KOH clearing solution for two days. Samples were then immersed in increasing concentrations of glycerol (1:4 glycerol / 1% KOH; 1:1 glycerol / 1% KOH; 8:2 glycerol / 1% KOH) for five to seven days per immersion. Finally, skeletal preparations were stored in 100% glycerol, photographed using a Leica DMRB microscope and measured using ImageJ (National Institutes of Health, Bethesda, MD). Images were processed using Adobe Photoshop CS6 (Adobe, San Jose, CA).

Histology and X-gal staining

Postnatal day 1 mice were collected, decapitated and heads fixed in 4% paraformaldehyde overnight at 4^{o}C. After washing in PBS, heads were incubated in 30% sucrose, embedded in OCT medium (Tissue-Tek, Torrance, CA), frozen, and sectioned at 12-15 µm. Sections were either stained with hematoxylin and eosin (H&E) (Sigma) for histological analysis, or X-gal for expression analysis as previously described[6]. Sections

were photographed by light microscopy on a Leica upright DMRB microscope and processed in Photoshop CS2 (Adobe, San Jose, CA).

Immunofluorescence and Cre lineage tracing

For *Cre* lineage tracing and anti-CHD7 immunofluorescence, E11.5 *Foxg1-Cre;ZsGreen;Chd7*$^{+/+}$ and *Wnt1-Cre;ZsGreen;Chd7*$^{+/+}$ embryos were harvested, dissected, and embedded in OCT cryosectioning media (Tissue-Tek, Torrance, CA). Embryos were cryosectioned at 14 μm, stained with 1:7500 anti-CHD7 rabbit IgG monoclonal antibody (in TSA block, #6505 Cell Signaling Technology (Danvers, MA) and counterstained with 1:200 biotinylated anti-rabbit IgG goat secondary antibody (in TSA block, BA-1000, Vector Laboratories (Burlingame, CA)). Strepavidin-HRP (1:100 in TSA block) was added to slides and Alexa 555 tyramide (1:100 in Amplification Buffer, Molecular Probes (Grand Island, NY)) was applied to generate fluorescence. DAPI (5 μg/mL) was added and slides mounted for imaging using a Leica DMRB microscope. Final image processing was performed using Adobe Photoshop CS6 (Adobe, San Jose, CA).

Cardiac Evaluation

For gross inspection, E16.5 embryos were harvested and dissected. For the hematoxylin/eosin stained sections, embryos were fixed in 4% paraformaldehyde for 12–18 hours at 4°C, dehydrated and embedded in Leica Histowax according to standard procedures. After embedding, sections were cut at 5–7 μm. Images were analyzed by brightfield microscopy. For India ink injections, E10.5 embryos were dissected and placed in ice cold PBS. Using a pulled glass pipette, India ink was injected into the ventricles

until the ink penetrated the small vessels. Embryos were post-fixed in 10% buffered formalin for 12 hours, dehydrated and cleared in benzylbenzoate: benzyl alcohol (2:1v/v).

Statistical analysis

Measurements of anatomical regions were performed on control (*N*=16), *Chd7* heterozygous mutant (*N*=6), *Foxg1* conditional heterozygous mutant (*N*=7), *Wnt1* conditional heterozygous mutant (*N*=2), *Foxg1* conditional knockout mutant (*N*=7) and *Wnt1* conditional knockout mutant (*N*=7) mice using stereoscope-standardized pictures analyzed with ImageJ (National Institutes of Health, Bethesda, MD). Discrete observations (i.e. presence or absence of dysplasia) were scored in a binomial fashion. Bone lengths were measured using ImageJ (National Institutes of Health, Bethesda, MD). All measurements were analyzed in SPSS (v.19.0) by MANOVA with a *post hoc* Tukey's honest significant difference (HSD) test; significance was limited to $p \leq 0.05$.

Acknowledgements

We thank John L. Zeller, M.D., Ph.D. (Division of Anatomical Sciences, University of Michigan) for assistance with interpretation of skeletal anatomy. This work was supported by the CHARGE Syndrome Foundation (EAH and ABS), Elizabeth E. Kennedy Research Award (EAH), Hearing Health Foundation (EAH), and NIH grants 5T32GM007863-33 (EDS), 5T35GL007690-30 (ENR), and R01-DC009410 (DMM).

Chapter II Note

[1]A revised version of Chapter II has been published as: Sperry, E. D., Hurd, E. A., Durham, M. A., Reamer, E. N., Stein, A. B., and Martin, D. M. The chromatin remodeling protein

CHD7, mutated in CHARGE syndrome, is necessary for proper craniofacial and tracheal development. *Developmental Dynamics* **243**:1055-1066 (2014).

Region	Feature	*Foxg1-Cre* Genotype			*Wnt1-Cre* Genotype	
		Chd7$^{+/flox}$ (*N*=9)	*Chd7*$^{Gt/flox}$ (*N*=6)	CKO (*N*=7)	Control (*N*=6)	CKO (*N*=7)
Cranium	Interocular distance	4.66	4.34	3.72 *	5.12	5.01
	Frontal bone dysplasia†	3	4	7 *	0	6 *
	Eye dysplasia†	0	0	7 *	0	0
	Intersquamosal distance	6.58	6.38	5.90 *	6.23	6.24
	Parietal/interparietal bone dysplasia†	0	0	0	0	0
	Occipital bone length	3.92	4.10	3.86	3.58	3.47
	Occipital bone dysplasia†	0	0	0	1	7 *
	Rostral-caudal length	9.54	9.27	8.99	9.75	9.46
	Ventral conchae dysplasia†	0	4 *	7 *	1	7 *
	Dorsal conchae dysplasia†	0	5 *	7 *	1	7 *
	Palatal shelf dysplasia†	0	0	7*	1	7 *
	Cleft palate†	0	0	0	0	3 *
	Mandible length	5.29	5.28	5.05	5.55	4.95 *
Cervical spine	Atlas (C1) dysplasia†	0	0	0	0	0
	Axis (C2) dysplasia†	0	0	0	0	2
Thoracic spine	Rib count	13.0	13.0	12.9	12.9	12.9
	Rib dysplasia (bifid)†	1	3	1	2	4
Thorax	Clavicle length	2.49	2.49	2.48	2.60	2.56
	Tracheal ring count	17.8	19.3	11.0 *	16.7	18.9

Table 2.1. Foxg1-Cre or Wnt1-Cre conditional loss of Chd7 in mice results in multiple skeletal abnormalities.
All measurements are in millimeters.
†These observations were scored in a binomial fashion (e.g. dysplasia of the frontal bone was identified as "present" or "absent"). As such, the number of mice affected is scored across each genotype for each observation.
*Significance indicated at $p < 0.05$ relative to *Chd7*$^{+/flox}$ (for *Foxg1-Cre*) or control (*Chd7*$^{+/flox}$ or *Chd7*$^{flox/flox}$ for *Wnt1-Cre*) by MANOVA with *post hoc* Tukey's HSD test.

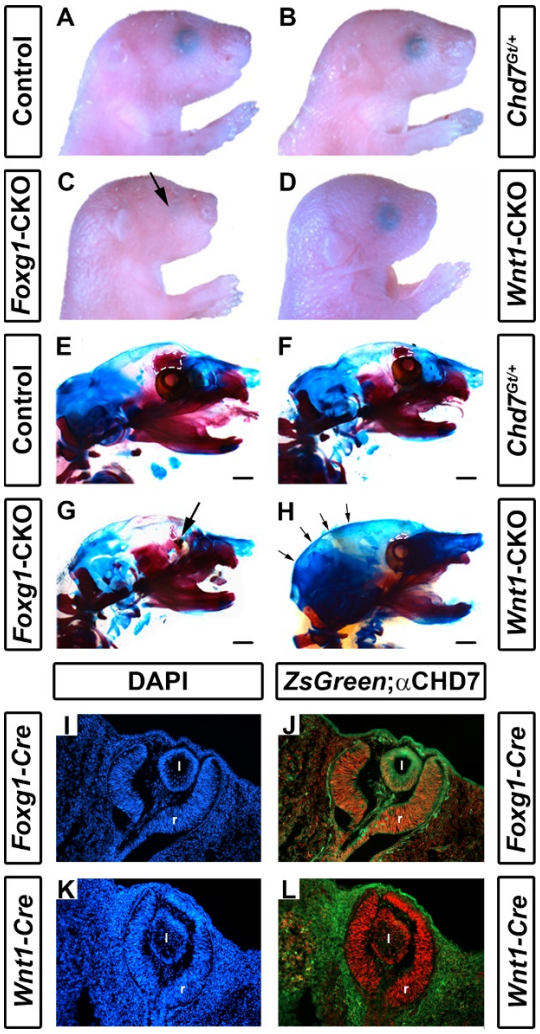


Figure 2.1. Conditional deletion of Chd7 results in ocular hypoplasia and cranial bone dysplasia. Brightfield images (A-D) and skeletal preparations (E-H) of postnatal day 1 control (*Cre*-negative, $Chd7^{+/f}$ or $Chd7^{f/f}$) (A,E), $Chd7^{Gt/+}$ (B,F), *Foxg1*-CKO (C,G) and *Wnt1*-CKO (D,H) pups. $Chd7^{Gt/+}$ mice appear similar to controls, whereas both *Foxg1*-CKO (C) and *Wnt1*-CKO (D) mice have shortened snouts, and *Foxg1*-CKO mice have ocular hypoplasia (arrows in C and G). There are no abnormalities in ossification, overall morphology or size of major craniofacial bones in $Chd7^{Gt/+}$ mice (B, F). In E-H, alizarin red and alcian blue staining reveal bone and cartilage, respectively. Ethmoid bones are hypoplastic in $Chd7^{Gt/+}$ (F), *Foxg1*-CKO (G) and *Wnt1*-CKO (H) mice (white dashed lines in E-H). *Wnt1*-CKO mice (H) have a more rounded posterior cranium (indicated by arrows) than mice of other genotypes. *Cre* expression in *Foxg1-Cre* and *Wnt1-Cre* mice was detected using ZsGreen reporter mice and compared to CHD7 protein levels in the developing eye (I-L). Shown are transverse sections of *Cre;ZsGreen* positive E11.5 embryos stained with DAPI (labels cellular nuclei) or anti-CHD7 (red). *Foxg1-Cre* is active in CHD7-positive cells in the retina (r) and posterior lens (l) of the developing eye (J), whereas *Wnt1-Cre* is restricted to the surrounding periocular mesenchyme and is absent in the retina and lens proper (L). Scale bars in E-H are 1 mm.

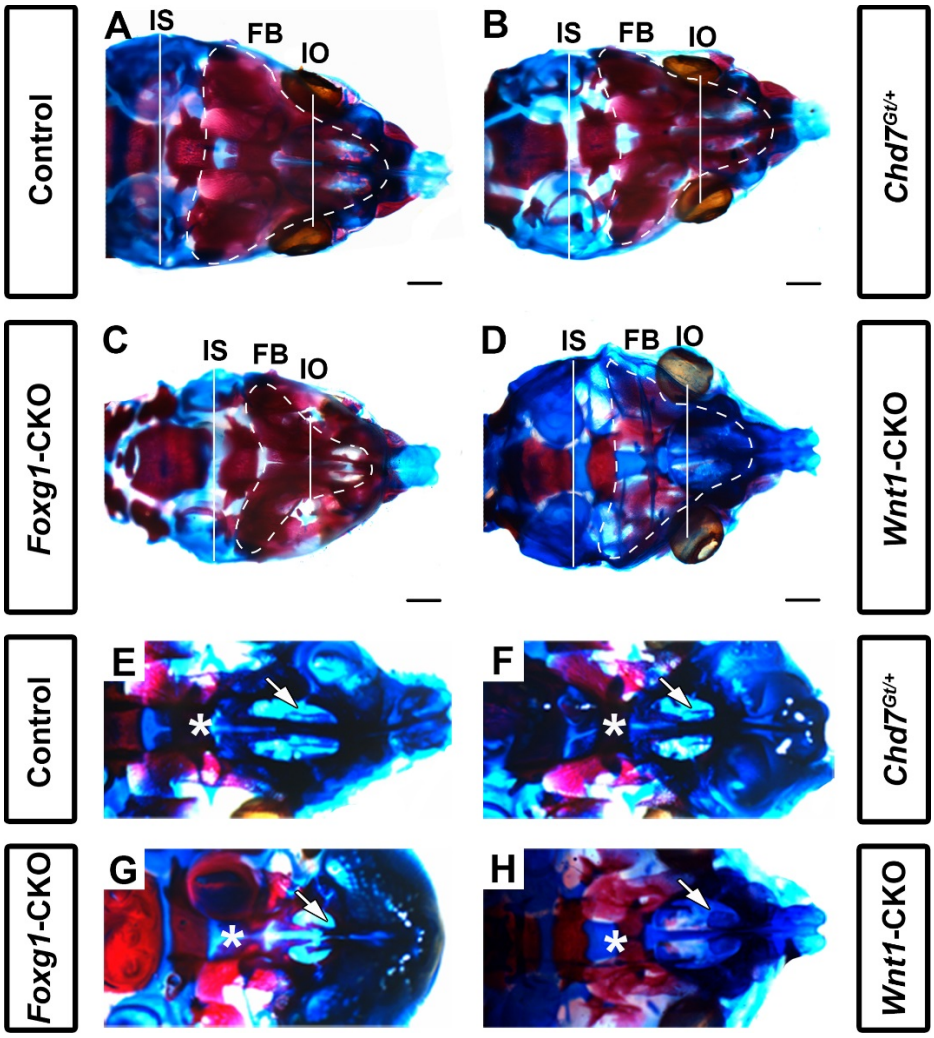


Figure 2.2. *Chd7* conditional mutants have shortened intraocular and intersquamosal distances, hypoplasia of the maxillary shelves, and dysplasia of nasal conchae.

Skeletal preparations of postnatal day 1 control (*Cre*-negative, $Chd7^{+/f}$ or $Chd7^{f/f}$) (A,E), $Chd7^{Gt/+}$ (B,F), *Foxg1*-CKO (C,G), and *Wnt1*-CKO (D,H) mice. Alizarin red and alcian blue staining show bone and cartilage, respectively. (A-D) are representative dorsal images of the calvaria while (E-H) are representative dorsal images of the developing maxillary shelves (with mandibles removed). *Foxg1*-CKO (C) mice exhibit shorter interocular (white line, IO; $p<0.001$, $N=7$) and intersquamosal (white line, IS; $p<0.001$, $N=7$) distances compared to control (A), $Chd7^{Gt/+}$ (B), and *Wnt1*-CKO (D) mice. *Foxg1*-CKO (C) mice exhibit a visibly smaller frontal bone (FB) surface area (white, dotted line) relative to control (A), $Chd7^{Gt/+}$ (B), and *Wnt1*-CKO (D) mice. *Wnt1*-CKO (D) mice lack frontal bone ossification (as demonstrated by alizarin red staining) relative to control (A), $Chd7^{Gt/+}$ (B), and *Foxg1*-CKO (C) mice. In control (E) and $Chd7^{Gt/+}$ (F) mice, appropriately formed palatal shelves (asterisk) and ventral nasal conchae (white arrow) are present. *Foxg1*-CKO (G) mice have hypoplastic palatal shelves which approximate the midline (asterisk) and absent ventral conchae (white arrow), whereas *Wnt1*-CKO (H) mice have severe palatal shelf hypoplasia (asterisk) and dysplastic ventral conchae (white arrow). Scale bars in A-D are 1 mm.

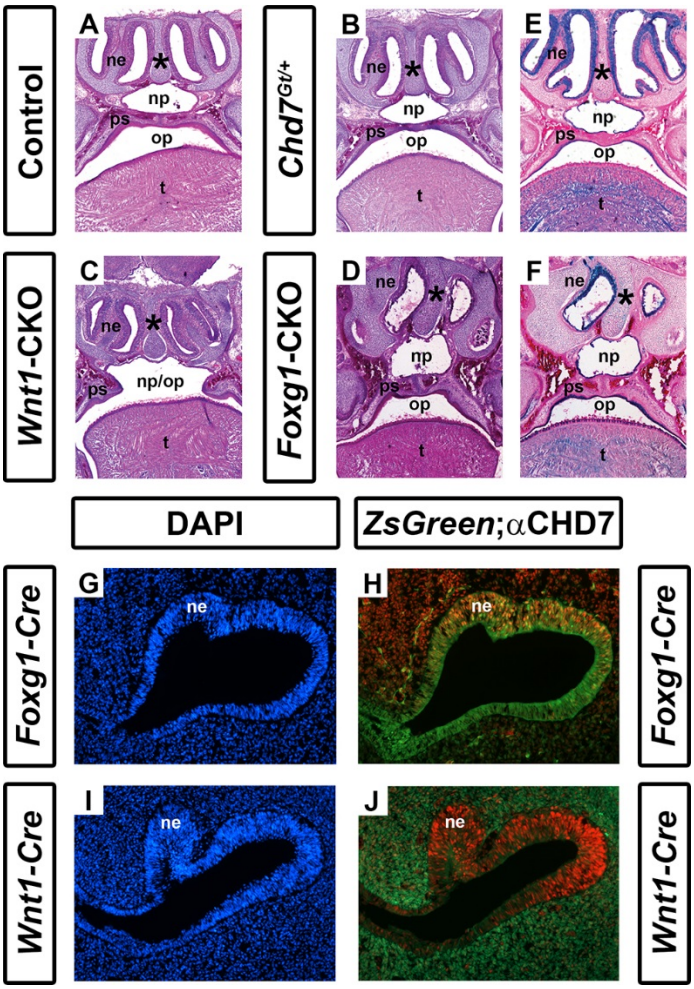


Figure 2.3. Conditional Chd7 deletion results in palatal and nasal epithelial dysplasia.
Transverse sections of postnatal day 1 control (*Cre*-negative, $Chd7^{+/f}$ or $Chd7^{f/f}$) (A), $Chd7^{Gt/+}$ (B), *Wnt1*-CKO (C), and *Foxg1*-CKO (D) mice stained with hematoxylin and eosin. Control (A) and $Chd7^{Gt/+}$ (B) mice exhibit fully fused palatal shelves (ps) with separation of the nasopharynx (np) from the oropharynx (op), whereas *Wnt1*-CKO(C) mice have severely hypoplastic palatal shelves (ps) resulting in a cleft palate and single pharyngeal cavity (np/op). *Foxg1*-CKO mice (D) have fused palatal shelves (ps) resulting in a highly-arched, intact palate, a thickened nasal septum (asterisk), and severely hypoplastic nasal epithelia (ne). (E) and (F) show X-gal/eosin stained sections of postnatal day 1 $Chd7^{Gt}$ mice, which express β-galactosidase under the control of the *Chd7* promoter. X-gal staining is present in the nasal epithelium (ne), tongue (t) and epithelial cells lining the palatal shelves and combined oral-nasal pharynx (op/np) of $Chd7^{Gt/flox}$ (E) and *Foxg1*-CKO (F) mice. Panels (G-J) are transverse sections of *Foxg1-Cre;ZsGreen* (G, H) or *Wnt1-Cre;ZsGreen* (I, J) E11.5 embryos stained with DAPI (blue, marking cellular nuclei) or anti-CHD7 (red). Green fluorescence (*ZsGreen* reporter) marks *Cre* expressing cells and is overlaid with anti-CHD7 (red) in (H) and (J). *Foxg1-Cre* and *Chd7* are both highly expressed in the developing nasal epithelium (ne) while *Wnt1-Cre* expression is restricted to the surrounding nasal mesenchyme (m) and is absent from the nasal epithelium proper.

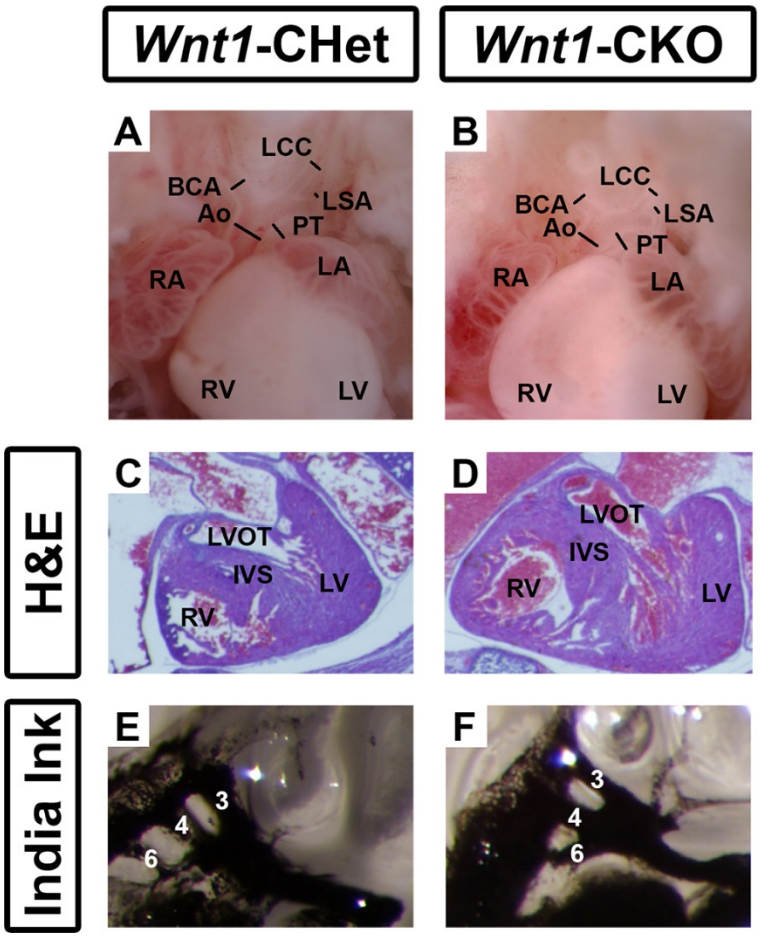


Figure 2.4. Neural crest-derived cardiac structures develop normally in *Wnt1*-CHet and *Wnt1*-CKO mice.

(A) E16.5 embryonic hearts from *Wnt1*-CHet and *Wnt1*-CKO embryos exhibited normal septation of the aorta (Ao) and pulmonary trunk (PT) with normal extension of the brachiocephalic (BCA), left common carotid (LCC), and left subclavian (LSA) arteries from the aortic arch. H&E staining of sectioned E16.5 embryonic hearts from *Wnt1-Cre* conditional heterozygous (B) and *Wnt1*-CKO (C) mice revealed normal development of the left ventricular outflow tract (LVOT) and inter ventricular septum (IVS). India ink injections of E10.5 *Wnt1-Cre* conditional heterozygous (CHet) (D) and *Wnt1*-CKO (E) mice demonstrate normal development of the 3rd, 4th, and 6th pharyngeal arch arteries. Other abbreviations: RA (right atrium); LV (left ventricle); RA (right atrium); LA (left atrium). Lines span lumina of arteries.

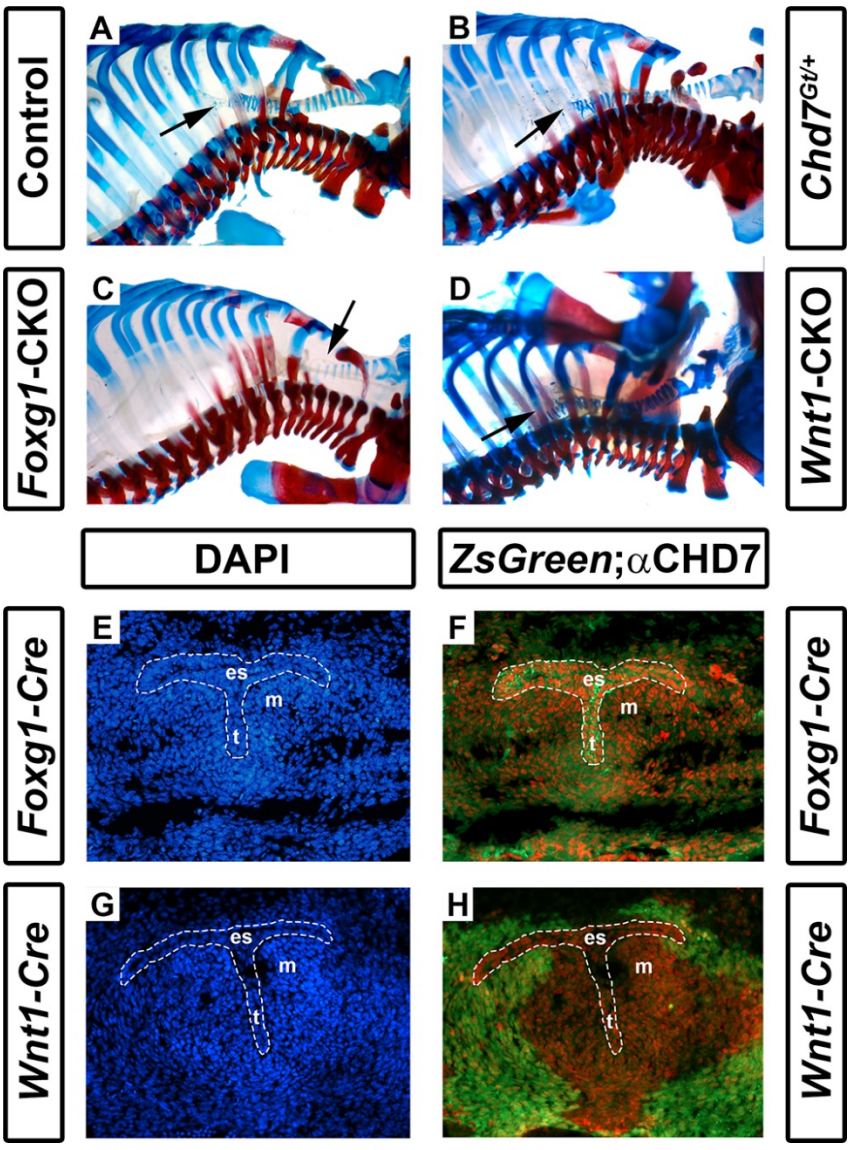


Figure 2.5. Foxg1-CKO mice have reduced numbers of cartilaginous tracheal rings.
Shown are skeletal preparations of postnatal day 1 control (*Cre*-negative, $Chd7^{+/f}$ or $Chd7^{f/f}$) (A), $Chd7^{Gt/+}$ (B), *Foxg1*-CKO (C), and *Wnt1*-CKO (D) mice. Alizarin red and alcian blue staining reveal bone and cartilage, respectively. Normal numbers of tracheal rings (17-19) (arrows point to distal trachea) are present in control, $Chd7^{Gt/+}$, and *Wnt1*-CKO mice, whereas *Foxg1*-CKO mice have fewer (11) tracheal rings. Panels E-H are transverse sections of *Foxg1-Cre;ZsGreen* (E, F) or *Wnt1-Cre;ZsGreen* (G, H) E11.5 embryos at the level of the laryngotracheal groove (indicated by the area within the dashed white lines) stained with DAPI (blue, labeling cellular nuclei) or anti-CHD7 (red). Green fluorescence (*ZsGreen* reporter) marks *Cre*-expressing cells and is overlaid with anti-CHD7 (red) in (F) and (H). *Chd7* and *Foxg1-Cre* are highly co-expressed in the developing esophagus (es), trachea (t), and the surrounding mesenchyme (m), whereas *Wnt1-Cre* activity is restricted to the surrounding mesenchymal tissues and does not overlap with *Chd7* expression in the presumptive esophagus or trachea.

References

1. Husu, E. *et al.* Phenotype in 18 Danish subjects with genetically verified CHARGE syndrome. *Clin Genet* **83**, 125-134 (2013).

2. Janssen, N. *et al.* Mutation update on the CHD7 gene involved in CHARGE syndrome. *Hum Mutat* **33**, 1149-1160 (2012).

3. Hughes, S. S., Welsh, H. I., Safina, N. P., Bejaoui, K. & Ardinger, H. H. Family history and clefting as major criteria for CHARGE syndrome. *Am J Med Genet A* **164A**, 48-53 (2014).

4. Zentner, G. E., Layman, W. S., Martin, D. M. & Scacheri, P. C. Molecular and phenotypic aspects of CHD7 mutation in CHARGE syndrome. *Am J Med Genet A* **152A**, 674-686 (2010).

5. Legendre, M. *et al.* Antenatal spectrum of CHARGE syndrome in 40 fetuses with CHD7 mutations. *J Med Genet* (2012).

6. Hurd, E. A. *et al.* Loss of Chd7 function in gene-trapped reporter mice is embryonic lethal and associated with severe defects in multiple developing tissues. *Mamm Genome* **18**, 94-104 (2007).

7. Hurd, E. A., Poucher, H. K., Cheng, K., Raphael, Y. & Martin, D. M. The ATP-dependent chromatin remodeling enzyme CHD7 regulates pro-neural gene expression and neurogenesis in the inner ear. *Development* **137**, 3139-3150 (2010).

8. Adams, M. E. *et al.* Defects in vestibular sensory epithelia and innervation in mice with loss of Chd7 function: implications for human CHARGE syndrome. *J Comp Neurol* **504**, 519-532 (2007).

9. Hurd, E. A. *et al.* Mature middle and inner ears express Chd7 and exhibit distinctive pathologies in a mouse model of CHARGE syndrome. *Hear Res* (2011).

10. Hurd, E. A., Micucci, J. A., Reamer, E. N. & Martin, D. M. Delayed fusion and altered gene expression contribute to semicircular canal defects in Chd7 deficient mice. *Mech Dev* (2012).

11. Layman, W. S., Hurd, E. A. & Martin, D. M. Reproductive dysfunction and decreased GnRH neurogenesis in a mouse model of CHARGE syndrome. *Hum Mol Genet* **20**, 3138-3150 (2011).

12. Layman, W. S. *et al.* Defects in neural stem cell proliferation and olfaction in Chd7 deficient mice indicate a mechanism for hyposmia in human CHARGE syndrome. *Hum Mol Genet* **18**, 1909-1923 (2009).

13. Bosman, E. A. *et al.* Multiple mutations in mouse Chd7 provide models for CHARGE syndrome. *Hum Mol Genet* **14**, 3463-3476 (2005).

14. Yu, T. *et al.* Deregulated FGF and homeotic gene expression underlies cerebellar vermis hypoplasia in CHARGE syndrome. *eLife* **2**, e01305 (2013).

15. Wright, E. M., O'Connor, R. & Kerr, B. A. Radial aplasia in CHARGE syndrome: a new association. *Eur J Med Genet* **52**, 239-241 (2009).

16. Prasad, C., Quackenbush, E. J., Whiteman, D. & Korf, B. Limb anomalies in DiGeorge and CHARGE syndromes. *Am J Med Genet* **68**, 179-181 (1997).

17. Hebert, J. M. & McConnell, S. K. Targeting of cre to the Foxg1 (BF-1) locus mediates loxP recombination in the telencephalon and other developing head structures. *Dev Biol* **222**, 296-306 (2000).

18. Danielian, P. S., Muccino, D., Rowitch, D. H., Michael, S. K. & McMahon, A. P. Modification of gene activity in mouse embryos in utero by a tamoxifen-inducible form of Cre recombinase. *Curr Biol* **8**, 1323-1326 (1998).

19. Bajpai, R. *et al.* CHD7 cooperates with PBAF to control multipotent neural crest formation. *Nature* **463**, 958-962 (2010).

20. Schnetz, M. P. *et al.* Genomic distribution of CHD7 on chromatin tracks H3K4 methylation patterns. *Genome Res* **19**, 590-601 (2009).

21. Randall, V. *et al.* Great vessel development requires biallelic expression of Chd7 and Tbx1 in pharyngeal ectoderm in mice. *J Clin Invest* **119**, 3301-3310 (2009).

22. Madisen, L. *et al.* A robust and high-throughput Cre reporting and characterization system for the whole mouse brain. *Nat Neurosci* **13**, 133-140 (2010).

23. Bergman, J. E. H. *et al.* CHD7 mutations and CHARGE syndrome: the clinical implications of an expanding phenotype. *Journal of Medical Genetics* **48**, 334-342 (2011).

24. Bergman, J. E. H., Bosman, E. A., van Ravenswaaij-Arts, C. M. A. & Steel, K. P. Study of smell and reproductive organs in a mouse model for CHARGE syndrome. *Eur J Hum Genet* **18**, 171-177 (2010).

25. Van de Laar, I. *et al.* Limb anomalies in patients with CHARGE syndrome: an expansion of the phenotype. *Am J Med Genet A* **143A**, 2712-2715 (2007).

26. Fujita, K. *et al.* Abnormal basiocciput development in CHARGE syndrome. *AJNR Am J Neuroradiol* **30**, 629-634 (2009).

27. Jiang, X., Rowitch, D. H., Soriano, P., McMahon, A. P. & Sucov, H. M. Fate of the mammalian cardiac neural crest. *Development* **127**, 1607-1616 (2000).

28. Hutson, M. R. & Kirby, M. L. Model systems for the study of heart development and disease. Cardiac neural crest and conotruncal malformations. *Semin Cell Dev Biol* **18**, 101-110 (2007).

29. Woo, J., Miletich, I., Kim, B. M., Sharpe, P. T. & Shivdasani, R. A. Barx1-mediated inhibition of Wnt signaling in the mouse thoracic foregut controls tracheo-esophageal septation and epithelial differentiation. *PLoS One* **6**, e22493 (2011).

30. Kastl, K. G., Rettinger, G. & Keck, T. The impact of nasal surgery on air-conditioning of the nasal airways. *Rhinology* **47**, 237-241 (2009).

31. Kim, K. S., Choi, Y. S., Kim, H. J. & Yoon, J. H. The risk of olfactory disturbance from conchal plate injury during ethmoidectomy. *American journal of rhinology* **17**, 307-310 (2003).

32. Jacob, A. & Chole, R. A. Survey anatomy of the paranasal sinuses in the normal mouse. *Laryngoscope* **116**, 558-563 (2006).

33. Coppola, D. & Craven, B. The effects of naris occlusion on mouse nasal turbinate development. *The Journal of experimental biology* (2013).

34. Wang, X. X. *et al.* Anterior maxillary segmental distraction for correction of maxillary hypoplasia and dental crowding in cleft palate patients: a preliminary report. *International journal of oral and maxillofacial surgery* **38**, 1237-1243 (2009).

35. Chapman, K. L. *et al.* Timing of palatal surgery and speech outcome. *The Cleft palate-craniofacial journal : official publication of the American Cleft Palate-Craniofacial Association* **45**, 297-308 (2008).

36. Eppley, B. L., van Aalst, J. A., Robey, A., Havlik, R. J. & Sadove, A. M. The spectrum of orofacial clefting. *Plastic and reconstructive surgery* **115**, 101e-114e (2005).

37. Akisu, M., Ozkinay, F., Ozyurek, R., Kucuktas, A. & Kultursay, N. The CHARGE association in a newborn infant. *The Turkish journal of pediatrics* **40**, 283-287 (1998).

38. Li, L. *et al.* BmprIa is required in mesenchymal tissue and has limited redundant function with BmprIb in tooth and palate development. *Dev Biol* **349**, 451-461 (2011).

39. Wang, Y., Song, L. & Zhou, C. J. The canonical Wnt/beta-catenin signaling pathway regulates Fgf signaling for early facial development. *Dev Biol* **349**, 250-260 (2011).

40. Bush, J. O. & Jiang, R. Palatogenesis: morphogenetic and molecular mechanisms of secondary palate development. *Development* **139**, 231-243 (2012).

41. Doshi, J. & Krawiec, M. E. Clinical manifestations of airway malacia in young children. *The Journal of allergy and clinical immunology* **120**, 1276-1278 (2007).

42. Perl, A. K., Wert, S. E., Nagy, A., Lobe, C. G. & Whitsett, J. A. Early restriction of peripheral and proximal cell lineages during formation of the lung. *Proc Natl Acad Sci U S A* **99**, 10482-10487 (2002).

43. Sinn, R. & Wittbrodt, J. An eye on eye development. *Mech Dev* **130**, 347-358 (2013).

44. Grocott, T., Johnson, S., Bailey, A. P. & Streit, A. Neural crest cells organize the eye via TGF-beta and canonical Wnt signalling. *Nature communications* **2**, 265 (2011).

45. Patten, S. A. *et al.* Role of Chd7 in zebrafish: a model for CHARGE syndrome. *PLoS One* **7**, e31650 (2012).

46. Sperber, G. H. *Craniofacial Embryology*. 4th edn, 58-68, 110-111 (Wright, 1989).

47. Nichols, D. H. Formation and distribution of neural crest mesenchyme to the first pharyngeal arch region of the mouse embryo. *Am J Anat* **176**, 221-231 (1986).

48. Takada, I. *et al.* A histone lysine methyltransferase activated by non-canonical Wnt signalling suppresses PPAR-gamma transactivation. *Nat Cell Biol* **9**, 1273-1285 (2007).

49. Minoux, M. & Rijli, F. M. Molecular mechanisms of cranial neural crest cell migration and patterning in craniofacial development. *Development* **137**, 2605-2621 (2010).

Chapter III: Duplication 2p25 in a Child with Clinical Features of CHARGE Syndrome[1]

Abstract

CHARGE syndrome is a dominant disorder characterized by ocular colobomata, heart defects, choanal atresia, retardation of growth and development, genital hypoplasia, and ear abnormalities including deafness and vestibular disorders. The majority of individuals with CHARGE have pathogenic variants in the gene encoding CHD7, a chromatin remodeling protein. Here we present a 15-year-old girl with clinical features of CHARGE syndrome and a *de novo* 6.5 Mb gain of genomic material at 2p25.3-p25.2. The duplicated region contained 24 genes, including the early and broadly expressed transcription factor gene *SOX11*. Analysis of 28 other patients with CHARGE showed no *SOX11* copy number changes or pathogenic sequence variants. To our knowledge, this child's chromosomal abnormality is unique and represents the first co-occurrence of duplication 2p25 and clinical features of CHARGE syndrome. We compare our patient's phenotype to ten previously published patients with isolated terminal duplication 2p, and elaborate on the clinical diagnosis of CHARGE in the context of atypical genetic findings.

Introduction

CHARGE syndrome is a multiple anomaly disorder that presents with ocular colobomata, heart defects, choanal atresia, growth retardation, genital anomalies, and ear malformations[1]. Heterozygous loss-of-function mutations in *CHD7*, an ATP-dependent chromatin remodeling protein, are present in 70% of individuals with CHARGE[2]. In addition, chromosomal aberrations have been reported in association with CHARGE features[3-5].

Duplication 2p25 syndrome is a rare and clinically heterogeneous disorder manifest by extra genetic material in variably sized portions of the short arm of chromosome 2. Common features include developmental delay, craniofacial dysmorphic features (including hypertelorism and prominent forehead), and cardiovascular malformations. Duplication 2p25 has thus far has been reported in only ten patients with an isolated aberration of the terminal region of 2p[6-13].

Here, we report a child with a complex duplication-triplication of 2p25 and clinical features of CHARGE syndrome. The aberrant region (2p25.3-p25.2) was 6.5 Mb in length, consisting of a duplication of the distal 3.0 Mb and a triplication of the proximal 3.5 Mb. We compare our patient's phenotype to ten previously published patients with isolated terminal duplication 2p, and elaborate on the diagnosis of CHARGE in the context of atypical genetic findings[6-13].

Materials and Methods

Clinical evaluation

Clinical evaluation and photographs of the proband were performed by DMM with written consent from the patients' parents. This research was approved by the University of Michigan Medical School IRB.

Chromosomal microarray (CMA)

CMA was performed on genomic DNA extracted from peripheral blood lymphocytes using the Illumina CytoSNP-850K array platform (Illumina, San Diego, CA, USA). Patient DNA was isolated, amplified, and enzymatically fragmented. DNA fragments were hybridized to array probes and extended with tagged terminating nucleotides. Aberrations were confirmed by relative-quantitative PCR (Applied Biosystems, Carlsbad, CA, USA).

Fluorescence in situ hybridization (FISH)

FISH of interphase and metaphase chromosomes was performed using peripheral blood lymphocytes. Bacterial artificial chromosomes were used as probes for the regions of interest on chromosome 2 (RP11-168K7, RP11-36C8; BlueGnome, UK), chromosome 15 (RP11-475F15; BlueGnome) and subtelomeric regions of chromosomes 2 and 15 (Abbott Molecular, Abbott Park, IL, USA). Probes used for FISH are listed in Table 3.2.

Relative-Quantitative PCR (RQ-PCR) and SOX11 gene sequencing

SOX11 RQ-PCR was performed on 28 individuals with clinical features of CHARGE syndrome and negative *CHD7* sequencing (Hs00839199_cn, Applied

Biosystems). PCR amplification of the *SOX11* coding DNA sequence was performed using the GC-Rich PCR system (Roche, Indianapolis, IN) followed by Sanger sequencing. Primers used for PCR amplification and sequencing are listed in Table 3.3.

Results

Clinical report

Our patient was initially evaluated at 19 months of age in the University of Michigan Pediatrics Genetics clinic for multiple congenital anomalies. She was born at 42 weeks by induced vaginal delivery following an uneventful pregnancy with a birth weight of 3.3 kg (25-50th centile) and length of 51.4 cm (50-75th centile). Parents were healthy and non-consanguineous. Newborn hearing screening was abnormal and she was subsequently diagnosed with right-sided profound sensorineural hearing loss by brainstem auditory evoked response testing. The left ear tested within normal limits.

At 19 months, she exhibited generalized growth delay, including short stature (76 cm, <3rd centile), low weight (9.48 kg, <3rd centile), and microcephaly (45 cm, <3rd centile). She also exhibited developmental delay, and several craniofacial dysmorphic features (Figure 3.1A-C and Table 3.1). She had a highly-arched palate, bifid uvula, and peg-shaped teeth. Ophthalmologic exam revealed bilateral colobomata involving the iris, retina, and optic nerves with sensory nystagmus, variable angle esotropia, and ptosis. No corneal opacity, microcornea, lens opacification, or increased intraocular pressures were noted. She had bilateral preauricular pits and posteriorly rotated, simplified external ears (Figure 3.1D-E). Discontinuous palmar creases and dysmorphic features of the fingers (i.e. hypoplasia of the left thumb and arachnodactyly) and toes (i.e. camptodactyly) with persistent fetal fingertip and toe pads were noted (Figure 3.1F-G). She had a small thoracic

cage with upturned xyphoid process and right-sided spinal muscular prominence in addition to widely-spaced nipples, supernumerary nipples, and hypoplastic labia minora.

Developmental milestones were delayed: she developed a social smile at 4 months, sat at 10 months, crawled at 19 months, pulled to a stand at 21 months, and walked at 4 years. At 21 months she was using three nonspecific consonant-vowel combinations; at 5.5 years she could hum and follow some commands but had no expressive verbal language. By age 11, she could speak in 2-3 word phrases.

Echocardiography at 2 years was normal. A temporal bone CT performed at 43 months showed dysplastic inner ears. The right ear contained a single dysplastic semicircular canal and a severely hypoplastic cochlea while the left inner ear had a Mondini malformation and an expanded endolymphatic duct. Renal ultrasonography revealed bilateral calculi and cysts. She had left-sided facial nerve palsy, night terrors with tongue fasciculations, and partial complex petit mal seizures (onset age 3 years). She developed tonic-clonic seizures at 5.5 years. Brain MRI at 23 months revealed white matter ischemic-hypoxic changes in both cerebral hemispheres. Biochemical panels for lysosomal enzymes, plasma amino acids, urine organic acids, and carbohydrate deficient transferrins were normal.

Past surgical history was significant for multiple bilateral myringotomies secondary to recurrent otitis media, and strabismus surgery at age 3 years. Preauricular pits were reported in multiple maternal relatives, including an aunt, uncle, grandmother, and cousin. Her mother reported a history of renal calculi.

Our patient met clinical diagnostic criteria for CHARGE syndrome, with two of three major criteria (ocular colobomata and hypoplastic semicircular canals) and three of

five minor criteria (cranial nerve dysfunction, abnormal outer/middle ear structure, and intellectual disability)[1,14].

Clinical genetic testing

Chromosomal analysis revealed a normal 46,XX karyotype. *CHD7* mutation testing revealed no pathogenic variants, deletions, or duplications. CMA revealed a female chromosomal profile with aberrations on chromosomes 2 and 15.

Chromosome 2 contained two contiguous regions of gain, together spanning 6.5 Mb of genomic material at 2p25.3-p25.2 (chr2:39193-6531231; hg38 (Figure 3.2A). There were four copies of the proximal 3.5 Mb region (chr2:3126461-6531231) containing 13 RefSeq genes, and three copies of the distal 3 Mb region (chr2:39193-3058475) containing 11 genes (Figure 3.2E). The 67,986 bp intervening genomic sequence with normal copy number contained no genes (chr2: 3058475-3126461). RQ-PCR confirmed these chromosomal gains in the proband, which were absent in both parents. FISH on interphase chromosomes from 100 cells identified three copies of the distal chromosome 2 gain in 75% of cells examined (Figure 3.2B), and three or four copies of the proximal genomic gain in 59% and 26% of the cells, respectively (Figure 3.2C). Importantly, 20% of cells examined by FISH had normal staining patterns, indicating mosaicism for both the distal and proximal gains. We did not assess co-localization of the distal and proximal gains within the same cells. In prophase cells, distal FISH probes bound to the same chromosomal strand (Figure 3.2D), consistent with a *de novo* interstitial duplication event resulting in mosaicism for three or four copies of the proximal region (2p25.3-p25.2) and three copies of the distal region (2p25.3). There was no evidence of a subtelomeric

deletion. Furthermore, FISH performed on cells from each parent revealed no chromosome 2p abnormalities, including inversion or subtelomeric deletion.

The proband had a 602 kb gain of genomic material at 15q11.2 (chr15:22572809-23174546). RQ-PCR confirmed maternal inheritance of this single-copy microduplication. FISH studies were unable to confirm the duplication in either the proband or her mother, likely because it was under the detection threshold of 700 kb. Importantly, there were no supernumerary chromosomes or chromosomal translocations.

RQ-PCR and sequencing for SOX11 in individuals with CHARGE syndrome

Among the 24 genes in the aberrant 2p region was the triplicated *SOX11*, encoding a SoxC group high mobility group (HMG) box-containing transcription factor. SOX11 has major roles in embryonic and adult neurogenesis, craniofacial osteogenesis, ocular morphogenesis, and cardiac development, all specifically disrupted in CHARGE[15-22]. Sanger sequencing and RQ-PCR on our patient and on 28 patients with CHARGE phenotypes, negative chromosomal microarray, and negative *CHD7* mutation testing showed no *SOX11* mutations or duplications.

Discussion

Here we report a child with features of CHARGE syndrome and a complex mosaic duplication-triplication 2p25, including triplication of the transcription factor *SOX11*. Given that a minority of cells had two copies of either the distal or proximal gains, and given that neither parent had a detectable chromosome 2p anomaly, it is possible that our patient's 2p anomaly is post-zygotic and thus represents a case of somatic mosaicism.

Analysis of 28 other individuals revealed no additional cases of CHARGE and gain of 2p25 or *SOX11* mutations. To our knowledge, our patient represents the first case of 2p25 gain with inner ear anomalies and other CHARGE features.

Comprehensive review of the literature revealed ten cases presenting with partial trisomy 2p, including our region of interest (Table 3.1)[6-13]. Interestingly, our patient had the smallest region of 2p duplication among these ten cases and was the only one to exhibit triplication (Figure 3.2E). Lack of reported key clinical findings in the three published cases precluded retrospective assignment of a CHARGE syndrome diagnosis; however, they did exhibit some CHARGE features including external ear malformations, hearing loss, cardiac anomalies, craniofacial dysmorphic features, and developmental delay. As with our patient, some of these ten cases also exhibited clinical findings not commonly observed in CHARGE, such as hypertelorism, seizure disorder, cerebral white matter ischemic-hypoxic changes, and arachnodactyly. While this phenotypic cluster could be the result of dysregulation of one gene within the chromosomal region of gain, such as *SOX11*, we cannot rule out other genes within the interval as contributory. Finally, we found 20 individuals in the ClinGen and DECIPHER databases with duplications wholly or partially contained within our patient's duplicated interval. Reported phenotypes are summarized in Tables 3.4 and 3.5, respectively. These findings indicate that 2p duplication is associated with developmental delay and craniofacial dysmorphic features.

Our patient's phenotype may be explained in part by duplication of the early and broadly expressed transcription factor *SOX11* which has been implicated in development of CHARGE-relevant structures, such as the eye, ear, and heart[21]. Interestingly, a recent report showed that *Sox11* is a direct target of CHD7 in neural stem cells; however, it is not

known whether CHD7 regulates *Sox11* expression in other developing tissues[23]. Of note, loss-of-function mutations in *SOX11* were recently reported in Coffin-Siris syndrome[24]. Our patient does not have clinical features or a genetic diagnosis consistent with Coffin-Siris syndrome. Further, our patient's clinical features overlap with those described in Kabuki syndrome, specifically her pre-auricular pits, persistent fetal fingertip pads, and craniofacial features. To date, no link between *KMT2D*, the gene most often associated with Kabuki, and any gene in our patient's relevant chromosomal region of gain has been observed. Finally, our patient's duplicated interval contains *PXDN*, a gene in which loss-of-function mutations have been associated with microphthalmia and anterior segment dysgenesis[25,26]. Duplications of *PXDN* have also been associated with autism without ocular involvement[27]. To date, there are no reports of *PXDN* duplication and coloboma. Taken together, these observations suggest that increased *PXDN* dosage is not sufficient to cause our patient's phenotype.

There are three important caveats to our analysis. First, we cannot rule out noncoding mutations in *CHD7* or elsewhere as contributing to her phenotype. Also, it is not known whether some or all of the duplicated genes in our patient were overexpressed during embryologic development. Finally, while the breakpoints surrounding her duplicated regions were devoid of coding DNA, critical regulatory regions could be disrupted.

In summary, this is the first account of a complex mosaic gain of 2p25 in an individual with features of CHARGE syndrome. This report may prompt detection and surveillance of CHARGE-related features in individuals with duplication 2p25.

Acknowledgments

We thank the patient and her family for allowing us to present this case. Further, we thank the University of Michigan Medical Genetics Laboratories, the Cytogenetics Laboratory, and the DNA Sequencing Core for clinical testing and sequencing support. EDS is supported by NIH grants 2T32-GM007863 and 5T32-DC000011. DMM is supported by NIH grant 5R01-DC009410 and the Donita B. Sullivan, M.D. Research Professorship.

Chapter III Note

[1]A revised version of Chapter III has been published as: Sperry, E. D., Schuette, J. L., Van Ravenswaaij-Arts, C. M. A., Green, G. E., and Martin, D. M. Duplication 2p25 in a child with clinical features of CHARGE syndrome. *American Journal of Medical Genetics Part A* **170**A:1148-1154 (2016).

Clinical Feature	Our Patient dup(2)(p25.3-p25.2)	Stoll et al., 1974 Case 1 dup(2)(pter-p22)	Stoll et al., 1974 Case 2 dup(2)(pter-p22)	Fineman et al., 1983 dup(2)(pter-p23)	Wakita et al., 1985 dup(2)(p25.3-p25.1)	Engels et al., 1999 dup(2)(pter-p23)	Aviram-Goldring et al., 2000 Case 1 dup(2)(p25.2-p23)	Al-Saffar et al., 2000 dup(2)(pter-p23)	Ishikawa et al., 2002 dup(2)(p25.3-p22.2)	Martinez-Juarez et al., 2014 Case 1 dup(2)(pter-p22.3)	Martinez-Juarez et al., 2014 Case 2 dup(2)(pter-p22.3)
Growth and development											
IUGR (<10%)	-	-	-	-		-	-	-	-	-	-
Postnatal growth failure (<3%)	+	+		+			+	+	+	+	+
Developmental delay (motor)	+	+		+	-	+	+	+	+	+	+
Intellectual disability	+	+		+		+	+	+		+	+
Craniofacial dysmorphic features											
High, prominent forehead	+, BC			+	TC		+	+	+	+	+
Hypertelorism	+				+				+		
Epicanthal folds	+	+	+			+	+			+	+
Nasal abnormalities	broad, prominent, short philtrum	broad	broad	broad	anteverted nares	short	broad	broad, short		broad, short	broad, short
Ocular abnormalities											
Coloboma	retinal – bilateral										
Myopia	+							+			
Ptosis	+										

Ear abnormalities									
External ear anomalies	+	+		+	+	+			
Sensorineural hearing loss	+							+	
Mondini malformation	+								
Semicircular canal dysplasia	+								
Other findings									
WM ischemic-hypoxic change	+ (seizures)					+	+ (seizures)		
Ventricular septal defect	-					+		+	
Finger dysmorphic features	hypoplastic left thumb, AD, FFP	AD, joint dysplasia	AD				slender	AD	AD
Toe dysmorphic features	CD						slender, clinodactyly	AD	AD
Supernumerary nipples	+			+					
Renal abnormalities	stones			pelvic dilation	VUR				
Hypoplasic external genitalia	+				-			+	+

BC = brachycephaly; TC = trigonocephaly; WM = white matter; AD = arachnodactyly; FFP = fetal fingertip pads CD = camptodactyly; VUR = vesico-ureteral reflux

Table 3.1: Clinical features of pure trisomy 2p patients.

This comprehensive list of clinical findings reveals significant overlap between our patient, diagnosed with typical CHARGE syndrome, and ten other individuals with the terminal 2p duplication.

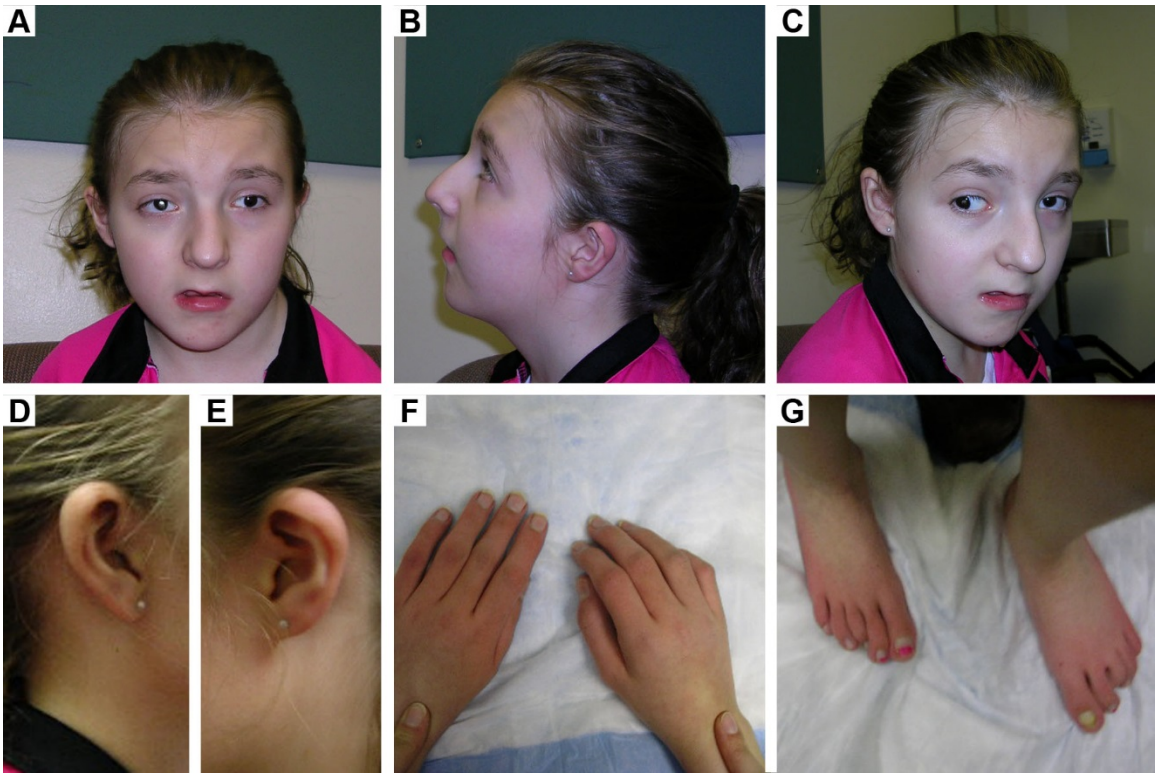


Figure 3.1: Clinical features of the proband.
Photographs taken at 11 years show a broad, sloping forehead with a slender, prominent nose and flattened nasal tip (A-C). Over-folded helices (D-E), shortened proximal phalanges of the thumbs (F), and elongated fingers and toes (F-G) are noted.

NB: The authors thank the family of the patient for allowing her images to be included in this manuscript.

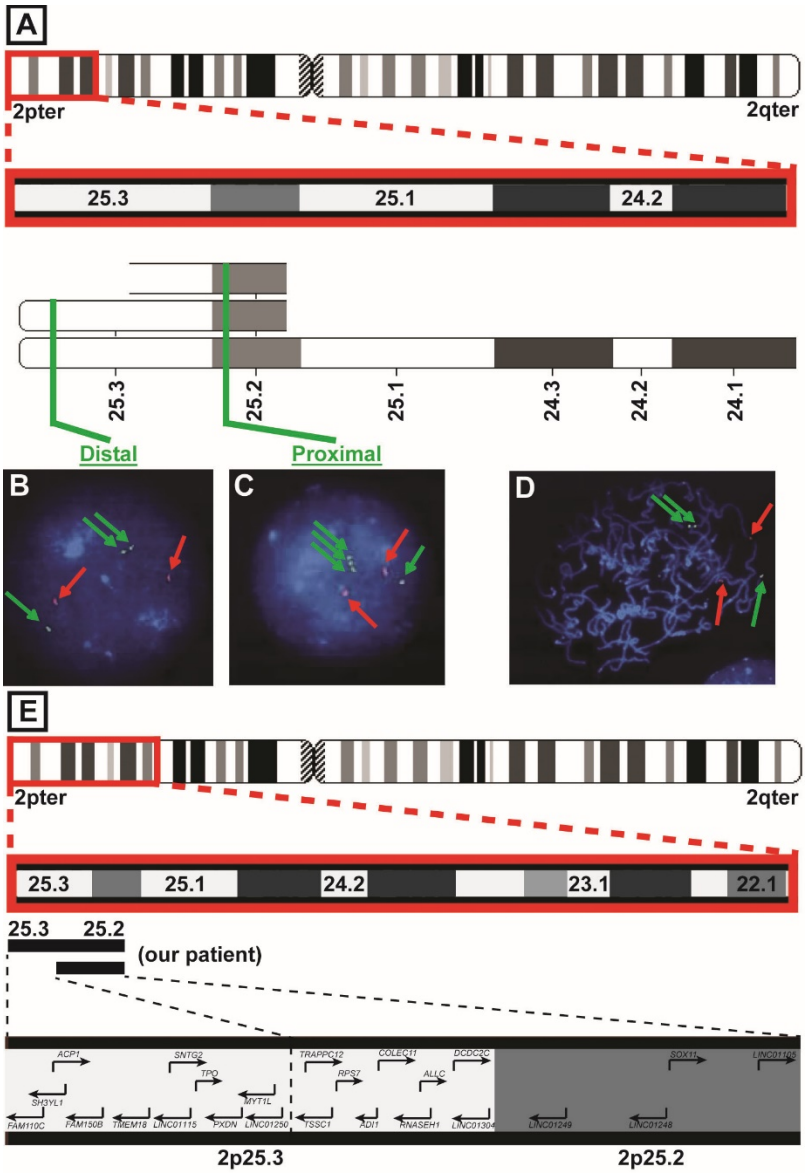


Figure 3.2: Chromosomal microarray analysis revealed a gain of genomic material on chromosome 2p25.3-p25.2, confirmed by FISH, and shared with three other cases.

CMA performed on whole blood revealed a *de novo*, distal duplication and proximal triplication of 2p25.3-p25.2 (A, highlighted in red). Interphase FISH confirmed the CMA findings, revealing a distal duplication (B, green probe RP11-168K7) and proximal triplication (C, green probe RP11-36C8). Red label in (B) and (C) corresponds to a 2qter probe, indicating normal dosage of 2q in each case. Visualization of pachytene chromosomes using prophase FISH (D) confirmed probe arrangement along 2p, confirmed the integrity of the 2p subtelomeric region (2pter red probe), and excluded translocation events. The 24 genes contained within the interval duplicated within our patient are shown (E). In our patient's diploid genome, the 11 distal genes were present in triplicate while the 13 proximal genes were in quadruplicate. Of interest, our patient had four copies of *SOX11*, an SRY-related HMG box-containing SoxC group transcription factor.

FISH Probe and Label	Use	Genetic Location (NCBI 37)
RP11-36C8 – Green	Detect 2p25.2 copy number	chr2:4,639,538-4,818,989
RP11-168K7 – Green	Detect 2p25.3 copy number	chr2:1,612,842-1,785,220
Abbott Molecular 2pter – Green	Detect 2pter copy number	2pter
Abbott Molecular 2qter – Orange	Control for chr2	2qter
RP11-475F15 – Green	Detect 15q11.2 copy number	chr15:20,249,886-20,851,728
Abbott Molecular 15qter – Orange	Control for chr15	15qter

Table 3.2: Probes utilized in FISH experiments.

BAC-derived, fluorescently labeled probes (BlueGnome, Illumina, San Diego, CA) were used to label the distal and proximal region of our patient's *de novo* 2p and maternally-inherited 15q duplicated interval as detected by chromosomal microarray. Probes against the 2p and 2q subtelomeric regions (Abbott Molecular, Abbott Park, IL) were used to label chromosome ends to detect translocation events and subtelomeric deletions.

Primer	Use	Genetic Location (NBCI 37)	Sequence or Label
SOX11_cds_F	Amplification and sequencing of human *SOX11* CDS	chr2:5,832,395 (*SOX11*)	5'-GGG CCT CCG AGT TAA TAA AGG A-3'
SOX11_cds_R	Amplification and sequencing of human *SOX11* CDS	chr2:5,834,370 (*SOX11*)	5'-TCC AAT TTC TTT GCG TCA CGA-3'
SOX11_hseq_F	Sequencing of human *SOX11* CDS	chr2:5,832,896 (*SOX11*)	5'-CCC CGG GAG GCG CTG GAC ACG-3'
SOX11_hseq_R	Sequencing of human *SOX11* CDS	chr2:5,834,156 (*SOX11*)	5'-AGA AGT TCG CCT CCA GCC AGT C-3'
TaqMan Hs00525014_cn	Confirm 2p25.3 duplication	chr2:5,832,920 (*SOX11*)	FAM dye-labeled MGB
TaqMan Hs00839199_cn	Confirm 15q11.2 duplication	chr15:22,956,550 (*CYFIP1*)	FAM dye-labeled MGB
TaqMan Copy Number Reference Assay RNaseP	Control for copy number assays	chr14:20,811,565 (*RPPH1*)	VIC dye-labeled TAMRA

Table 3.3: Primers utilized in experiments.

Custom-designed primers (Invitrogen, Carlsbad, CA) were used for amplification, sequencing, and cloning of the human *SOX11* coding region. TaqMan qPCR primers with the proprietary RNaseP control reference assay were utilized for detection of *SOX11* copy number.

ClinGen Duplication	Wholly Contained within Proband's Duplicated Interval?	Citation	Phenotype(s)
nssv578818	yes	Kaminsky et al. 2011[28]	ASD
nssv576382	yes	Miller et al. 2010[29]	cerebral palsy
nssv582314	no	Miller et al. 2010	DD and/or SDMP
nssv578816	no	Kaminsky et al. 2011	DD and/or SDMP
nssv578817	no	Kaminsky et al. 2011	DD and/or SDMP
nssv578819	no	Kaminsky et al. 2011	DD and/or SDMP
nssv578820	no	Kaminsky et al. 2011	abnormality of skeletal system; DD
nssv578821	no	Kaminsky et al. 2011	DD and/or SDMP
nssv582360	yes	Miller et al. 2010	micrognathia; ID (specific)
nssv1415155	no	Miller et al. 2010	DD and/or SDMP
nssv1603658	yes	Miller et al. 2010	DD and/or SDMP
nssv1608835	no	Miller et al. 2010	DD
nssv3397014	no	Miller et al. 2010	DD
nssv3397118	no	Miller et al. 2010	ASD; OCD
nssv3397394	no	Miller et al. 2010	abnormal palmar creasing; agenesis of corpus callosum; arachnodactyly; feeding difficulties; flexion contractures; high palate; IUGR; malar flattening; premature birth; short, webbed neck; smooth philtrum

NB: Only duplications wholly or partially contained within our patient's duplicated interval were considered. These data were obtained using the ISCA database accessed via ClinGen (National Institutes of Health).
Key: ASD = autism spectrum disorder; DD = developmental delay; SDMP = other significant developmental or morphological phenotypes; ID = intellectual disability; OCD = obsessive-compulsive disorder; IUGR = intrauterine growth retardation

Table 3.4: Summary of relevant 2p duplication cases from ClinGen Database.

We queried the ClinGen Database (National Institutes of Health) for patients with pathogenic duplications which included at least a portion of our patient's duplicated interval. Observed phenotypes in these individuals indicate that 2p duplication is associated with developmental delay and craniofacial dysmorphic features.

DECIPHER Duplication	Wholly Contained within Proband's Duplicated Interval?	Citation	Phenotype(s)
285961	yes	none	anteverted nares; conductive HL; depressed nasal bridge; short nose; DD; thick vermillion border (upper lip)
286201	yes	none	abnormal finger flexion creases; clinodactyly; DD
287586	no	none	ASD; DD
287871	yes	none	ASD; holoprosencephaly; ID; abnormal facies
291403	no	none	DD; kyphoscoliosis; tall stature

NB: Only duplications wholly or partially contained within our patient's duplicated interval were considered. These data were obtained using DECIPHER v.9.4 (Wellcome Sanger Trust Institute).
Key: HL = hearing loss; DD = developmental delay; ASD = autism spectrum disorder; ID = intellectual disability

Table 3.5: Summary of relevant 2p duplication cases from DECIPHER Database.

We queried the DECIPHER Database (Wellcome Sanger Trust Institute) for patients with pathogenic duplications which included at least a portion of our patient's duplicated interval. Observed phenotypes in these individuals indicate that 2p duplication is associated with developmental delay and craniofacial dysmorphic features.

References

1. Verloes, A. Updated diagnostic criteria for CHARGE syndrome: a proposal. *American journal of medical genetics. Part A* **133A**, 306-308 (2005).

2. Vissers, L. E. *et al.* Mutations in a new member of the chromodomain gene family cause CHARGE syndrome. *Nature genetics* **36**, 955-957 (2004).

3. Lev, D. *et al.* CHARGE association in a child with de Novo chromosomal aberration 46, X,der(X)t(X;2)(p22.1;q33) detected by spectral karyotyping. *Journal of medical genetics* **37**, E47 (2000).

4. North, K. N., Wu, B. L., Cao, B. N., Whiteman, D. A. & Korf, B. R. CHARGE association in a child with de novo inverted duplication (14)(q22-->q24.3). *American journal of medical genetics* **57**, 610-614 (1995).

5. Wieczorek, D., Bolt, J., Schwechheimer, K. & Gillessen-Kaesbach, G. A patient with interstitial deletion of the short arm of chromosome 3 (pter-->p21.2::p12-->qter) and a CHARGE-like phenotype. *American journal of medical genetics* **69**, 413-417 (1997).

6. Al-Saffar, M., Lemyre, E., Koenekoop, R., Duncan, A. M. & Der Kaloustian, V. M. Phenotype of a patient with pure partial trisomy 2p(p23-->pter). *American journal of medical genetics* **94**, 428-432 (2000).

7. Aviram-Goldring, A. *et al.* Molecular cytogenetic studies in three patients with partial trisomy 2p, including CGH from paraffin-embedded tissue. *American journal of medical genetics* **91**, 74-82 (2000).

8. Engels, H. *et al.* The use of CGH in the analysis of constitutive de novo chromosome aberrations: examples and comparison with other molecular-cytogenetic methods. *Cytogenet Cell Genet* **85**, 174-174 (1999).

9. Fineman, R. M., Buyse, M. & Morgan, M. Variable phenotype associated with duplication of different regions of 2p. *American journal of medical genetics* **15**, 451-456 (1983).

10. Ishikawa, T., Inukai, K. & Kanayama, M. Paradoxical eyelid movement in trisomy 2p. *Pediatric neurology* **26**, 236-238 (2002).

11. Martinez-Juarez, A., Uribe-Figueroa, L., Quintana-Palma, M., Razo-Aguilera, G. & Sevilla-Montoya, R. Pure trisomy 2p syndrome in two siblings with an unbalanced translocation and minimal terminal 12q monosomy characterized by high-density microarray. *Cytogenetic and genome research* **142**, 249-254 (2014).

12. Stoll, C., Messer, J. & Vors, J. Equilibrated 2-14 translocation in a mother and partial trisomy of a pair of the short branches of a number 2 chromosome in 2 of her children. *Annales de genetique* **17**, 193-196 (1974).

13. Wakita, Y. *et al.* Duplication of 2p25: confirmation of the assignment of soluble acid phosphatase (ACP1) locus to 2p25. *Human genetics* **71**, 259-260 (1985).

14. Hale, C. L., Niederriter, A. N., Green, G. E. & Martin, D. M. Atypical phenotypes associated with pathogenic CHD7 variants and a proposal for broadening CHARGE syndrome clinical diagnostic criteria. *American journal of medical genetics. Part A* (2015).

15. Gadi, J. *et al.* The transcription factor protein Sox11 enhances early osteoblast differentiation by facilitating proliferation and the survival of mesenchymal and osteoblast progenitors. *The Journal of biological chemistry* **288**, 25400-25413 (2013).

16. Hargrave, M. *et al.* Expression of the Sox11 gene in mouse embryos suggests roles in neuronal maturation and epithelio-mesenchymal induction. *Developmental dynamics : an official publication of the American Association of Anatomists* **210**, 79-86 (1997).

17. Jankowski, M. P., Cornuet, P. K., McIlwrath, S., Koerber, H. R. & Albers, K. M. SRY-box containing gene 11 (Sox11) transcription factor is required for neuron survival and neurite growth. *Neuroscience* **143**, 501-514 (2006).

18. Paul, M. H., Harvey, R. P., Wegner, M. & Sock, E. Cardiac outflow tract development relies on the complex function of Sox4 and Sox11 in multiple cell types. *Cellular and molecular life sciences : CMLS* **71**, 2931-2945 (2014).

19. Pillai-Kastoori, L. *et al.* Sox11 is required to maintain proper levels of Hedgehog signaling during vertebrate ocular morphogenesis. *PLoS genetics* **10**, e1004491 (2014).

20. Potzner, M. R. *et al.* Sequential requirement of Sox4 and Sox11 during development of the sympathetic nervous system. *Development* **137**, 775-784 (2010).

21. Sock, E. *et al.* Gene targeting reveals a widespread role for the high-mobility-group transcription factor Sox11 in tissue remodeling. *Mol Cell Biol* **24**, 6635-6644 (2004).

22. Wang, Y., Lin, L., Lai, H., Parada, L. F. & Lei, L. Transcription factor Sox11 is essential for both embryonic and adult neurogenesis. *Developmental dynamics : an official publication of the American Association of Anatomists* **242**, 638-653 (2013).

23. Feng, W. *et al.* The chromatin remodeler CHD7 regulates adult neurogenesis via activation of SoxC transcription factors. *Cell Stem Cell* **13**, 62-72 (2013).

24. Tsurusaki, Y. *et al.* De novo SOX11 mutations cause Coffin-Siris syndrome. *Nature communications* **5**, 4011 (2014).

25. Choi, A. *et al.* Novel mutations in PXDN cause microphthalmia and anterior segment dysgenesis. *European journal of human genetics : EJHG* **23**, 337-341 (2015).

26. Khan, K. *et al.* Homozygous mutations in PXDN cause congenital cataract, corneal opacity, and developmental glaucoma. *American journal of human genetics* **89**, 464-473 (2011).

27. Meyer, K. J., Axelsen, M. S., Sheffield, V. C., Patil, S. R. & Wassink, T. H. Germline mosaic transmission of a novel duplication of PXDN and MYT1L to two male half-siblings with autism. *Psychiatric genetics* **22**, 137-140 (2012).

28. Kaminsky, E. B. *et al.* An evidence-based approach to establish the functional and clinical significance of copy number variants in intellectual and developmental disabilities. *Genetics in medicine : official journal of the American College of Medical Genetics* **13**, 777-784 (2011).

29. Miller, D. T. *et al.* Consensus statement: chromosomal microarray is a first-tier clinical diagnostic test for individuals with developmental disabilities or congenital anomalies. *American journal of human genetics* **86**, 749-764 (2010).

Chapter IV: SOX11 and CHD7 Act in a Common Gene Regulatory Network to Promote Inner Ear Development[1]

Abstract

Development of the inner ear depends on accurate spatiotemporal control of gene expression via transcriptional networks in the cell nucleus. SoxC transcription factors (i.e. SOX4, SOX11, and SOX12) are a class of proteins that are emerging as critical mediators of inner ear morphogenesis. Prior studies in neural stem cells have demonstrated that SOX11 is a genetic target of CHD7, an ATP-dependent chromatin remodeler with roles in transcriptional regulation. Haploinsufficiency of *CHD7* results in CHARGE syndrome, which presents with hearing loss and balance impairment related to inner ear dysplasia. The specific mechanisms by which loss of *CHD7* results in inner ear malformation are incompletely understood. Here, we explored potential common molecular genetic pathways of *Sox11* and *Chd7* in the developing mouse inner ear. Using histologic analyses in mice, we discovered that *Sox11* is necessary for lateral and posterior semicircular canal morphogenesis through control of cellular proliferation around the canal fusion plate. Additionally, *Sox11* regulates expression of *Bmp4* in the presumptive lateral crista ampullaris. Finally, homozygous loss of *Chd7* results in reduced expression of otic *Sox11*, providing insight into the genetic regulation of lateral semicircular canal development. These studies suggest that *Sox11* is a putative effector of CHD7 function in the developing

ear, and that a *Chd7-Sox11* regulatory network serves to promote both neural and otic development.

Introduction

The mammalian inner ear receives both external auditory and vestibular signals, which are transmitted to the brain via the eighth cranial nerve to generate the sensations of hearing and balance. The inner ear is a highly evolutionarily conserved and remarkable example of three-dimensional morphogenesis which results from rapid and accurate cellular proliferation and differentiation. Inner ear morphogenesis begins with the formation of the otic placode from the pre-placodal region[1-3]. Following this, the otic placode elongates along the ectodermal ridge and invaginates to form the optic cup and ultimately the otic vesicle contained between the ectodermal layer and the lateral wall of the neural tube. As embryogenesis progresses, the otic vesicle grows and segregates into the various epithelial compartments (e.g. semicircular canals, cochlea) and sensory structures (sensory cristae and maculae, the organ of Corti) of the inner ear. Coordination of this complex developmental process depends on accurate spatiotemporal control of gene expression via transcriptional networks in the cell nucleus.

SoxC transcription factors are a class of proteins emerging as critical mediators of inner ear morphogenesis. In humans, heterozygous mutations in *SOX11* cause a phenotypically mild, rare variant of Coffin-Siris syndrome[4]. Individuals with Coffin-Siris syndrome, including those with mutations in *SOX11*, generally exhibit craniofacial dysmorphisms, microcephaly, posteriorly rotated ears, intellectual disability, endocrine deficiencies, congenital heart defects, and hypo/aplasia of the fifth finger/toenails[5-10].

Developmental delay is common in Coffin-Siris and some children exhibit autism spectrum disorder and sensorineural hearing loss[6,8,11]. Most cases of Coffin-Siris syndrome have been attributed to mutations in one of the five subunits found in the human SWI/SNF (BAF) complex (*ARID1A/B* and *SMARCA4/B1/E1*), placing this disorder within the rapidly expanding group of neurodevelopmental disorders caused by defects in chromatin remodeling with significant implications for embryologic development[8-10,12,13].

Studies in the developing mouse highlight the importance of SOX11 for proper embryogenesis. *Sox11* germline mutant mice exhibit abnormalities in craniofacial, axial skeletal, cardiopulmonary, and neurologic structures[14]. Interestingly, concomitant loss of another SoxC transcription factor, *Sox4*, mimics, and in some cases, amplifies the various developmental defects observed in *Sox11* deficient mice. Little is known about the role of *Sox11* in the developing ear despite its broad expression in the zebrafish and chicken ear[15,16]. SOX11 and SOX4 were recently studied in the developing murine utricle and found to be important for proliferation in the utricular macula[17]. *Sox11* deficiency also led to reduced proliferation of otic sensory progenitor cells and impaired differentiation of otic progenitors into hair cells (versus supporting cells).

In mouse central nervous system neural stem cells, *Sox11* expression is regulated by CHD7, an ATP-dependent chromatin remodeling protein mutated in human CHARGE syndrome[18,19]. CHD7 functions through nucleosome sliding, exposing regions of genomic DNA to the milieu of trans-acting factors critical for maintenance of gene expression[20,21]. As in Coffin-Siris syndrome, individuals with CHARGE syndrome exhibit complex craniofacial anomalies and sensory impairments, including hearing and balance dysfunction[22-24]. Specifically, *CHD7* haploinsufficiency leads to abnormalities of the

outer, middle, and inner ear, resulting in difficulties with sound capture, transduction, and processing. Individuals with CHARGE syndrome and *CHD7* mutations exhibit highly penetrant lateral and posterior semicircular canal abnormalities manifesting delayed gross motor development and balance disturbances[25]. Studies in *Chd7* mutant mice largely replicate the otic findings reported in humans, with *Chd7* haploinsufficiency resulting in highly penetrant (over 95% of mutant mice) hearing loss, lateral and posterior semicircular canal malformations, and vestibular sensory epithelial innervation defects[26-29].

The specific molecular genetic mechanisms by which CHD7 impacts inner ear development are incompletely understood. Given that CHD7 regulates *Sox11* expression in mouse neural stem cells, and SOX11 is critical for utricular development, we postulated that SOX11 may have a role as a downstream effector of CHD7 during semicircular canal morphogenesis. Specifically, we hypothesized that the highly penetrant inner ear malformations present in *Chd7* haploinsufficient mice may be recapitulated in mice with loss of *Sox11*. We demonstrate here that loss of *Sox11* results in malformation of the developing lateral and posterior cristae and associated semicircular canals. Specifically, loss of both copies of *Sox11* results in fusion plate formation failure, periotic mesenchymal proliferation defects, and misexpression of effector genes critical for canal development. We also show that loss of *Chd7* results in misexpression of *Sox11* in the mouse otocyst, likely impacting canal specification during otic morphogenesis. Our results provide evidence for a *Chd7-Sox11* regulatory network crucial for both neural and otic development, and provide additional insights into the pathophysiology of both CHARGE and Coffin-Siris syndromes.

Methods

Mouse husbandry

Sox11$^{+/-}$ mice were obtained from L. Lei (University of New England), maintained on a C57BL/6J X 129/Sv mixed background, and genotyped as described[30]. *Chd7*$^{Gt/+}$ mice were maintained on a C57BL/6J X 129/Sv mixed background, and genotyped as described[31]. All mouse husbandry and experimental handling were approved by and performed according to the standards of the University of Michigan University Committee on the Use and Care of Animals (UCUCA).

Histology

Timed pregnancies were established between *Sox11*$^{+/-}$ or *Chd7*$^{Gt/+}$ mice with the morning of copulatory plug identification designated as E0.5. E10.5-E14.5 embryos were collected following cervical dislocation and hysterectomy of the pregnant dam, dehydrated (1X PBS – 25% EtOH – 50% EtOH – 70% EtOH), and embedded in paraffin (30-90 min cycles dependent on age). Paraffin embedded embryos were sectioned at 7 µm, mounted on Superfrost Plus slides (ThermoFisher Scientific, Waltham, MA) and further processed according to experimental design. Sections were stained with hematoxylin and eosin (H&E) (Sigma, St. Louis, MO) as previously described[31]. Sections were photographed by light microscopy on a Leica upright DMRB microscope and processed in Photoshop CS6 (Adobe, San Jose, CA). For H&E staining, multiple sections from at least three ears (N=3) of each genotype were tested.

Anti-CHD7, Anti-SOX11, and Anti-Cleaved Caspase-3 (D175) Immunofluorescence

Embryos were prepared as described above. Paraffin sections (7 µm) were stained with 1:2500 anti-SOX11 (in TSA block, #sc-17347 Santa Cruz Biotechnology, Dallas, TX), 1:100 anti-CHD7 (in TSA block, #6505 Cell Signaling Technology, Danvers, MA), or 1:100 anti-cleaved Caspase-3 (D175) (in TSA block, #9661 Cell Signaling Technology) antibodies. Anti-SOX11 stained sections were counterstained with 1:200 biotinylated horse anti-goat IgG secondary antibody (in Tyramide Signal Amplification (TSA) block, BA-9500, Vector Laboratories, Burlingame, CA). Strepavidin-horseradish peroxidase (1:100 in TSA block) was added to slides and Alexa 488 tyramide (1:100 in Amplification Buffer) was applied to generate indirect fluorescence (Molecular Probes, Grand Island, NY). Anti-CHD7 stained sections were counterstained with 1:200 goat anti-rabbit Alexa Fluor 555 (#A21429 ThermoFisher Scientific). Anti-cleaved Caspase-3 (D175) stained sections were counterstained with 1:200 goat anti-rabbit Alexa Fluor 555 (#A21429 ThermoFisher Scientific). All immunofluorescence processed sections were counterstained with 1:2500 DAPI (#D1306 ThermoFisher Scientific) and photographed by fluorescence microscopy on a Leica upright DMRB microscope followed by Photoshop CS6 (Adobe) processing. For anti-SOX11 and anti-CHD7 antibody staining, multiple sections from at least three ears (N=3) of each genotype were tested. For anti-cleaved Caspase-3 (D175) antibody staining, serial sections through the vestibular structures of at least four ears (N=4) of each genotype were tested.

Anti-Laminin Immunochemistry

Sections were stained with 1:100 rabbit anti-laminin antibody (in TSA block, Abcam, Cambridge, UK), and counterstained with 1:250 biotinylated goat anti-rabbit antibody (in TSA block, #BA-1000, Vector Laboratories). Immunoperoxidase detection of the biotin antigen was performed using the Vectastain Elite ABC Kit (Vector Laboratories). Finally, slides were developed using 3,3'-diaminobenzidine (DAB, Sigma) for 5 minutes. Sections were photographed by light microscopy on a Leica upright DMRB microscope and processed in Photoshop CS6 (Adobe). For anti-laminin staining, multiple sections from three ears (*N*=3) of each genotype were tested.

In situ hybridization

Sections were prepared as described above and subjected to *in situ* hybridization using digoxigenin-labeled riboprobes as previously described[32]. Riboprobes used included *Bmp4* (55°C, gift of Brigid Hogan), *Lrig3* (55°C, gift of Lisa Goodrich), *Ntn1* (60°C, gift of Lisa Goodrich), and *Otx1* (65°C)[28]. Sections were photographed by light microscopy on a Leica upright DMRB microscope and processed in Photoshop CS6 (Adobe). For each anti-sense RNA probe, multiple sections from at least four ears (*N*=4) of each genotype were tested, except where noted in the Results.

BrdU proliferation studies

Pregnant *Sox11*$^{+/-}$ dams were intraperitoneally (IP) injected with 100 mg/kg 0.2 µm filter-sterilized 5-bromo-2'-deoxyuridine (BrdU) (#B5002, Sigma) at 11.5, 12.0, and 12.5 days post-conception. Sections from E12.0-E12.5 *Sox11*$^{+/+}$ and *Sox11*$^{-/-}$ embryos were

prepared as described above and stained with 1:200 rat anti-BrdU (in TSA block, Bio-Rad Antibodies, Raleigh, NC). Sections were secondarily labeled with 1:200 rabbit anti-rat Alexa Fluor 488 (ThermoFisher Scientific), counterstained with DAPI (ThermoFisher Scientific), and mounted in aqueous solution. Sections were photographed by fluorescence microscopy on a Leica upright DMRB microscope and processed in Photoshop CS6 (Adobe). For anti-BrdU staining, serial sections through the vestibular structures of at least five ears (N=5) of each genotype were tested. Quantification of BrdU-positive cells was performed using ImageJ (NIH, Bethesda, MD). An unpaired Student's t-test with Welch correction was performed on pooled counts between age-matched genotypes to determine statistical significance ($p<0.05$).

Paintfill analyses

E11.5-E14.5 embryos were collected, washed in 1X PBS, placed in Bodian's fixative, cleared using 100% methyl salicylate, and filled with 3% titanium dioxide/47% methyl salicylate/50% 1X PBS[28,33]. E12.5-E14.5 heads were subjected to craniotomy and excision of the brain prior to filling the ears.

RNA isolation and qRT-PCR analyses

E10.5 (N=3) and E12.5 (N=3) embryos were harvested into 1X PBS on ice. Immediately following collection, embryos were bisected along the sagittal midline. Otic tissue was microdissected bilaterally (with care taken to remove periotic mesenchyme) into 100 µL of 1X PBS, spun at 100 rpm for 10 seconds, micropipette aspirated, and flash-frozen on dry ice. The remaining tissue was collected for genotyping. Total RNA was

isolated using the RNAqueous-Micro RNA Isolation Kit (Ambion, Austin, TX) and treated with DNaseI prior to cDNA synthesis. cDNA was generated using the SuperScript First-Strand cDNA Synthesis System with oligo(dT) primers (Invitrogen, Carlsbad, CA). Gene expression levels were assayed using the TaqMan system (Applied Biosystems, Foster City, CA). TaqMan probes for *Bmp2*, *Bmp4*, *Chd7*, *Lrig3*, *Ntn1*, *Otx1*, *Otx2*, and *Sox11* are listed in Table 4.1. *Gapdh* probe was used as a reference control. Each sample was run in quadruplicate using a StepOne-Plus Real-Time qPCR System (Applied Biosystems). Fold change of the assayed gene relative to *Gapdh* was defined as $2^{-\Delta\Delta C_T}$. An unpaired *t*-test with Welch correction was performed on *Gapdh*-normalized fold change values to determine statistical significance ($p<0.05$).

Results

Sox11 mutant mice have abnormal semicircular canals

Sox11-null mice exhibit cardiac, skeletal, craniofacial, and ocular malformations, consistent with a broad role for this transcription factor in embryogenesis[14]. Interestingly, *Sox11* mutant mouse phenotypes resemble those found in *Chd7* haploinsufficient mice and in humans with *CHD7* mutations and CHARGE syndrome[19,31,34]. Loss of *Sox11* results in brain hypoplasia as a result of early neural progenitor cell ablation[30]. Notably, CHD7 regulates *Sox11* expression in neural stem cells and is required for proliferation of neural progenitors in the developing mouse brain[18]. Study of SOX11 in the inner ear has been limited to the utricular macula, where similar proliferation defects in otic progenitors were observed with homozygous loss of *Sox11*[17]. Given these reports, we hypothesized that loss of *Sox11* may disrupt semicircular canal development.

We examined E11.5-E14.5 *Sox11*$^{+/+}$, *Sox11*$^{+/-}$, and *Sox11*$^{-/-}$ inner ears by paintfill (Figure 4.1A-4.1L). In all *Sox11*$^{+/+}$ ears (*N*=18), we observed normal anatomic development from the initial post-otocyst phase (E11.5) to completion of the major morphologic development of the endolymphatic duct, semicircular canals and associated cristae ampullaris, and cochlea by E14.5 (Figure 4.1A-4.1D). By contrast, we observed lateral semicircular canal narrowing and truncation in 42% of E14.5 *Sox11*$^{+/-}$ ears (*N*=11/26) tested (Figure 4.1E-4.1H). In 31% of E14.5 *Sox11*$^{+/-}$ ears (*N*=8/26), we also observed structural malformations or absence of the posterior semicircular canal. An increased frequency of semicircular canal defects was noted in *Sox11*$^{-/-}$ ears (*N*=12/12) compared to *Sox11*$^{+/-}$, with 100% of tested ears exhibiting both lateral and posterior canal malformations (Figure 4.1K-4.1L). Interestingly, in ears with malformed lateral and posterior canals, the associated cristae were predominantly found to be small or absent. While the overall size of *Sox11*$^{+/-}$ ears was similar to wild type, there was moderate widening of the canals and endolymphatic ducts in many ears. Closer examination of E11.5 *Sox11*$^{-/-}$ ears revealed smaller rostral-caudal size with less-developed dorsal structures, including the endolymphatic duct (Figure 4.1I). There were no consistent differences in severity or type of lateral or posterior semicircular defects between left and right ears.

As some individuals with CHARGE syndrome exhibit under-coiling of the cochlea, known as Mondini malformation, we also used the paintfill technique to examine *Sox11* mutant mice for defects in cochlear structure[35]. None of the E14.5 *Sox11* mutant ears examined by paintfill (*N*=0/38) exhibited cochlear coiling defects (Figure 4.1D, 4.1H, 4.1L).

Lateral canal fusion plate formation is impaired in Sox11 deficient mice

The three-dimensional semicircular canal is generated from a small dorsal portion of the spherical otocyst. This sheet of cells comprising this dorsal portion of the otocyst invaginates towards the center of the otocyst and allows for the approximation of two cellular planes[36,37]. When these planes are in close proximity, a proportion of the cells undergoes an epithelial-to-mesenchymal transition (EMT) precisely governed by opposing gradients of the pro-EMT molecule NETRIN-1 and the anti-EMT molecule LRIG3[38-41]. Where *Lrig3* is expressed, *Ntn1* expression is repressed, allowing cells to remain epithelialized and form the semicircular canal lumen. In cells expressing *Ntn1*, the underlying basement membrane is broken down, which can be visualized by observing disruption to the fibrous protein Laminin. *Ntn1*-positive cells then mobilize and intermingle, forming a single column, or fusion plate, that delineates the boundary of the developing canal. Disruption of fusion plate formation results in malformations of the canals, including complete aplasia in the most severe cases[39]. Given the observed lateral and posterior semicircular canal defects in *Sox11*-null embryos (varying from truncation to aplasia), we hypothesized that proper expression of *Sox11* is critical for canal fusion plate formation.

To test this hypothesis, we examined transverse sections of E11.5 and E12.5 mouse inner ears by hematoxylin and eosin staining. In the mouse, posterior semicircular canal morphogenesis begins around E11.0 with cellular proliferation along the dorsolateral wall of the otocyst and formation of the posterior canal projection (Figure 4.2A). By E12.0, the projection has begun to approximate the final shape of the posterior semicircular canal and by E12.5, the fusion plate is fully formed, separating the canal from the remainder of the

otocyst (Figure 4.2C). In E11.5 *Sox11*-null ears, the canal projection is markedly hypoplastic (Figure 4.2B) and at E12.5 no fusion plate is present (Figure 4.2D). A similar process is observed during lateral semicircular canal formation (data not shown). Thus, posterior and lateral semicircular canal formation is arrested with homozygous loss of *Sox11*, resulting in incomplete canal formation by E12.5.

Based on these findings, we postulated that *Sox11* may be required for proper spatiotemporal expression of *Ntn1* and/or *Lrig3*, genes critical for fusion plate formation[38,39]. *In situ* hybridization at E12.5 showed no observable differences in *Ntn1* between *Sox11* wild type and null ears (Figure 4.2E-4.2F), suggesting that misexpression these EMT regulators is not sufficient to cause the fusion plate delay. We then asked whether the integrity of the *Sox11*-null basement membrane may be altered, given that signaling between cells in the surrounding mesenchyme and developing epithelium is critical for EMT success. We observed normal anti-laminin-DAB staining along *Ntn1*-negative regions in E12.5 *Sox11*-wild type and null ears, indicating that *Sox11* is not necessary for proper basement membrane integrity at the fusion plate (Figure 4.2G-4.2H).

Given that fusion plate gene expression was unaffected by loss of *Sox11*, we next tested whether cellular proliferation within the lateral and posterior canal projections was impaired in *Sox11* mutant ears. We crossed $Sox11^{+/-}$ mice to generate E12.0 and E12.5 timed pregnancies and pulsed each pregnant dam with BrdU for 30 minutes prior to embryo harvesting. Transverse sections through the developing ear from wild type and *Sox11*-null embryos were stained with anti-BrdU antibody and BrdU-positive cells in the tissue space between the lateral border of the embryo and the lateral border of the dorsal ear were counted. Using a modification of the method described by Salminen et al. (2000), BrdU-

positive cells in the medial half of this region were compared with the total (medial + lateral) BrdU-positive cell population to determine the proportion of cells proliferating within the lateral projection (Figure 4.3A-4.3B)[39]. The number of BrdU-positive cells in *Sox11*-null ears was statistically significantly reduced by 19% at E12.0 compared to wild type ears and by 17% E12.5, indicating that cellular proliferation in the medial compartment is impaired with loss of *Sox11* (Figure 4.3C). By contrast, loss of *Sox11* did not affect the number of apoptotic cells observed via anti-cleaved caspase-3 (D175) staining within the developing canal epithelia and surrounding mesenchyme (data not shown). Together, these data suggest that *Sox11* is necessary for cell proliferation within semicircular canal projections, which allow the walls of the fusion plate to approximate one another and form the semicircular canal lumen.

Sox11 dosage is critical for proper gene expression in the developing ear

Specification of the semicircular canals occurs early in otic development, with all three canals originating from the dorsolateral compartment of the otocyst[2,42]. This process requires both accurate spatial orientation and localization of differentiating cells as well as precise temporal control of the transcriptional networks involved. In the mouse, the otocyst is fully formed by E10.5 and semicircular canal buds are present by E11.5. Specifically, dorsal-ventral patterning, as specified by co-repressive WNT and SHH signaling during early ear development, is critical for specification of two canal pouches: the vertical (corresponding to the anterior and posterior canals) and the horizontal (corresponding to the lateral canal) canal pouches[43]. These vertical and horizontal canal pouches are marked by the LIM-domain transcriptional regulator LMO4[44]. LMO4 regulates several

downstream effectors during inner ear development, including *Fgf10* and *Bmp2/4*. FGF signaling (principally FGF10) marks each (anterior, posterior, and lateral) canal prosensory zone contained within its respective canal pouch[45]. These prosensory zones develop into their respective crista ampullaris, explicitly marked by FGF10 and BMP4. Adjacent to each crista, a canal genesis zone develops which expresses *Bmp2*[45,46]. The epithelial canal structure emanates from the canal genesis zone to form the mature semicircular canal.

Early disruption of the TGF-beta signaling pathway, specifically expression of *Bmp2/4*, results in ablation of the lateral canal in mice[47]. Further, the transcription factors OTX1 and OTX2 have been implicated specifically in lateral canal morphogenesis, with corresponding germline null mice exhibiting failure of lateral canal development[48]. Additionally, the developing posterior semicircular canal is dependent on TGF-beta signaling and expression of *Bmp4*[49]. The homeobox-containing transcription factor *Gbx2* is required for posterior canal development[50].

CHD7 serves as a crucial regulatory protein both during the specification of the prosensory domain at E10.5-E11.5 and during the expansion of the lateral semicircular canal genesis zone at E11.5-E12.5. Loss of *Chd7* results in downregulation of several genes important in prosensory domain specification and crista formation, including *Fgf10* and *Jag1*[28]. One day later, loss of *Chd7* is associated with disruption to *Bmp2* and *Bmp4* signaling within the crista ampullaris and the associated canal genesis zones. CHD7 is also necessary for *Otx1* expression, further highlighting its role in promoting development of the lateral semicircular canal[28].

We hypothesized that SOX11, acting as a transcription factor with broad influence on gene expression, may regulate expression of one or more of these downstream genes

critical for canal development. To test this, we microdissected ears from *Sox11* wild type and null embryos at the E10.5 otocyst stage and used TaqMan qRT-PCR chemistry to query gene expression. We uncovered marked reductions in *Bmp2*, *Otx1*, and *Otx2* transcripts in *Sox11*$^{-/-}$ ears compared to wild type (Figure 4.4). Interestingly, at E12.5, expression of *Otx2* was higher in *Sox11*-null ears versus wild type. *Bmp4* expression was elevated in *Sox11*$^{-/-}$ ears at both time points. We further queried *Ntn1* and *Lrig3* expression at both time points. Finally, we observed that *Chd7* levels were mildly upregulated with loss of *Sox11* at E10.5 and E12.5.

Bmp4, *Otx1* and *Otx2* exhibit highly restricted expression domains within the developing otocyst. *Bmp4* expression is specifically located at the lateral aspect of the dorsoventral boundary delineating the presumptive anterior and lateral cristae[45]. We observed normal expression of *Bmp4* at E10.5 in wild type ears; however, its expression was expanded dorsally in *Sox11*-null ears (Figure 4.5A-4.5B). *Otx1/2* expression is located within the ventrolateral quadrant of the E10.5 otocyst[48,51]. *Otx1* is required for lateral semicircular canal development in the chicken and mouse[48]. In contrast, *Otx2* is thought to be dispensable for lateral canal development, but required for ventral otic patterning[51]. Notably, expression of *Otx2*, but not of *Otx1*, is reduced with loss of *Chd7*[28,29]. Somewhat surprisingly, we observed that loss of *Sox11* results in no appreciable changes to the expression pattern of either *Otx1* or *Otx2* in E10.5 ears by *in situ* hybridization (Figure 4.5C-4.5F).

By E11.5, *Bmp4* expression clearly defines the regions of the presumptive anterior and lateral cristae, with an intermediate region of relatively reduced *Bmp4* expression delineating the segmentation of the two cristae[52]. Given the expanded dorsal expression of

Bmp4 in the E10.5 otocyst, we examined *Bmp4* expression in *Sox11*$^{-/-}$ E11.5 otocysts. In wild type ears (*N*=2), *Bmp4* was highly expressed in the presumptive anterior crista in the rostral otocyst (Figure 4.6A). *Bmp4* transcript was also present at the caudal end of the otocyst demarcating the presumptive lateral crista (Figure 4.6C). In the midline, *Bmp4* expression was absent, confirming adequate segmentation of the anterior and lateral cristae (Figure 4.6B). In *Sox11*-null ears (*N*=2), the *Bmp4* expression domain was continuous along the rostral-caudal aspect of the lateral wall (Figure 4.6D-4.6F). These results indicate an important role for *Sox11* in restricting *Bmp4* expression along the rostral-caudal axis at the level of the developing anterior and lateral cristae ampullae.

Sox11 expression depends on Chd7 dosage but not vice versa

Lateral and posterior semicircular canal hypo/aplasia are highly penetrant with *CHD7* haploinsufficiency and CHARGE syndrome[26,29,53]. Loss of *Chd7* disrupts expression of several genes critical for canal formation, including *Bmp2/4* and *Otx1*, and results in fusion plate formation failure as evident by delayed *Ntn1* expression[28]. Additionally, CHD7 positively regulates *Sox11* in mouse neural stem cells[18]. Given these data, we hypothesized that CHD7 may also positively regulate *Sox11* during otic development.

By qRT-PCR, we detected a 60% reduction in *Sox11* transcript levels in E10.5 microdissected *Chd7*$^{Gt/Gt}$ inner ears compared to *Chd7*$^{+/+}$ and *Chd7*$^{Gt/+}$ (Figure 4.7). We also assayed SOX11 protein by immunofluorescence in E10.5 *Chd7*$^{+/+}$, *Chd7*$^{Gt/+}$, and *Chd7*$^{Gt/Gt}$ embryos. SOX11 protein was distributed along the dorsolateral, ventrolateral, and ventromedial walls of the *Chd7*$^{+/+}$ otocyst, with expression highest in the ventrolateral

quadrant (Figure 4.8A-4.8B). SOX11 protein localization was expanded laterally in the *Chd7*$^{Gt/+}$ mutant otocyst (Figure 4.8C-4.8D) and was absent in the *Chd7*$^{Gt/Gt}$ ear (Figure 4.8E-4.8F). These observations suggest that otic expression of *Sox11* is dependent on expression of *Chd7* in the ear. Consistent with this, E10.5 *Sox11*$^{-/-}$ ears exhibited robust CHD7 staining in the ventral otocyst and vestibulocochlear (CN-VIII) ganglion (Figure 4.8G-4.8H).

To test whether *Chd7* and *Sox11* operate with the same genetic pathway, we crossed mice with heterozygous deletions and analyzed inner ears by the paintfill technique. *Chd7*$^{Gt/+}$*;Sox11*$^{+/-}$ ears exhibited malformed lateral (*N*=12/12; 100%) and posterior (*N*=10/12; 83%) semicircular canal structures similar to those observed in *Chd7*$^{Gt/+}$ ears (*N*=6) (Figure 4.9A-4.9C). The remaining structures, including the endolymphatic duct, anterior semicircular canal, and cochlea, were unaffected in *Chd7;Sox11* double heterozygotes.

Discussion

We showed that homozygous loss of *Sox11* results in malformation of the developing lateral and posterior cristae and associated semicircular canals. Specifically, *Sox11* deficiency results in fusion plate formation failure, periotic mesenchymal proliferation defects, and misexpression of *Bmp4* within the region containing the nascent anterior and lateral cristae ampullae. We also show that loss of *Chd7* results in misexpression of *Sox11* in the mouse otocyst, likely impacting canal specification during otic morphogenesis. Our results provide evidence for a *Chd7-Sox11* regulatory network crucial for both neural and otic development.

Sox11 is required for lateral and posterior semicircular canal development

Germline loss of one or both copies of *Sox11* resulted in malformations to the lateral and posterior semicircular canals by E14.5. These malformations are readily apparent by paintfill analyses and via histologic staining, demonstrating delay of fusion plate formation by E12.5 for both canals. Loss of *Sox11* also resulted in delay of fusion plate formation but no changes to expression of *Ntn1* by *in situ* hybridization, suggesting an alternate mechanism underlying fusion plate formation failure in *Sox11*$^{-/-}$ mice. Development of the fusion plate requires proliferation of the adjacent periotic mesenchyme, which in turn allows invagination of the cellular sheet to approximate a fusion plate[39]. Quantification of the periotic mesenchyme adjacent to the dorsolateral quadrant of the developing E12.0 and E12.5 ear revealed moderate reductions in proliferating cells in the *Sox11*$^{-/-}$ ear relative to wild type. It has been reported that *Sox11* is required for cellular proliferation, including neural progenitors in the developing brain and proto-sensory cells in the utricular maculae[17,30]. Our results indicate disruption to cellular proliferation in the periotic mesenchyme of *Sox11*-null mice. Given that *Sox11*-null mice exhibit moderate decreases in periotic cellular proliferation but relatively severe defects in lateral and posterior canal formation, it is possible that *Sox11* may have other roles in inner ear development beyond promoting cell proliferation.

Our results also build on a previous study which reported normal vestibular structures in *Sox11* mutant mice[17]. In their study, Gnedeva and Hudspeth reported normal inner ear anatomy in E18.5 *Pax2-Cre;Sox11*$^{f/f}$ conditional knockout mice. One possible explanation for the discrepancy between their study and ours is that they used a whole-mount preparatory technique with lower resolution than paintfill. Alternatively, there may

be differences in *Sox11* dosage, *Cre* expression and deletion efficiency, or genetic background. While *Pax2* is expressed in the early otic anlage, use of *Pax2-Cre* to delete *Sox11* may result in late, mosaic, or incomplete deletion of *Sox11* in the periotic mesenchyme that is not sufficient to disrupt canal development[54]. If true, then germline loss of *Sox11* may be associated with temporally and spatially restricted requirements that could be recovered by gene re-introduction or regulation later in development (at least by E18.5). This is an intriguing possibility and is consistent with previous studies showing that semicircular canal morphogenesis is highly dependent on accurate timing of gene expression[1,28,42]. Further study of *Sox11* conditional and mutant mice will be helpful in establishing how the specific timing of *Sox11* function contributes to semicircular canal formation.

Sox11 function in the lateral semicircular canal

Analysis of *Sox11*$^{-/-}$ ears revealed reduced *Bmp2* expression and increased *Bmp4* expression. Complementary *in situ* hybridization studies showed expanded *Bmp4 i*n the dorsolateral quadrant of the E10.5 otocyst. Further, preliminary analysis of *Bmp4* at E11.5 indicated that this expansion obscures the segmentation of the anterior and lateral cristae, a process demarcated by incremental *Bmp4* expression along the rostral-caudal axis at the dorsoventral boundary[52]. Interestingly, our paintfill analyses revealed small or absent cristae associated with the developing lateral canal in the majority of *Sox11*-null ears. The observed disruption to *Bmp4* expression observed at E10.5 and E11.5 did not disrupt *Otx1* expression by *in situ* hybridization. This was surprising as our qRT-PCR results indicated

severe reductions to *Otx1* expression at both E10.5 and E12.5. Together, these findings suggest a role for *Sox11* in proper segmentation of the lateral crista from the anterior crista.

Expression of *Bmp4* in the lateral canal crista is thought to drive expression of *Bmp2* in the adjacent canal genesis zone[45,46]. Our quantitative RT-PCR results indicate that *Bmp2* levels are reduced in *Sox11* mutant ears, consistent with delayed or failed specification of the lateral canal genesis zone. Further examination of *Bmp2* expression in *Sox11* mutant inner ears is necessary to conclusively determine how loss of *Sox11* impacts specification of the canal genesis zone.

Sox11 does not contribute to ventral otic patterning

Like all anatomic development, inner ear morphogenesis occurs in three dimensions. Within the inner ear, the dorsal-ventral boundary separates the vestibular and auditory components[2,3]. The ventral half of the developing ear gives rise to the cochlea, which contains the organ of Corti responsible for detection of sound. Examination of *Sox11* mutant mice by paintfill revealed no disruptions to cochlear development. Further, the cells of the vestibulocochlear (CN-VIII) ganglion were present in appropriate sections through the *Sox11* mutant ear at time points E10.5, E11.5, and E12.5 (data not shown). By contrast, previous studies suggest that *Sox4* and *Sox11* together are required for proper cochlear hair cell morphogenesis and hearing[17]. However, these authors reported minimal defects in cochlear anatomy and organ of Corti cellular composition. Our findings concur with these previously reported results.

Chd7 and Sox11 may reside within a common genetic pathway crucial for semicircular canal development

As an ATP-dependent chromatin remodeler, *Chd7* has wide-ranging effects on gene expression in the developing ear (unpublished data)[28,29]. Mutations in *Chd7* and *Sox11* independently generate similar phenotypes across multiple organ systems in the developing mouse, including ocular anterior segment dysgenesis and retinal differentiation, simplication of the nasal passageways, oropharyngeal clefting, septal heart defects, and broad cortical neurogenic deficits[17,27-29,31,34,55-62]. A recent report suggests that CHD7 regulates adult neurogenesis via direct binding to regulatory regions upstream of *Sox11*[18]. From these data, we anticipated that *Chd7* and *Sox11* might share a common regulatory pathway in the developing ear. Our data suggest that loss of *Chd7* impairs expression of *Sox11* in the E10.5 otocyst and that *Chd7;Sox11* double heterozygotes exhibit similar defects in lateral and posterior semicircular canal morphogenesis. Further, we observed a mild-moderate increase in *Chd7* transcript in *Sox11*-null E10.5 and E12.5 microdissected ears, indicating that a potential feedback mechanism could exist between these two genes.

By qRT-PCR and *in situ* hybridization, we explored the expression of four genes in *Sox11* mutant ears. Critically, these four genes, *Bmp4*, *Ntn1*, *Otx1*, and *Otx2*, are also downstream of *Chd7* during ear development. We found that loss of *Sox11* did not impair spatiotemporal localization of *Ntn1*, *Otx1*, and *Otx2* by *in situ* hybridization despite qRT-PCR evidence suggesting altered expression levels in *Sox11*-null ears. However, we uncovered upregulation and expansion of the *Bmp4* expression domain in *Sox11* mutant ears. Taken together, our data suggest that *Sox11* can be placed downstream of *Chd7* in a

pathway regulating *Bmp4* distribution in the presumptive lateral canal crista (Figure 4.10). Specifically, *Sox11* may help to restrict *Chd7*-mediated expression of *Bmp4* in the developing lateral semicircular canal crista. Further analysis, perhaps by ChIP-sequencing in an appropriate cell model, could provide additional insights into how *Sox11* negatively regulates *Bmp4* expression, and other genes, in the developing crista. Interestingly, SOX11 binds its own regulatory regions and to regulatory regions of *Chd7* and *Bmp4* based on ChIP-seq analyses of neural-derived transit amplifying progenitors and Granta-519 mantle cell lymphoma cells[63,64].

The data presented here describe a heretofore unappreciated role for SOX11 in lateral and posterior semicircular canal morphogenesis. Additionally, this study examines the interaction of CHD7 and SOX11 in crista specification and outgrowth of the semicircular canal epithelium. We posit that CHD7 and SOX11 together function within a common genetic pathway that is likely conserved in multiple developing tissues.

Acknowledgments

The authors would like to acknowledge the intellectual and technical contributions of Dr. Elizabeth Hurd and Dr. Joseph Micucci.

Chapter IV Note

[1]A revised version of Chapter IV is being prepared for submission and review under the following authorship: Sperry, E. D., Hojjati, R., Swiderski, D. L., Raphael, Y., Lei, L., and Martin, D. M. SOX11 and CHD7 act in a common gene regulatory network to promote inner ear development. (in preparation)

Gene	ABI Reference #
Gapdh	Mm99999915_g1
Bmp2	Mm01340178_m1
Bmp4	Mm00432087_m1
Chd7	Mm01219527_m1
Lrig3	Mm00622768_m1
Ntn1	Mm00500896_m1
Otx1	Mm01616047_m1
Otx2	Mm00446859_m1
Sox11	Mm01281943_s1

Table 4.1. TaqMan probes used in this study.

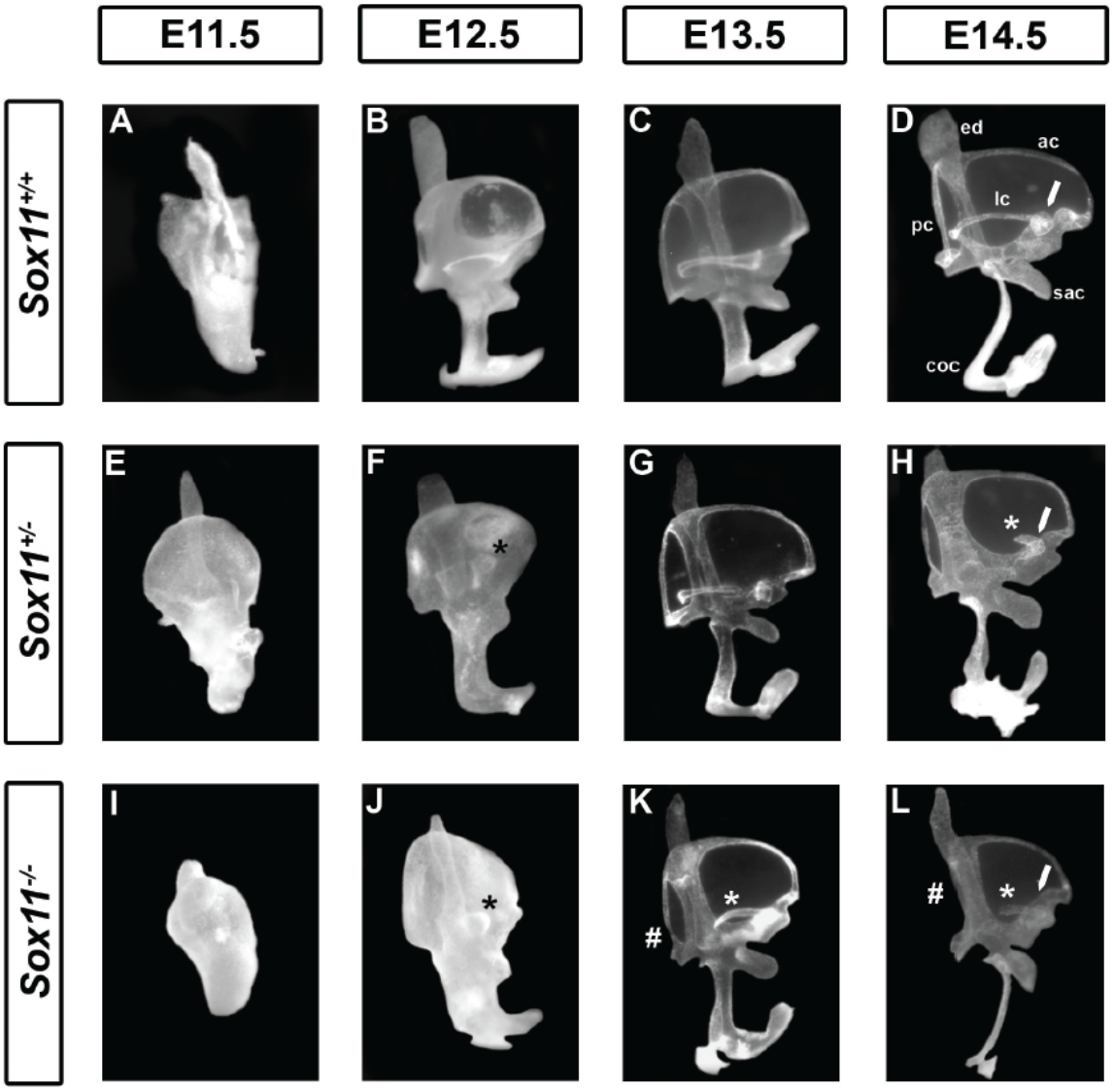


Figure 4.1. *Sox11* mutant mice exhibit lateral and posterior semicircular canal dysplasia.
Sox11 wild type, heterozygous, and null ears at ages (A, E, I) E11.5 (*N*=4, *N*=6, *N*=6), (B, F, J) E12.5 (*N*=6, *N*=6, *N*=6), (C, G, K) E13.5 (*N*=4, *N*=6, *N*=6), and (D, H, L) E14.5 (*N*=18, *N*=26, *N*=12) were subjected to paintfill. E11.5 *Sox11*$^{-/-}$ ears (I) were smaller than wild type (A) or heterozygous (E). Lateral semicircular canal defects were apparent in *Sox11* heterozygous (F, G, H) and null (J, K, L) ears at time points E12.5, E13.5, and E14.5. Lateral (*) and posterior (#) canal defects are demarcated where observed. An arrow points to the region of the developing lateral crista ampullaris, which is hypoplastic or absent where lateral canal malformations are observed (D, H, L). Abbreviations: ed = endolymphatic duct; ac = anterior semicircular canal; pc = posterior semicircular canal; lc = lateral semicircular canal; sac = saccule; coc = cochlea.

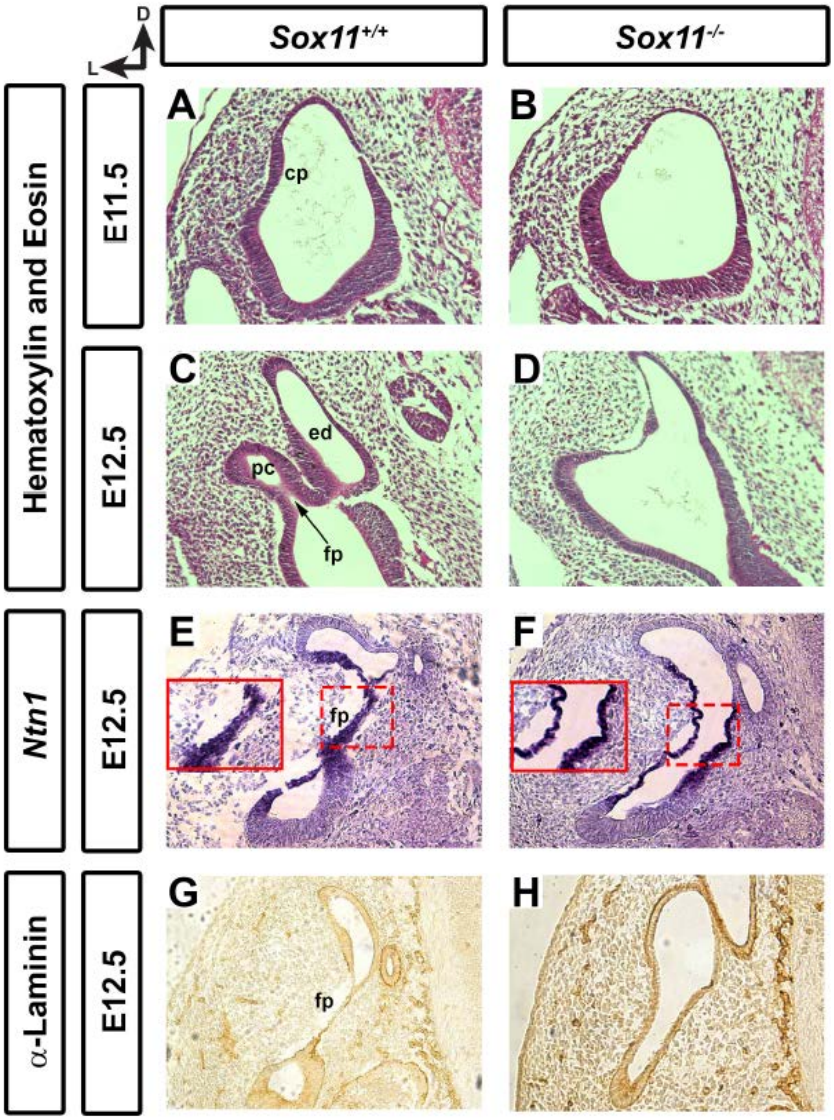


Figure 4.2. Posterior canal projections fail to form in *Sox11*-null mice despite normal EMT gene expression along the fusion plate.

Transverse sections of E11.5 (A-B) and E12.5 (C-D) mouse inner ears were stained with hematoxylin and eosin. *Sox11* wild type ears showed normal development of the canal pouch at E11.5 (A) with an intact canal fusion plate by E12.5 (C). Compared to *Sox11* wild type tissues, all *Sox11*-null specimens exhibited absent canal projections at E11.5 (B) and fusion plates at E12.5 (D). *In situ* hybridization on E12.5 inner ears showed no observable changes in *Ntn1* expression in *Sox11* wild type (E) compared to null (F) ears. Inset panels in (E-F) demonstrate merging of the two cell layers in the *Sox11*-wild type (E) but not in the *Sox11*-null (F). Anti-laminin-DAB staining showed disruption of laminin along the *Ntn1*-positive domain and intact laminin along the *Ntn1*-negative domain in both the *Sox11* wild type (G) and the null (H) ears. All panels are oriented so that the dorsal and lateral aspects respectively correspond to the upper and left borders of the panel. Abbreviations: cp = canal projection; fp = fusion plate; pc = posterior semicircular canal; ed = endolymphatic duct.

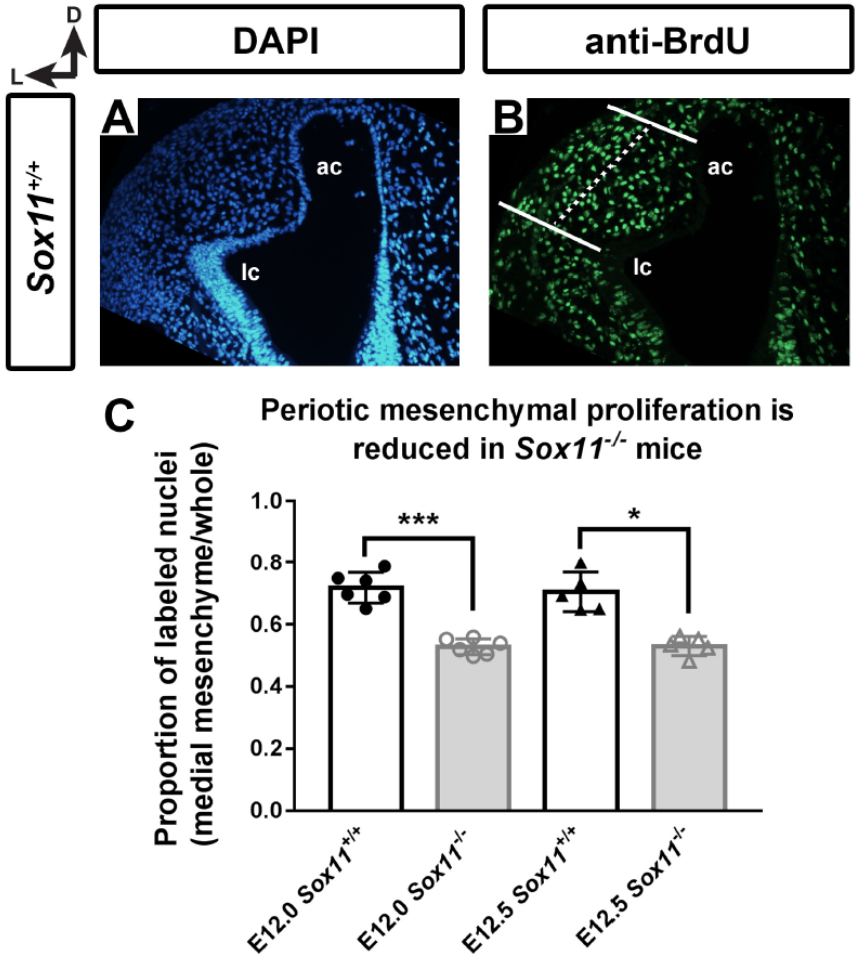


Figure 4.3. *Sox11*-null mouse ears demonstrate impaired cellular proliferation.
Transverse sections through the developing ear from E12.0 (*N* = 6 ears per genotype) and E12.5 (*N* = 6 ears per genotype) *Sox11* wild type and null embryos were stained with anti-BrdU antibody for detection of proliferating cells and counter-stained with DAPI. BrdU positive cells in the medial mesenchyme and the total BrdU cell population were counted using a modification of the method described by Salminen et. al (2000) and with ImageJ[39]. A representative DAPI-stained (A) and anti-BrdU-stained (B) image from an E12.0 wild type embryo is shown. The counting region is bounded by solid white lines while the lateral and medial aspects of the canal projection are separated by a dashed white line in panel (B). The proportion of cells proliferating within the canal projection was determined by dividing medial mesenchyme cells from the total BrdU cell population and plotted in (C). E12.0 *Sox11*-null ears exhibited a 19% reduction in BrdU-positive cells compared to age-matched wild type ears. E12.5 *Sox11*-null ears had a 17% reduction in BrdU-positive cells compared to age-matched wild type ears. Panels (A) and (B) are oriented so that the dorsal and lateral aspects respectively correspond to the upper and left borders of the panel. A Student's *t*-test with Welch correction was performed across genotypes at each time point: * = $p<0.05$; *** = $p<0.001$. Abbreviations: ac = presumptive anterior semicircular canal; lc = presumptive lateral semicircular canal.

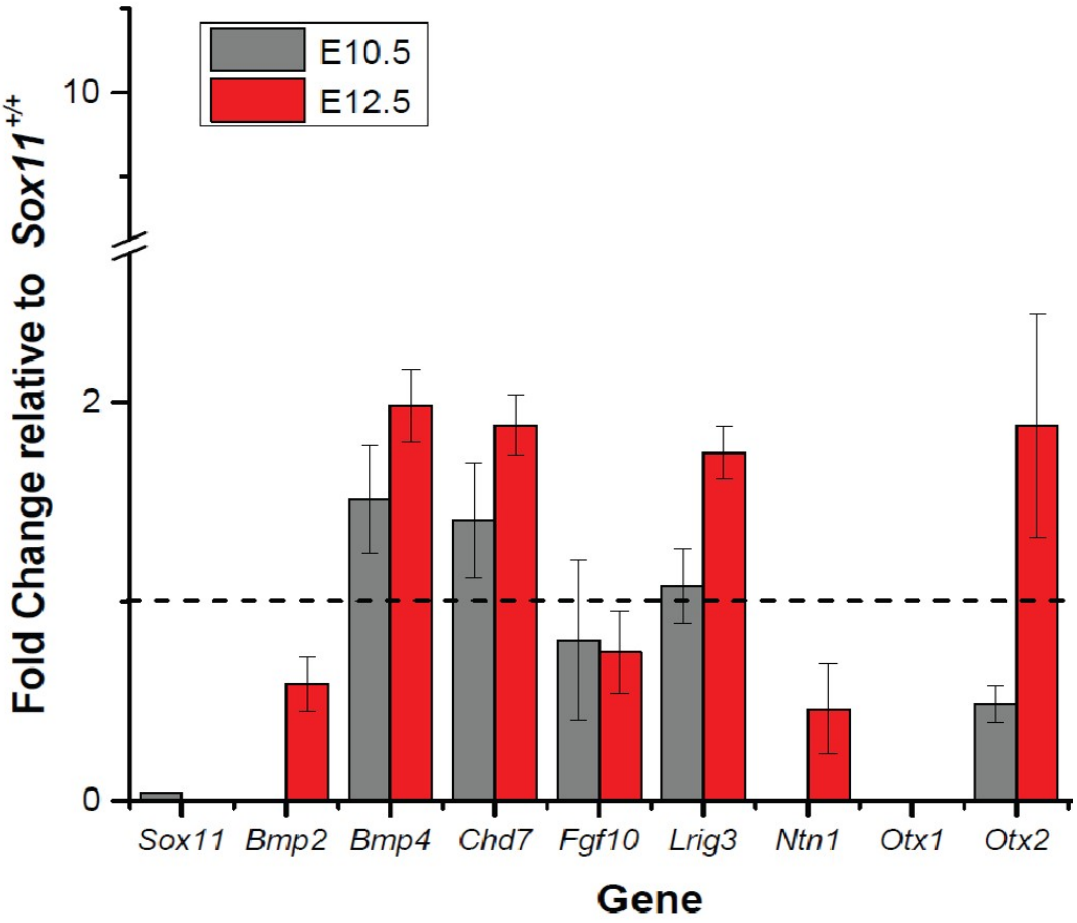


Figure 4.4. Germline absence of *Sox11* results in misexpression of several genes critical for vestibular development.

RNA extracted from E10.5 and E12.5 microdissected *Sox11* wild type and null otocysts was assayed by TaqMan-qPCR for changes in the expression levels of *Bmp2/4*, *Fgf10*, *Lrig3*, *Ntn1*, and *Otx1/2*, all genes important in semicircular canal development. Misregulation of these genes was observed at both time points. *Sox11* transcript was absent in *Sox11* null otocysts, consistent with its germline deletion. *Gapdh* was used as an endogenous control.

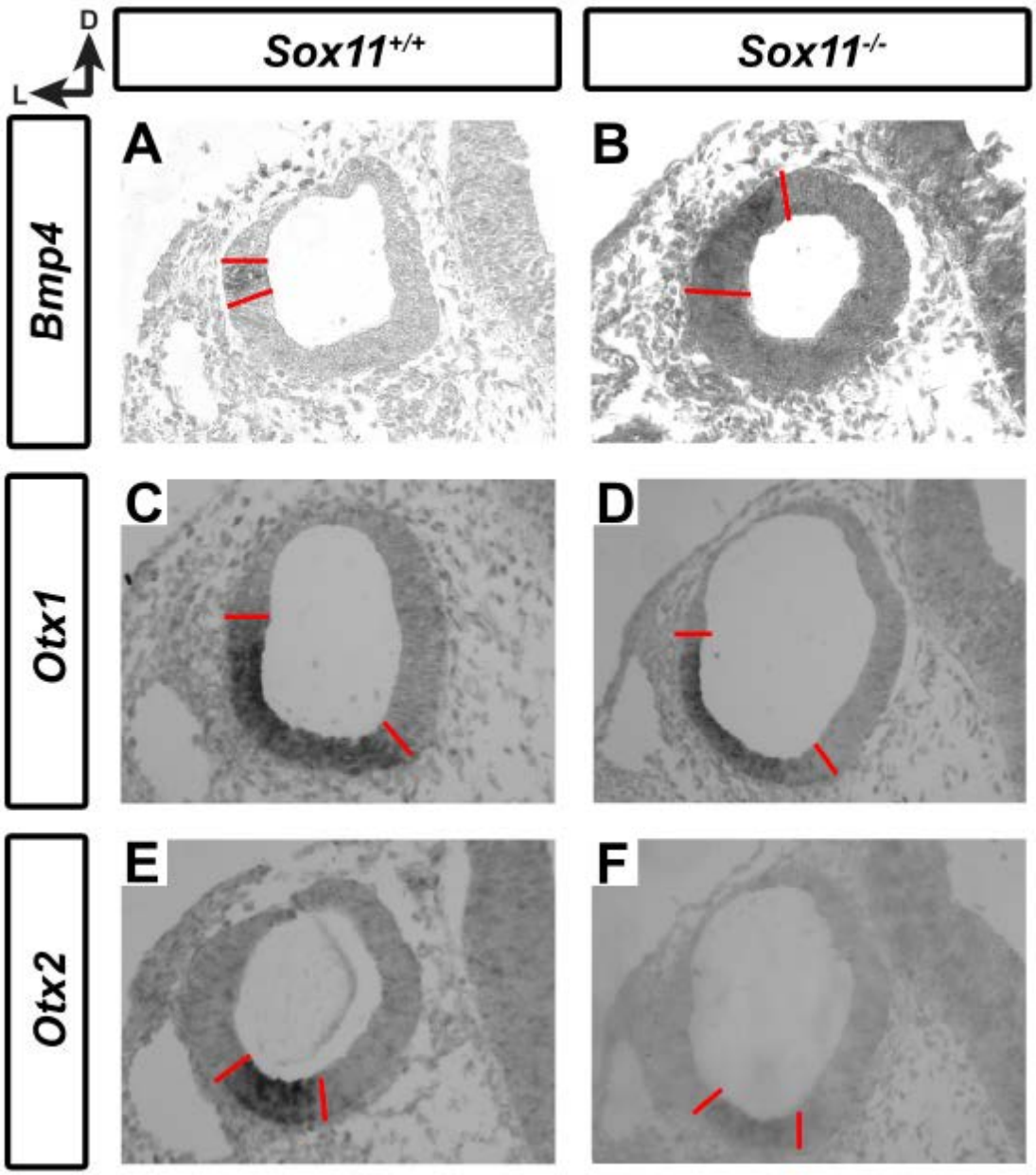


Figure 4.5. Loss of *Sox11* results in expansion of *Bmp4*, but not *Otx1/2*, expression at E10.5.
In situ hybridization studies were performed in E10.5 *Sox11* wild type and null sectioned ears to examine changes in the expression domains for *Bmp4*, *Otx1*, and *Otx2*. *Bmp4* expression was expanded dorsally at the level of the presumptive anterior and lateral crista (B) compared to wild type (A). The expression domains for *Otx1* and *Otx2* were unchanged in *Sox11* null ears (D, F) compared to wild type (C, E). All panels are oriented so that the dorsal and lateral aspects respectively correspond to the upper and left borders of the panel. Red lines demarcate the expression domains visualized under Brightfield microscopy.

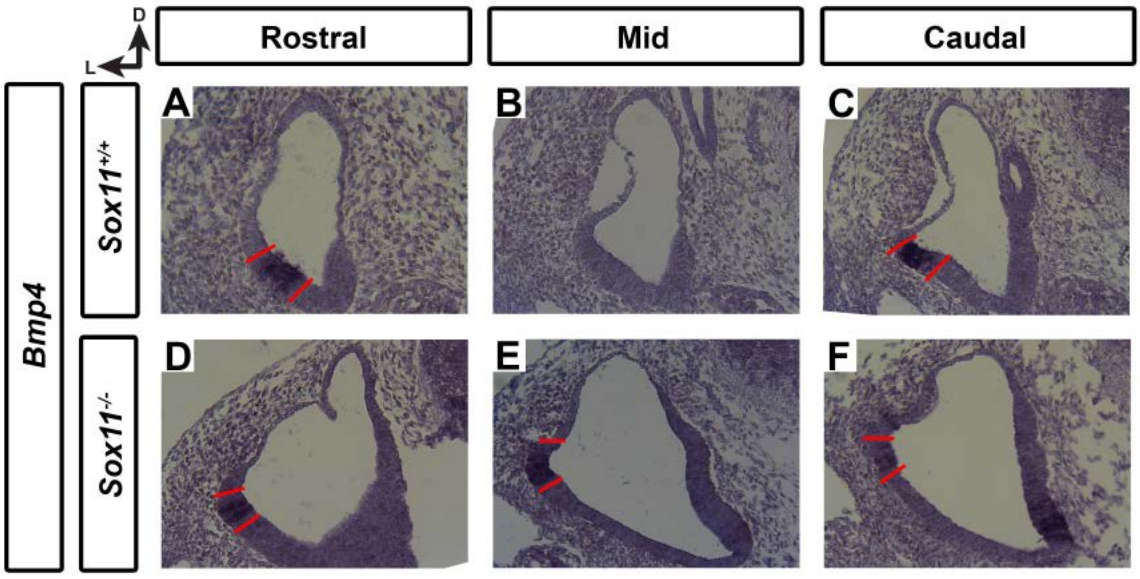


Figure 4.6. *Bmp4* expression is expanded across the presumptive lateral and anterior cristae of E11.5 *Sox11*$^{-/-}$ mice.

In situ hybridization studies were performed in E11.5 *Sox11* wild type and null sectioned ears to further examine changes in the expression domains for *Bmp4*. In wild type ears, *Bmp4* expression was identified in the region of the anterior crista (A) and lateral crista (C), but absent in the intervening region (B), consistent with previously published data. In the *Sox11*-null ear, *Bmp4* expression was continuously present from the anterior to lateral cristae regions, obscuring the exact locations of each crista (D-F). All panels are oriented so that the dorsal and lateral aspects respectively correspond to the upper and left borders of the panel. Red lines demarcate the expression domains visualized under Brightfield microscopy.

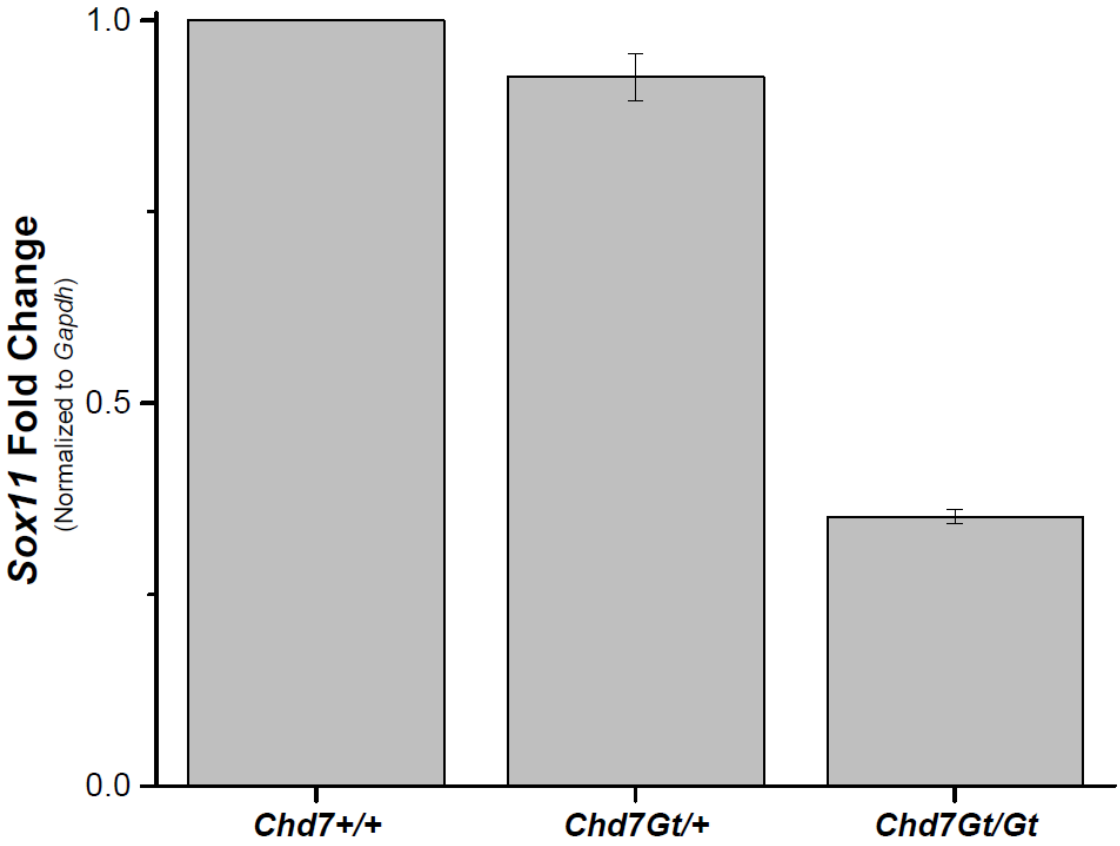


Figure 4.7. CHD7 positively regulates *Sox11* expression in the developing inner ear.
Chd7-heterozygous (*N*=3) and null (*N*=3) otocysts were microdissected and analyzed with TaqMan-qPCR for *Sox11* mRNA levels. E10.5 *Chd7*-heterozygous ears demonstrated insignificant reduction in *Sox11* levels while E10.5 *Chd7*-null ears showed a significant reduction in *Sox11* levels. *Gapdh* was used an endogenous control.

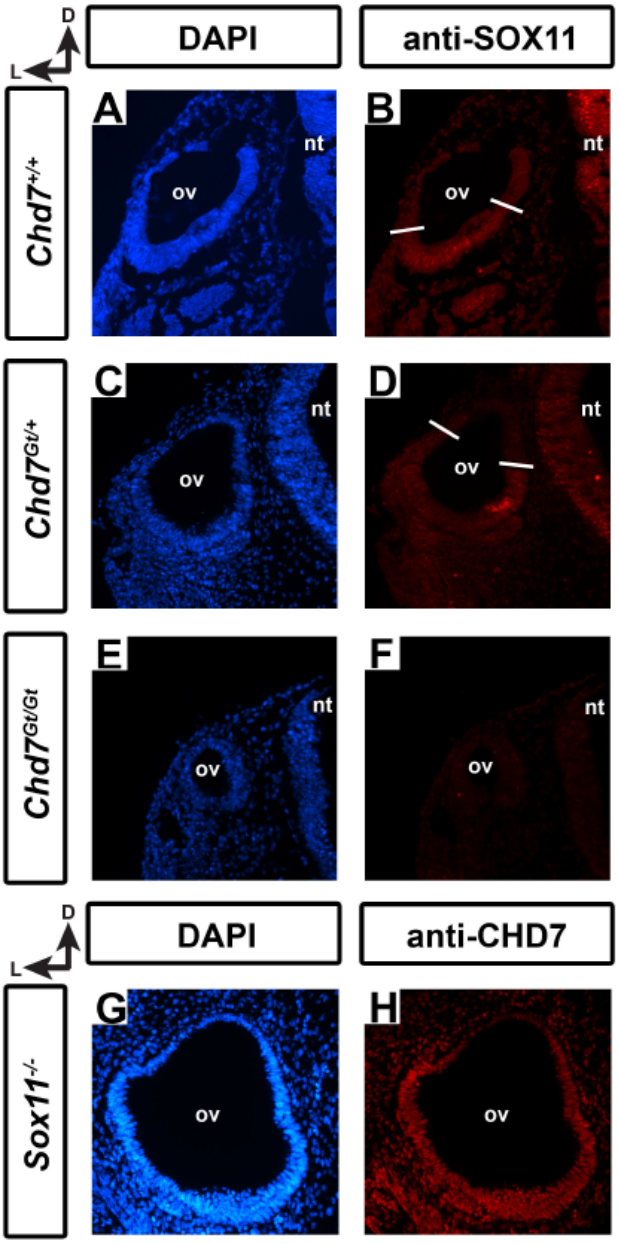


Figure 4.8. SOX11 protein levels are reduced in *Chd7* mutant inner ears but CHD7 protein levels are preserved in *Sox11*-null ears.

Anti-SOX11 (B, D, F) staining and DAPI (A, C, E) counterstaining of transverse E10.5 sections of *Chd7*$^{+/+}$, *Chd7*$^{Gt/+}$, and *Chd7*$^{Gt/Gt}$ ears with anti-SOX11 antibody showed SOX11 protein is abundant along the ventral, medial, and lateral E10.5 wild type mouse otocyst (ov) and lateral neural tube (nt) (A-B). SOX11 protein is dorsally expanded in *Chd7*$^{Gt/+}$ otocysts (D-E); however, SOX11 is absent from the otocyst and neural tube of *Chd7*-null mice (E-F). E11.5 *Sox11*-null ears stained with anti-CHD7 antibody and counterstained with DAPI showed significant staining throughout the ear (G-H). All panels are oriented so that the dorsal and lateral aspects respectively correspond to the upper and left borders of the panel. White lines demarcate the expression domains visualized under fluorescence microscopy.

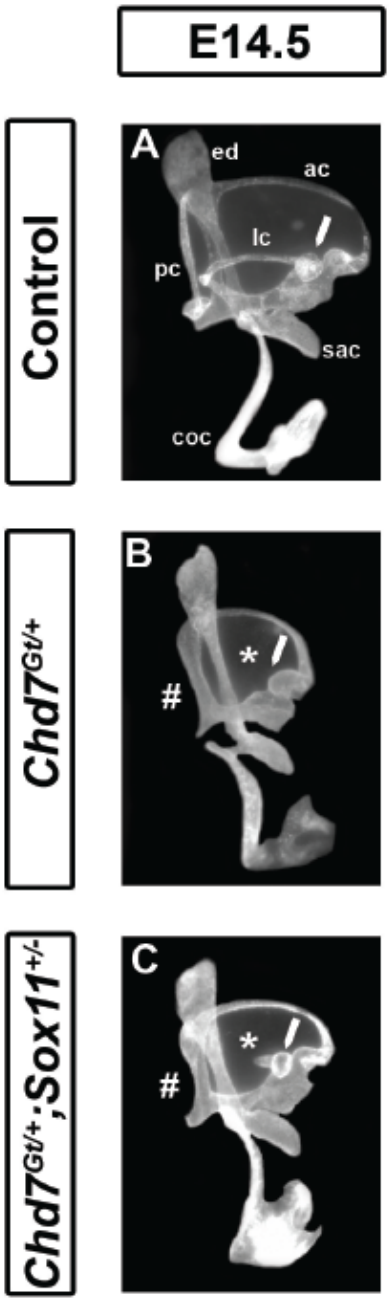


Figure 4.9. Mice doubly heterozygous for *Chd7* and *Sox11* exhibited lateral and posterior semicircular canal dysplasia.

Ears from E14.5 control (*N*=18), $Chd7^{Gt/+}$ (*N*=6), and $Chd7^{Gt/+};Sox11^{+/-}$ (*N*=6) mice were subjected to paintfilling. Relative to control (A) mice, $Chd7^{Gt/+}$ mice (B) exhibited characteristic defects in the lateral (*) and posterior (#) canals. *Chd7;Sox11* double heterozygous mice (C) demonstrated identical lateral and posterior canal defects. An arrow points to the region of the developing lateral crista ampullaris, which is hypoplastic in $Chd7^{Gt/+}$ ears, but present in *Chd7;Sox11* double heterozygous ears. Abbreviations: ed = endolymphatic duct; ac = anterior semicircular canal; pc = posterior semicircular canal; lc = lateral semicircular canal; sac = saccule; coc = cochlea.

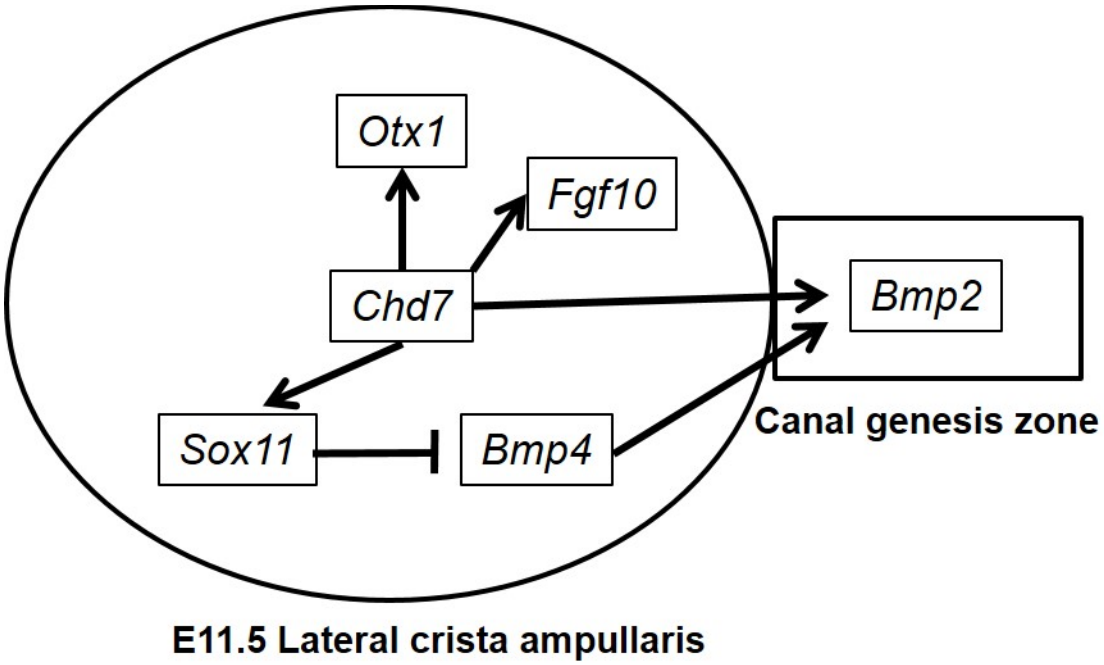


Figure 4.10. Model of CHD7 and SOX11 function in the lateral crista ampullaris and adjacent canal genesis zone.

Schematic of downstream effectors of *Chd7* expression at the developing E11.5 lateral crista ampullaris. *Sox11* expression is placed downstream of *Chd7* and serves to restrict *Chd7*-driven *Bmp4* expression specifying the crista and canal genesis zone. *Otx1* and *Fgf10* expression within the crista are driven by *Chd7*, but not *Sox11*.

References

1. Alsina, B. & Whitfield, T. T. Sculpting the labyrinth: Morphogenesis of the developing inner ear. *Semin Cell Dev Biol* **65**, 47-59 (2017).

2. Fekete, D. M. Cell fate specification in the inner ear. *Curr Opin Neurobiol* **6**, 533-541 (1996).

3. Fekete, D. M. Development of the vertebrate ear: insights from knockouts and mutants. *Trends Neurosci* **22**, 263-269 (1999).

4. Tsurusaki, Y. *et al.* De novo SOX11 mutations cause Coffin-Siris syndrome. *Nat Commun* **5**, 4011 (2014).

5. Coffin, G. S. & Siris, E. Mental retardation with absent fifth fingernail and terminal phalanx. *Am J Dis Child* **119**, 433-439 (1970).

6. Fleck, B. J., Pandya, A., Vanner, L., Kerkering, K. & Bodurtha, J. Coffin-Siris syndrome: review and presentation of new cases from a questionnaire study. *Am J Med Genet* **99**, 1-7 (2001).

7. Haspeslagh, M., Fryns, J. P. & van den Berghe, H. The Coffin-Siris syndrome: report of a family and further delineation. *Clin Genet* **26**, 374-378 (1984).

8. Hoyer, J. *et al.* Haploinsufficiency of ARID1B, a member of the SWI/SNF-a chromatin-remodeling complex, is a frequent cause of intellectual disability. *Am J Hum Genet* **90**, 565-572 (2012).

9. Santen, G. W. *et al.* Mutations in SWI/SNF chromatin remodeling complex gene ARID1B cause Coffin-Siris syndrome. *Nat Genet* **44**, 379-380 (2012).

10. Tsurusaki, Y. *et al.* Mutations affecting components of the SWI/SNF complex cause Coffin-Siris syndrome. *Nat Genet* **44**, 376-378 (2012).

11. Kellermayer, R. *et al.* Upper gastrointestinal malformations in Coffin-Siris syndrome. *Am J Med Genet A* **143A**, 1519-1521 (2007).

12. Kleefstra, T. *et al.* Disruption of an EHMT1-associated chromatin-modification module causes intellectual disability. *Am J Hum Genet* **91**, 73-82 (2012).

13. Wieczorek, D. *et al.* A comprehensive molecular study on Coffin-Siris and Nicolaides-Baraitser syndromes identifies a broad molecular and clinical spectrum converging on altered chromatin remodeling. *Hum Mol Genet* **22**, 5121-5135 (2013).

14. Sock, E. *et al.* Gene targeting reveals a widespread role for the high-mobility-group transcription factor Sox11 in tissue remodeling. *Mol Cell Biol* **24**, 6635-6644 (2004).

15. de Martino, S. *et al.* Expression of sox11 gene duplicates in zebrafish suggests the reciprocal loss of ancestral gene expression patterns in development. *Dev Dyn* **217**, 279-292 (2000).

16. Sinkkonen, S. T. *et al.* Serial analysis of gene expression in the chicken otocyst. *J Assoc Res Otolaryngol* **12**, 697-710 (2011).

17. Gnedeva, K. & Hudspeth, A. J. SoxC transcription factors are essential for the development of the inner ear. *Proc Natl Acad Sci U S A* **112**, 14066-14071 (2015).

18. Feng, W. *et al.* The chromatin remodeler CHD7 regulates adult neurogenesis via activation of SoxC transcription factors. *Cell Stem Cell* **13**, 62-72 (2013).

19. Vissers, L. E. *et al.* Mutations in a new member of the chromodomain gene family cause CHARGE syndrome. *Nat Genet* **36**, 955-957 (2004).

20. Bouazoune, K. & Kingston, R. E. Chromatin remodeling by the CHD7 protein is impaired by mutations that cause human developmental disorders. *Proc Natl Acad Sci U S A* **109**, 19238-19243 (2012).

21. Manning, B. J. & Yusufzai, T. The ATP-dependent chromatin remodeling enzymes CHD6, CHD7, and CHD8 exhibit distinct nucleosome binding and remodeling activities. *J Biol Chem* **292**, 11927-11936 (2017).

22. Hall, B. D. Choanal atresia and associated multiple anomalies. *J Pediatr* **95**, 395-398 (1979).

23. Hittner, H. M., Hirsch, N. J., Kreh, G. M. & Rudolph, A. J. Colobomatous microphthalmia, heart disease, hearing loss, and mental retardation--a syndrome. *J Pediatr Ophthalmol Strabismus* **16**, 122-128 (1979).

24. Pagon, R. A., Graham, J. M., Jr., Zonana, J. & Yong, S. L. Coloboma, congenital heart disease, and choanal atresia with multiple anomalies: CHARGE association. *J Pediatr* **99**, 223-227 (1981).

25. Sanlaville, D. *et al.* Phenotypic spectrum of CHARGE syndrome in fetuses with CHD7 truncating mutations correlates with expression during human development. *J Med Genet* **43**, 211-217 (2006).

26. Adams, M. E. *et al.* Defects in vestibular sensory epithelia and innervation in mice with loss of Chd7 function: implications for human CHARGE syndrome. *J Comp Neurol* **504**, 519-532 (2007).

27. Hurd, E. A. *et al.* Mature middle and inner ears express Chd7 and exhibit distinctive pathologies in a mouse model of CHARGE syndrome. *Hear Res* **282**, 184-195 (2011).

28. Hurd, E. A., Micucci, J. A., Reamer, E. N. & Martin, D. M. Delayed fusion and altered gene expression contribute to semicircular canal defects in Chd7 deficient mice. *Mech Dev* **129**, 308-323 (2012).

29. Hurd, E. A., Poucher, H. K., Cheng, K., Raphael, Y. & Martin, D. M. The ATP-dependent chromatin remodeling enzyme CHD7 regulates pro-neural gene expression and neurogenesis in the inner ear. *Development* **137**, 3139-3150 (2010).

30. Wang, Y., Lin, L., Lai, H., Parada, L. F. & Lei, L. Transcription factor Sox11 is essential for both embryonic and adult neurogenesis. *Dev Dyn* **242**, 638-653 (2013).

31. Hurd, E. A. *et al.* Loss of Chd7 function in gene-trapped reporter mice is embryonic lethal and associated with severe defects in multiple developing tissues. *Mamm Genome* **18**, 94-104 (2007).

32. Martin, D. M., Skidmore, J. M., Fox, S. E., Gage, P. J. & Camper, S. A. Pitx2 distinguishes subtypes of terminally differentiated neurons in the developing mouse neuroepithelium. *Dev Biol* **252**, 84-99 (2002).

33. Kiernan, A. E. The paintfill method as a tool for analyzing the three-dimensional structure of the inner ear. *Brain Res* **1091**, 270-276 (2006).

34. Sperry, E. D. *et al.* The chromatin remodeling protein CHD7, mutated in CHARGE syndrome, is necessary for proper craniofacial and tracheal development. *Dev Dyn* **243**, 1055-1066 (2014).

35. Wright, C. G., Brown, O. E., Meyerhoff, W. L. & Rutledge, J. C. Auditory and temporal bone abnormalities in CHARGE association. *Ann Otol Rhinol Laryngol* **95**, 480-486 (1986).

36. Martin, P. & Swanson, G. J. Descriptive and experimental analysis of the epithelial remodellings that control semicircular canal formation in the developing mouse inner ear. *Dev Biol* **159**, 549-558 (1993).

37. Sher, A. E. The embryonic and postnatal development of the inner ear of the mouse. *Acta Otolaryngol Suppl* **285**, 1-77 (1971).

38. Abraira, V. E. *et al.* Cross-repressive interactions between Lrig3 and netrin 1 shape the architecture of the inner ear. *Development* **135**, 4091-4099 (2008).

39. Salminen, M., Meyer, B. I., Bober, E. & Gruss, P. Netrin 1 is required for semicircular canal formation in the mouse inner ear. *Development* **127**, 13-22 (2000).

40. Yan, W. *et al.* Netrin-1 induces epithelial-mesenchymal transition and promotes hepatocellular carcinoma invasiveness. *Dig Dis Sci* **59**, 1213-1221 (2014).

41. Yokdang, N. *et al.* LRIG1 opposes epithelial-to-mesenchymal transition and inhibits invasion of basal-like breast cancer cells. *Oncogene* **35**, 2932-2947 (2016).

42. Fekete, D. M. & Wu, D. K. Revisiting cell fate specification in the inner ear. *Curr Opin Neurobiol* **12**, 35-42 (2002).

43. Bissonnette, J. P. & Fekete, D. M. Standard atlas of the gross anatomy of the developing inner ear of the chicken. *J Comp Neurol* **368**, 620-630 (1996).

44. Deng, M., Pan, L., Xie, X. & Gan, L. Requirement for Lmo4 in the vestibular morphogenesis of mouse inner ear. *Dev Biol* **338**, 38-49 (2010).

45. Chang, W., Brigande, J. V., Fekete, D. M. & Wu, D. K. The development of semicircular canals in the inner ear: role of FGFs in sensory cristae. *Development* **131**, 4201-4211 (2004).

46. Chang, W., ten Dijke, P. & Wu, D. K. BMP pathways are involved in otic capsule formation and epithelial-mesenchymal signaling in the developing chicken inner ear. *Dev Biol* **251**, 380-394 (2002).

47. Hammond, K. L. *et al.* A late role for bmp2b in the morphogenesis of semicircular canal ducts in the zebrafish inner ear. *PLoS One* **4**, e4368 (2009).

48. Acampora, D. *et al.* Differential transcriptional control as the major molecular event in generating Otx1-/- and Otx2-/- divergent phenotypes. *Development* **126**, 1417-1426 (1999).

49. Omata, Y. *et al.* Role of Bone morphogenetic protein 4 in zebrafish semicircular canal development. *Dev Growth Differ* **49**, 711-719 (2007).

50. Lin, Z., Cantos, R., Patente, M. & Wu, D. K. Gbx2 is required for the morphogenesis of the mouse inner ear: a downstream candidate of hindbrain signaling. *Development* **132**, 2309-2318 (2005).

51. Morsli, H. *et al.* Otx1 and Otx2 activities are required for the normal development of the mouse inner ear. *Development* **126**, 2335-2343 (1999).

52. Hwang, C. H., Simeone, A., Lai, E. & Wu, D. K. Foxg1 is required for proper separation and formation of sensory cristae during inner ear development. *Dev Dyn* **238**, 2725-2734 (2009).

53. Janssen, N. *et al.* Mutation update on the CHD7 gene involved in CHARGE syndrome. *Hum Mutat* **33**, 1149-1160 (2012).

54. Torres, M., Gomez-Pardo, E. & Gruss, P. Pax2 contributes to inner ear patterning and optic nerve trajectory. *Development* **122**, 3381-3391 (1996).

55. Bhattaram, P. *et al.* Organogenesis relies on SoxC transcription factors for the survival of neural and mesenchymal progenitors. *Nat Commun* **1**, 9 (2010).

56. Chen, C., Lee, G. A., Pourmorady, A., Sock, E. & Donoghue, M. J. Orchestration of Neuronal Differentiation and Progenitor Pool Expansion in the Developing Cortex by SoxC Genes. *J Neurosci* **35**, 10629-10642 (2015).

57. Jiang, X. *et al.* The mutation in Chd7 causes misexpression of Bmp4 and developmental defects in telencephalic midline. *Am J Pathol* **181**, 626-641 (2012).

58. Lin, L. *et al.* Sox11 regulates survival and axonal growth of embryonic sensory neurons. *Dev Dyn* **240**, 52-64 (2011).

59. Paul, M. H., Harvey, R. P., Wegner, M. & Sock, E. Cardiac outflow tract development relies on the complex function of Sox4 and Sox11 in multiple cell types. *Cell Mol Life Sci* **71**, 2931-2945 (2014).

60. Potzner, M. R. *et al.* Sequential requirement of Sox4 and Sox11 during development of the sympathetic nervous system. *Development* **137**, 775-784 (2010).

61. Usui, A. *et al.* The early retinal progenitor-expressed gene Sox11 regulates the timing of the differentiation of retinal cells. *Development* **140**, 740-750 (2013).

62. Wurm, A., Sock, E., Fuchshofer, R., Wegner, M. & Tamm, E. R. Anterior segment dysgenesis in the eyes of mice deficient for the high-mobility-group transcription factor Sox11. *Exp Eye Res* **86**, 895-907 (2008).

63. Bergsland, M. *et al.* Sequentially acting Sox transcription factors in neural lineage development. *Genes Dev* **25**, 2453-2464 (2011).

64. Kuo, P. Y. *et al.* High-resolution chromatin immunoprecipitation (ChIP) sequencing reveals novel binding targets and prognostic role for SOX11 in mantle cell lymphoma. *Oncogene* **34**, 1231-1240 (2015).

Chapter V: Discussion and Future Directions

Summary of dissertation

The data presented in my dissertation expand our understanding of roles for CHD7 in craniofacial and inner ear development. Importantly, my studies highlight the necessity for CHD7 in craniofacial and respiratory development and expand on its known role in neural crest cell-dependent developmental processes. I also describe a novel chromosome 2 duplication in an individual with clinical features of CHARGE syndrome. Finally, I demonstrate that SOX11 is required for lateral and posterior semicircular canal development in the mouse and may be an effector of CHD7 function in the developing ear, complementary to its published role in the central nervous system.

In the following three sections, I will briefly review the pertinent findings from each of my projects. Following this, I will highlight open questions for further study.

CHD7 in craniofacial and tracheal development[1]

In Chapter II, I discussed my research into the role of CHD7 during mouse craniofacial and oropharyngeal development. Specifically, I found that CHD7 is required for mouse head and neck morphogenesis in the same structures altered in human CHARGE syndrome. Using germline and conditional *Chd7* mouse mutants, I determined that loss of *Chd7* results in postnatal respiratory distress and death, dysplasia of the eye, concha, and

frontal bone, hypoplastic maxillary shelves and nasal epithelia, and reduced tracheal cartilaginous ring formation. The tracheal findings represent the first non-human evidence for *Chd7* deletion causing tracheomalacia, a serious condition experienced by many individuals with CHARGE. Results from this study 1) highlight the role of *Chd7* in craniofacial and respiratory development, including development of cartilage and bone, 2) demonstrate that *Chd7* is required for proper generation of the surface ectoderm, endoderm, and migrating neural crest cells, and 3) confirm the utility of available *Chd7* mutant mouse models in studying these phenotypes.

This study provides a detailed phenotypic framework for future study of CHD7 in pharyngeal arch derivatives and in migrating neural crest cell populations. Structures derived from the pharyngeal arches rely on proper migration of neural crest cells and appropriate interaction of these cells with the overlying ectoderm. Indeed, the role of CHD7 in neural crest cell-derived structures extends to migration, guidance, and terminal differentiation of these cells once they occupy the pharyngeal arches. Loss of *Chd7* disrupts neural crest cell guidance and migration[2,3]. Histologic examination of the cartilaginous precursor cell pools contributing to the nasal conchae, which are significantly altered in *Chd7* conditional mutant mice, would help determine if loss of *Chd7* is affecting neural crest cell migration and/or integration within the contributory pharyngeal arches.

Given that CHD7 is a chromatin remodeler, it likely has a role in a genetic pathway impacting neural crest cell function. Deregulation of *Sox10* expression with loss of *Chd7* recapitulates neural crest cell-dependent malformations in the zebrafish[4]. Recapitulating these studies in the developing mouse would help determine the downstream genetic network affecting observed *Chd7* mutant mouse craniofacial malformations. Finally, BMP

signaling has been reported to be crucial for craniofacial neural crest cell induction[5]. As CHD7 positively regulates *Bmp2* and *Bmp4* in other tissues, specifically the inner ear, further exploration of this molecular relationship in craniofacial neural crest and overlying ectoderm is warranted[6,7].

Clefting of the palate is a common finding in many craniofacial syndromes, including CHARGE. Several signaling pathways associated with cleft palate, including SHH, WNT, TGF-B, and FGF[8]. Members of these signaling pathways are commonly disrupted with loss of *Chd7*, particularly in the developing olfactory system and inner ear[6,7,9,10]. It remains to be seen if CHD7 exhibits spatiotemporal control over any of the transcription factors and morphogens critical for palatal shelf growth, approximation, and fusion. Histologic and genomic analyses of the contributory structures could help place CHD7 within a common regulatory pathway governing palatogenesis.

One unexpected result from my study was the lack of observable cardiac defects with conditional loss of *Chd7*. Specifically, I expected to observe neural crest cell-derived cardiac malformations in *Wnt1-Cre;Chd7*$^{Gt/f}$ mice consistent with the pharyngeal arch artery and septal malformations observed in humans with CHARGE[11-14]. Absence of these malformations in *Chd7* conditional knockout mice raises the question as to whether cardiac neural crest cell migration and function are dependent on *Chd7*. Careful molecular study of cardiac neural crest cells is required to more fully understand how loss of *Chd7* generates this common array of phenotypes. Alternatively, loss of *Chd7* may impact other cardiac structures not derived from neural crest, such as the endocardial cushions. These structures are critical for guiding neural crest cell-derived structural morphogenesis in the cardiac

outflow tract, affected in CHARGE syndrome; however, CHD7 contribution, if any, to the endocardial cushions has not been studied[15].

My analyses further revealed that conditional homozygous loss of *Chd7* restricts tracheal development. This result provides insight into the perinatal respiratory issues observed in both *Chd7*-deficient mice and humans with CHARGE syndrome[11,14]. Tracheoesophageal fistula and tracheomalacia are commonly reported in individuals with CHARGE[16]. As both the trachea and esophagus derive from the primitive foregut, further exploration into how CHD7 helps separate these two commonly-derived structures is required. Furthermore, the TGF-beta signaling pathway has been implicated in tracheal cartilage ring formation[17]. A recent study indicating upregulation of TGF-beta pathway members in *Chd7*-deficient mice provides an avenue for further study of tracheal ring morphogenesis in CHARGE syndrome[10].

In summary, much remains to be understood concerning CHD7 function in neural crest cell function and in development of craniofacial, cardiac, and tracheal structures.

Duplication 2p25 in a child with clinical features of CHARGE syndrome[18]

In Chapter III, I reported on an individual diagnosed with clinical features of CHARGE syndrome who did not exhibit any genetic aberrations in or around the *CHD7* locus. This study was inspired by continuing efforts in the field to better understand the genetic causes of CHARGE as well as the high degree of clinical overlap between CHARGE and phenotypically similar syndromes. I confirmed that this patient exhibited a complex partial duplication of chromosome 2p (2p25.3-p25.2), including increased dosage

of *SOX11* and 23 other genes. Further, I identified ten cases of pure partial trisomy 2p and reviewed these cases for clinical features of CHARGE syndrome.

Given the presence of 24 genes in the chromosome 2p duplicated interval in this patient, it would be an infeasible, if not impossible, task to ascertain the contributions of each gene to the affected individual's phenotype. Determination of the individual contributions of all duplicated genes would require use of a screening paradigm to observe the effects of mRNA overexpression in embryonic zebrafish[19]. Intriguingly, the duplicated interval includes *SOX11*, which is required for development of CHARGE-relevant structures, including the eye, ear, and heart[20]. Analysis of cells from the affected individual would help in determining whether duplication of *SOX11* leads to increased expression in CHARGE-relevant tissues. Development of mice with *Sox11* overexpression followed by careful morphologic phenotyping could also help determine how *Sox11* overexpression influences development of CHARGE-related structures.

SOX11 and CHD7 act in a common gene regulatory network to promote inner ear development

In Chapter IV, I present results of my analysis of the role of SOX11 in the developing mouse ear. Extensive phenotypic similarity between *Chd7* and *Sox11* mutant mice led me to hypothesize that SOX11 may have a complementary role during inner ear development. Consistent with this, CHD7 had been shown by others to act as an upstream regulator of *Sox11* expression in neural stem cells[21]. While loss of *Chd7* disrupts gene expression and morphologic development of the mouse inner ear, the precise genetic mechanism underlying CHD7's role in inner ear development is unknown. I hypothesized that similar to its role in neural stem cell development, CHD7 may directly regulate *Sox11*

during ear development. I focused my studies on lateral and posterior semicircular canal dysplasia, the most highly penetrant inner ear phenotypes observed in *Chd7* mutant mice. I showed that loss of *Sox11* disrupts lateral and posterior canal development. Next, I determined that SOX11 positively regulates cell proliferation around the lateral and posterior canal anlagen and is required for canal fusion plate formation. *Sox11* is important for restricting expression of *Bmp4*, a gene critical for specifying the semicircular canal crista ampullaris and adjacent canal genesis zones. Finally, loss of *Chd7* disrupts *Sox11* expression in the developing ear, suggesting that *Sox11* resides downstream of *Chd7* in semicircular canal morphogenesis.

Results of these studies raise many new and interesting questions. The paintfill analyses revealed that *Sox11*$^{-/-}$ mice have abnormal lateral and posterior cristae and their associated semicircular canals are truncated or hypoplastic. Normal semicircular canal development requires specification of cells that form a presumptive crista ampullaris, containing cells that will generate the sensory epithelium associated with that canal as well as cells that contribute to the canal. The nascent crista ampullaris is marked by FGF10 and BMP4[22-24]. The developing canal extends outward from the presumptive crista following specification of an adjacent canal genesis zone, which expresses *Bmp2*[22,23]. RNA i*n situ* hybridization for *Bmp2* in *Sox11* mutant ears will help determine whether Sox11 is also important in this region of the developing dorsal otocyst and in specification of the canal genesis zone.

The similarities in the lateral and posterior semicircular canal phenotypes within *Chd7* and *Sox11* mutant mice further suggests these canals share a common morphogenetic mechanism which could be different from the anterior semicircular canal. While the gene

expression changes in the *Chd7* lateral canal crista and adjacent canal genesis zone have been well-characterized, further examination of the posterior semicircular canal crista ampullaris in both *Chd7* and *Sox11* mutants is necessary to determine if these structures share a common developmental trajectory[6]. Comparison with the anterior semicircular canal genesis zone is crucial to delineating differences, if any, between these three structures. For example, differential regulation by *Chd7* and/or *Sox11* of early vestibular patterning genes, such as *Lmo4* or *Gbx2*, across the three semicircular canals could provide clues as to why the anterior canal remains grossly unaffected with loss of either *Chd7* or *Sox11*[25,26].

This study also provides insight into the genetic pathways responsible for the evolutionary specification and order of the semicircular canal system. The origin of the inner ear is considered a result of infolding of the lateral line complex in early fish[27]. Following this, putative anterior and posterior semicircular canal systems have been identified in the hagfish and other closely related species. Later vertebrates developed a third, orthogonal semicircular canal, giving rise to the three-canal system seen in advanced vertebrates. Exactly how this third (lateral) canal arose is currently unknown[27]. As loss of *Chd7* and *Sox11*, alone or together, give rise to posterior and lateral canal defects, it is reasonable to hypothesize that the lateral canal is derivative from the posterior. Further exploration of the CHD7-SOX11 genetic network within the development of the labyrinth could clarify if such an evolutionary relationship exists. Determination of transient expression, if any, of *Chd7* and *Sox11* within the nascent anterior semicircular canal and associated crista ampullaris would be crucial to delineating if these genes have any role in anterior canal morphogenesis.

Co-expression of *Sox4* and *Sox11* has been reported in several developing mouse organs, particularly neuronal tissues and structures derived from mesenchyme[28]. In the ear, *Sox4* and *Sox11* are required for sensory cell specification and organization in the five vestibular sensory organs (two maculae and three cristae)[29]. *Sox4;Sox11* double conditional mutant ears fail to undergo segmentation of the anterior and lateral cristae and have reduced posterior cristae. Supporting cell and hair cell proliferation are severely reduced in *Sox4;Sox11* double conditional mutant mice, indicating a prosensory role for SoxC proteins in the five vestibular sensory organs. Further examination of prosensory cell proliferation in germline *Sox11* mutant cristae will help define the dependency of the mammalian vestibular apparatus on solely SOX11. Careful examination of germline *Sox4* mutant mice may also reveal heretofore undetected defects in murine ear development.

Finally, the data presented in Chapter IV suggests that, at least in certain aspects of inner ear specification and subsequent morphogenesis, *Chd7* is genetically upstream of *Sox11*. To more conclusively demonstrate a molecular relationship between CHD7 and the *Sox11* locus, examination of CHD7 localization around the *Sox11* locus by chromatin immunoprecipitation could be informative. Further, evidence of hypermethylation of the promoter and proximal coding sequence of *Sox11* in the absence of CHD7 would indicate a role for CHD7 in preserving a hypomethylated, and thus more active, chromatin state around the *Sox11* locus[30]. These experiments could be conducted in a relevant cell type, including iMOPs or a primary neural cell line[31].

Conclusion

The body of work contained within this dissertation advances our understanding of the pathogenesis of CHARGE syndrome, with a focus on the roles of CHD7 and SOX11 in craniofacial and inner ear development. My studies have defined clear contributions for CHD7 in development of the upper and lower respiratory tracts and provided insight into the etiology of life-threatening tracheomalacia seen in many individuals with CHARGE syndrome. Further, I describe a novel chromosomal aberration in an individual with clinical features of CHARGE and highlight potential roles for the transcription factor SOX11 in this syndrome. Finally, I describe results of an extensive study of how SOX11 contributes to vestibular development and define potential roles for SOX11 in development and function of the lateral and posterior semicircular canals. Collectively, these studies raise important questions about the interaction of CHD7 and SOX11 in mammalian development and highlight a potentially conserved CHD7-SOX11 genetic pathway critical for several embryologic processes.

References

1. Sperry, E. D. *et al.* The chromatin remodeling protein CHD7, mutated in CHARGE syndrome, is necessary for proper craniofacial and tracheal development. *Dev Dyn* **243**, 1055-1066 (2014).

2. Bajpai, R. *et al.* CHD7 cooperates with PBAF to control multipotent neural crest formation. *Nature* **463**, 958-962 (2010).

3. Schulz, Y. *et al.* CHD7, the gene mutated in CHARGE syndrome, regulates genes involved in neural crest cell guidance. *Hum Genet* **133**, 997-1009 (2014).

4. Asad, Z. *et al.* Rescue of neural crest-derived phenotypes in a zebrafish CHARGE model by Sox10 downregulation. *Hum Mol Genet* **25**, 3539-3554 (2016).

5. Mimura, S. *et al.* Bone morphogenetic protein 4 promotes craniofacial neural crest induction from human pluripotent stem cells. *Int J Dev Biol* **60**, 21-28 (2016).

6. Hurd, E. A., Micucci, J. A., Reamer, E. N. & Martin, D. M. Delayed fusion and altered gene expression contribute to semicircular canal defects in Chd7 deficient mice. *Mech Dev* **129**, 308-323 (2012).

7. Layman, W. S. *et al.* Defects in neural stem cell proliferation and olfaction in Chd7 deficient mice indicate a mechanism for hyposmia in human CHARGE syndrome. *Hum Mol Genet* **18**, 1909-1923 (2009).

8. Li, C., Lan, Y. & Jiang, R. Molecular and Cellular Mechanisms of Palate Development. *J Dent Res*, 22034517703580 (2017).

9. Hurd, E. A., Poucher, H. K., Cheng, K., Raphael, Y. & Martin, D. M. The ATP-dependent chromatin remodeling enzyme CHD7 regulates pro-neural gene expression and neurogenesis in the inner ear. *Development* **137**, 3139-3150 (2010).

10. Tian, C. *et al.* Otitis media in a new mouse model for CHARGE syndrome with a deletion in the Chd7 gene. *PLoS One* **7**, e34944 (2012).

11. Bergman, J. E. *et al.* CHD7 mutations and CHARGE syndrome: the clinical implications of an expanding phenotype. *J Med Genet* **48**, 334-342 (2011).

12. Janssen, N. *et al.* Mutation update on the CHD7 gene involved in CHARGE syndrome. *Hum Mutat* **33**, 1149-1160 (2012).

13. Randall, V. *et al.* Great vessel development requires biallelic expression of Chd7 and Tbx1 in pharyngeal ectoderm in mice. *J Clin Invest* **119**, 3301-3310 (2009).

14. Zentner, G. E. *et al.* CHD7 functions in the nucleolus as a positive regulator of ribosomal RNA biogenesis. *Hum Mol Genet* **19**, 3491-3501 (2010).

15. Miquerol, L. & Kelly, R. G. Organogenesis of the vertebrate heart. *Wiley Interdiscip Rev Dev Biol* **2**, 17-29 (2013).

16. Perl, A. K., Wert, S. E., Nagy, A., Lobe, C. G. & Whitsett, J. A. Early restriction of peripheral and proximal cell lineages during formation of the lung. *Proc Natl Acad Sci U S A* **99**, 10482-10487 (2002).

17. Turcatel, G. *et al.* Cartilage rings contribute to the proper embryonic tracheal epithelial differentiation, metabolism, and expression of inflammatory genes. *Am J Physiol Lung Cell Mol Physiol* **312**, L196-L207 (2017).

18. Sperry, E. D., Schuette, J. L., van Ravenswaaij-Arts, C. M., Green, G. E. & Martin, D. M. Duplication 2p25 in a child with clinical features of CHARGE syndrome. *Am J Med Genet A* **170A**, 1148-1154 (2016).

19. Davis, E. E., Frangakis, S. & Katsanis, N. Interpreting human genetic variation with in vivo zebrafish assays. *Biochim Biophys Acta* **1842**, 1960-1970 (2014).

20. Sock, E. *et al.* Gene targeting reveals a widespread role for the high-mobility-group transcription factor Sox11 in tissue remodeling. *Mol Cell Biol* **24**, 6635-6644 (2004).

21. Feng, W. *et al.* The chromatin remodeler CHD7 regulates adult neurogenesis via activation of SoxC transcription factors. *Cell Stem Cell* **13**, 62-72 (2013).

22. Chang, W., Brigande, J. V., Fekete, D. M. & Wu, D. K. The development of semicircular canals in the inner ear: role of FGFs in sensory cristae. *Development* **131**, 4201-4211 (2004).

23. Chang, W., ten Dijke, P. & Wu, D. K. BMP pathways are involved in otic capsule formation and epithelial-mesenchymal signaling in the developing chicken inner ear. *Dev Biol* **251**, 380-394 (2002).

24. Omata, Y. *et al.* Role of Bone morphogenetic protein 4 in zebrafish semicircular canal development. *Dev Growth Differ* **49**, 711-719 (2007).

25. Deng, M., Pan, L., Xie, X. & Gan, L. Requirement for Lmo4 in the vestibular morphogenesis of mouse inner ear. *Dev Biol* **338**, 38-49 (2010).

26. Lin, Z., Cantos, R., Patente, M. & Wu, D. K. Gbx2 is required for the morphogenesis of the mouse inner ear: a downstream candidate of hindbrain signaling. *Development* **132**, 2309-2318 (2005).

27. Carey, J. & Amin, N. Evolutionary changes in the cochlea and labyrinth: Solving the problem of sound transmission to the balance organs of the inner ear. *Anat Rec A Discov Mol Cell Evol Biol* **288**, 482-489 (2006).

28. Dy, P. *et al.* The three SoxC proteins--Sox4, Sox11 and Sox12--exhibit overlapping expression patterns and molecular properties. *Nucleic Acids Res* **36**, 3101-3117 (2008).

29. Gnedeva, K. & Hudspeth, A. J. SoxC transcription factors are essential for the development of the inner ear. *Proc Natl Acad Sci U S A* **112**, 14066-14071 (2015).

30. Schnetz, M. P. *et al.* Genomic distribution of CHD7 on chromatin tracks H3K4 methylation patterns. *Genome Res* **19**, 590-601 (2009).

31. Azadeh, J., Song, Z., Laureano, A. S., Toro-Ramos, A. & Kwan, K. Initiating Differentiation in Immortalized Multipotent Otic Progenitor Cells. *J Vis Exp* (2016).